Proposed Methods For Measuring and Interpreting Mueller Matrices in In Vivo Retinal Polarimetry

by

Steven Kenneth Esau

A thesis
presented to the University of Waterloo
in fulfillment of the
thesis requirement for the degree of
Master of Science
in
Physics

Waterloo, Ontario, Canada, 2020

Author's Declaration

This thesis consists of material all of which I authored or co-authored: see Statement of Contributions included in the thesis. This is a true copy of the thesis, including any required final revisions, as accepted by my examiners.

I understand that my thesis may be made electronically available to the public.

Statement of Contributions

Some of the content included in chapter 4 has been presented previously at Photonics North 2020 under the coauthorship of Dr. Melanie Campbell (Steven Esau and Melanie Campbell. Design for Faster Measurement of Mueller Matrices in Double Pass Retinal Imaging. *Photonics North*, 2020).

Rachel Redekop, Peter Neathway, Monika Kitor, Erik Mason, Julia Zangoulos, and Dr. Melanie Campbell read this thesis in part or in whole and provided feedback.

The author benefited from many discussions with other members of Campbell Labs: Dr. Melanie Campbell, Rachel Redekop, Peter Neathway, Julia Zangoulos, Olivia Tong, Yunyi Qui, Erik Mason, Laura Emptage, Jonathan Chen, Hannah Rosenberg, Monika Kitor, Yifan Ding, Tao Jin, Alexander Rajapakse, Yifei Gu, Nathan DeJong, and Yanming Qi. The author also engaged in helpful correspondences with Dr. Juan Bueno, Dr. Colin Sheppard, Dr. Razvigor Ossikovski, and Dr. Ignacio Ojeda.

Abstract

Mueller matrix polarimetry is the examination of how a sample transforms the polarization state of light. This requires probing the sample with input light of a variety of generated polarization states and analyzing the resulting output states, using a total of at least sixteen irradiance measurements. This allows one to calculate the Mueller matrix, which provides insight into the microstructure of the sample. In imaging applications this can yield additional contrast between different types of materials. Examination of the human retina has the potential to reveal not only ocular conditions, but also neurological disorders due to the fact that the retina is made up of neural tissue. Deposits of amyloid-β in the brain are a standard biomarker for Alzheimer's disease. Similar deposits have been identified in the retina. By studying *ex vivo* human retinae, members of Campbell Labs have shown that these deposits can be imaged label-free using Mueller matrix polarimetry, and that their number correlates with the severity of Alzheimer's disease as assessed using brain pathology post-mortem. Imaging these deposits in the living eye using *in vivo* retinal polarimetry could provide an affordable and noninvasive biomarker for Alzheimer's disease, aiding in diagnosis.

This thesis uses a "double pass model" to describe *in vivo* retinal polarimetry: it is assumed that light passes through the ocular tissue (*i.e.* the cornea, lens, and upper layers of the retina) before reflecting within the retina, and traversing polarimetrically similar tissue in the opposite direction. This model implies a particular mathematical structure for the Mueller matrix in *in vivo* retinal polarimetry. This thesis proposes ways in which this mathematical structure can be used advantageously when measuring and interpreting double pass Mueller matrices. While other authors have used the double pass model for *in vivo* retinal polarimetry, it is believed that this thesis is the first work to examine its implications without also making assumptions about the polarimetric properties of the ocular tissue.

Following other authors, this thesis first describes the reciprocity theorem which relates a Mueller matrix for opposite paths through a sample, and uses it to apply the double pass model to Mueller matrices. It is shown that double pass Mueller matrices have fewer degrees of freedom than ordinary Mueller matrices. This allows double pass Mueller matrices to be calculated from as few as ten irradiance measurements. Several designs are developed for the generating and analyzing branches of a polarimeter, capable of measuring double pass Mueller matrices in ten measurements while being optimized for the best possible error performance. These are found using a novel extension of standard polarimeter optimization techniques that allows them to take into account the aforementioned restrictions on double pass Mueller matrices. These designs could be used to improve the speed of an *in vivo*

retinal polarimeter used for Alzheimer's disease diagnosis, reducing patient discomfort and eye movement during the measurement. Next, the double pass Mueller matrix is compared to the corresponding single pass Mueller matrix for transmission once through the ocular tissue. New methods are found to calculate possible single pass polarimetric properties from the double pass Mueller matrix. This may provide additional insight into the microstructure of the sample and yield results that are more similar to the transmission properties of retinal amyloid deposits previously measured *ex vivo*.

This thesis proposes new methods for measuring and interpreting Mueller matrices measured in *in vivo* retinal polarimetry assuming the double pass model. These methods could be applied in order to improve a future instrument for Alzheimer's disease diagnosis through observation of retinal amyloid deposits.

Acknowledgements

Thank you to my supervisor Dr. Melanie Campbell for her guidance and encouragement, and to all my fellow members of Campbell Labs.

This work was supported by the Natural Sciences and Engineering Research Council of Canada (NSERC), the Canadian Institutes of Health Research (CIHR), the Queen Elizabeth II Graduate Scholarship in Science and Technology, and the University of Waterloo.

Dedication

To my family.

Table of Contents

List of Figures

List of Tables

List of Abbreviations

AD Alzheimer's Disease 1

cSLO Confocal Scanning Laser Opthalmoscope 31

MM Mueller Matrix 1

PSA Polarization State Analyzer 19

PSG Polarization State Generator 19

QWP Quarter Wave Plate 19

RI Reciprocal Invariant 3

RNFL Retinal Nerve Fiber Layer 2

Chapter 1

Introduction

Electromagnetic waves, including visible light, have a fundamental property known as *polarization* [19]. The polarization state of light carries a lot of information, but is usually imperceptible to the human eye[1]. Similar to how the colour of an object is determined by how it reflects, transmits, or absorbs different wavelengths of visible light [58], objects can also be classified by how they alter the polarization state of light. A Mueller Matrix (MM) is a set of sixteen numbers that describes the effect an object has on the polarization state of incident light. *MM polarimetry* is the measurement of MMs, by probing the object with a variety of different polarization states and measuring the resulting output states [40]. This requires at least sixteen irradiance measurements [40]. MMs can be interpreted in terms of polarimetric properties such as retardance, diattenuation, and depolarization, which are indicative of the microstructural features of the sample [57]. These properties have been used successfully in biological studies to distinguish between normal and diseased tissue [1, 50, 57, 101, 119].

Examination of the human retina is used for diagnosis of a wide range of different ocular conditions [16, 122]. In addition, the retina is an embryological extension of the central nervous system, that can be easily imaged due to the transparency of ocular tissue [92]. For this reason, there has been significant attention to the possibility of using the retina to diagnose neurological diseases [84, 92]. Alzheimer's Disease (AD) is a neurodegenerative disease that is the most common form of dementia, and in the U.S. in 2019 it affected approximately 5.8 million people [11]. It may be diagnosed based on cognitive tests and attempts to rule out other causes of dementia, but this does not always reliably predict brain

[1] There are some rare situations in which humans can discern the difference between polarization states; *e.g.* [111, 124, 135]

pathology [11]. A biomarker is an objectively measurable "indicator of normal biological processes, pathogenic processes or pharmacological response to a therapeutic intervention" [12]. Biomarkers are important to provide a more reliable diagnosis for AD, and to allow researchers to assess the effectiveness of drug trials [92]. Brain biomarkers of AD are well established but expensive and invasive to assess *in vivo* [92].

A standard brain biomarker of AD, amyloid-β protein in the form of deposits, has also been identified in the retina [35, 75]. In recent years, a project of Campbell Labs (with which the author is affiliated) has been to study *ex vivo* retinae with matched brain pathology [35, 43, 45, 67]. Deposits were discovered in the retinae that fluoresced when stained with Thioflavin-S, an amyloid dye [35]. It was found that these could also be imaged without dyes using MM polarimetry, and that their number correlated with the severity of AD diagnosis from brain pathology [43, 45]. The primary cause of their visibility is linear retardance, likely due to the fibrillar nature of amyloid, but there are also other significant polarimetric signals [68]. Polarimetric data has been collected of over one thousand deposits at Campbell Labs. These deposits are a promising candidate for a retinal biomarker of AD. However, these were *ex vivo* retinal polarimetry measurements, studying the light that was transmitted through isolated retinae. Future work is planned to be *in vivo* in order to realize the diagnostic potential of this method. Due to the anatomy of the eye, in *in vivo* retinal polarimetry light must pass through the cornea, pupil, lens, and upper layers of the retina, before being reflected and traversing each of those structures again in the opposite direction. This is a different measurement than past *ex vivo* images of retinal amyloid deposits, not only due to the polarimetric effects of the cornea and lens [32, 30, 121], but also because of the change from a transmission to a reflection geometry.

A number of instruments have been used in the past for *in vivo* retinal polarimetry. The Carl Zeiss Meditec (formerly Laser Diagnostics) GDx and GDx-VCC were commercially available instruments used for glaucoma diagnosis through assessment of the thickness of the Retinal Nerve Fiber Layer (RNFL) [140, 143, 142]. They were also applied in many different studies aimed at understanding how retinal structure changes in different conditions (*e.g.* [51, 71, 99, 123]). These instruments were partial polarimeters, meaning that they could not determine the full MM. Rather, they relied on the assumption that both the *anterior segment* (consisting of the cornea and lens together) and the retina each acted as a linear retarder, while also accounting for an isotropic depolarization term [73, 74, 142]. Additionally, they used what this thesis will define as the *double pass model*: that the beam transmits through the ocular tissue before experiencing an idealized reflection within the retina, after which it traverses polarimetrically similar tissue in the reverse direction [24, 64, 73, 74, 142]. There are two main advantages to this kind of partial polarimeter approach. Firstly, it allows for a simpler polarimeter design due to not requiring measurement of the

full MM. Secondly, under these assumptions the interpretation of the polarimetric results is straightforward, and the linear retardance from a single pass through the RNFL can be calculated and used to estimate its thickness [73, 74, 142].

However, this approach is unable to measure diattenuation or non-isotropic depolarization, and will be in error when these polarimetric properties are present [25, 26, 126]. While diattenuation is usually small in the human eye [25, 28, 126], depolarization varies and may increase in older eyes [22, 30, 26, 126]. Additionally, retinal amyloid deposits measured *ex vivo* show some diattenuation and depolarization [68, 106]. Other research groups have produced full MM *in vivo* retinal polarimeters which are able to measure any combination of polarimetric properties [27, 21, 29, 49, 72, 79, 100, 126]. This comes at the cost of increased complexity of the instrument and/or increased total measurement time.

This thesis proposes using the double pass model, without any other assumptions about the polarimetric properties of the retina (or retinal amyloid deposits), as the basis for a new type of partial *in vivo* retinal polarimetry. The double pass model alone implies a specific mathematical structure for the MM that is measured in *in vivo* retinal polarimetry. It will be shown that any double pass MM is restricted to have only ten degrees of freedom rather than sixteen. While the term "double pass" is often used to describe measurements in the eye (*e.g.* [7, 27, 21, 28, 108]), to the best of the author's knowledge this thesis is the first work to propose using the restrictions on the MM that are implied by the double pass model for partial *in vivo* retinal polarimetry. This approach has several benefits for the application of detecting retinal amyloid deposits *in vivo* as a biomarker for AD diagnosis. A double pass MM can be determined from as few as ten measurements, while still being sensitive to diattenuation and depolarization as well as retardance. This may decrease the time required for each patient, reducing patient discomfort and the number of disruptions such as blinks, involuntary eye movements [88], and tear film drying [62]. Additionally, the double pass model relates the transmission properties of the retina and amyloid deposits, which have been measured *ex vivo* by Campbell Labs, with the full *in vivo* MM. This aids in the interpretation of the *in vivo* MM.

Chapter 2 outlines the important background concepts of polarization, Jones and Mueller matrices, and polarimetry. Chapter 3 describes the double pass model and the mathematical structure of double pass MMs. It is shown that double pass MMs have a property called *reciprocal invariance*, which is due to the symmetry of the double pass model upon switching the incident and reflected beam. As well, a polarization ray tracing model is used to provide additional support for the claim that the MM measured in *in vivo* retinal polarimetry should be Reciprocal Invariant (RI).

Chapter 4 shows how to choose which generating and analyzing polarization states to

use for a partial polarimeter assuming the MM is RI. These states are optimized based on the objective of reducing the impact of experimental errors on the measured MM. The methodology used in this chapter is related to other author's work in the field of polarimeter optimization (*e.g.* [125, 130, 139]) but has novel elements. Several example optimized polarimeter designs are found which can determine a double pass MM in as few as ten measurements. A simulation is used to examine the performance of these designs and compare them to a conventional full MM polarimeter design. These designs could be used for faster measurement of double pass MMs in *in vivo* retinal polarimetry.

Chapter 5 examines the relationship between a double pass MM and its corresponding *single pass* MM (that is, the MM for transmission once through the ocular tissue). It is shown how to calculate possible single pass polarimetric properties from the double pass MM. These may provide more direct information about the microstructural features of the ocular tissue than the double pass polarimetric properties do. Chapter 5 also highlights how some of the information in the single pass MM is inaccessible in double pass. This has implications for studies of the transmission *ex vivo* retinal data currently being collected by Campbell Labs.

This thesis demonstrates the potential advantages of partial *in vivo* retinal polarimetry based on the double pass model without any assumptions about the polarimetric properties of ocular tissue. As well, methodologies are developed for the practical tasks of optimizing such a polarimeter and interpreting the resulting MMs. This work could be used by a future instrument identifying retinal amyloid deposits *in vivo* for AD diagnosis.

Chapter 2

Background

2.1 Polarization of Light

2.1.1 Electromagnetic Waves

In vacuum, Maxwell's equations involving the electric ($\mathbf{E}$) and magnetic ($\mathbf{B}$) fields can be used to derive the vector wave equations

$$\nabla^2\mathbf{E} - \epsilon_0\mu_0\frac{\partial^2\mathbf{E}}{\partial t^2} = 0 \tag{2.1}$$

$$\nabla^2\mathbf{B} - \epsilon_0\mu_0\frac{\partial^2\mathbf{B}}{\partial t^2} = 0. \tag{2.2}$$

where ϵ_0 is the vacuum permittivity and μ_0 is the vacuum permeability. Consider *plane wave* solutions for $\mathbf{E}$; *i.e.*, those for which $\mathbf{E}$ is constant on every plane perpendicular to some unit vector $\hat{\mathbf{n}}$. This implies that $\mathbf{E}$ can be written as a function of $\mathbf{r}\cdot\hat{\mathbf{n}}$ and t only. Combining this assumption with that of separable time dependence,

$$\mathbf{E}(\mathbf{r},t) = \mathbf{E}_0 e^{i(\mathbf{k}\cdot\mathbf{r}-\omega t)} \tag{2.3}$$

where $\mathbf{E}_0$ is a constant (generally complex) vector, ω is the frequency, and $\mathbf{k} \equiv \hat{\mathbf{n}}\sqrt{\mu_0\epsilon_0}\omega$. Using the Maxwell equations it can be shown that $\mathbf{E}_0\cdot\mathbf{k} = 0$, that is, harmonic plane waves are transverse.

Define unit vectors $\hat{\mathbf{t}}_1$ and $\hat{\mathbf{t}}_2$ such that $\hat{\mathbf{t}}_1\times\hat{\mathbf{t}}_2 = \hat{\mathbf{n}}$. $\mathbf{E}_0$ can be described in terms of its scalar projections onto $\hat{\mathbf{t}}_1$ and $\hat{\mathbf{t}}_2$:

$$\mathbf{E}_0 = E_{\hat{\mathbf{t}}_1}\hat{\mathbf{t}}_1 + E_{\hat{\mathbf{t}}_2}\hat{\mathbf{t}}_2 = a_1 e^{i\delta_1}\hat{\mathbf{t}}_1 + a_2 e^{i\delta_2}\hat{\mathbf{t}}_2 \tag{2.4}$$

where $E_{\hat{\mathbf{t}}_i} = \mathbf{E}_0 \cdot \hat{\mathbf{t}}_i$, and a_i and δ_i are real, for $i = 1, 2$.

Because of the Lorentz force equation

$$\mathbf{F} = q(\mathbf{E} + \mathbf{v} \times \mathbf{B}) \quad [66],$$

where $\mathbf{F}$ is the force on a point charge, q is the charge, and $\mathbf{v}$ is the velocity, complex $\mathbf{E}$ or $\mathbf{B}$ would imply complex forces, which would be unphysical. Due to the linearity of the equations involved, one can always construct a real solution using $\mathbf{E}_{real} \equiv \frac{1}{2}(\mathbf{E} + \mathbf{E}^*) = \Re(\mathbf{E})$. However, during intermediate calculations it is often convenient to work with the complex versions, understanding that $\mathbf{E}_{real}$ can be produced at the end of the calculation if needed.

2.1.2 The Polarization Ellipse

The vector nature of the complex amplitude $\mathbf{E}_0$ leads to a large variety of behaviour, beyond what is possible for scalar waves. The orientation of $\mathbf{E}_0$ is time-independent, but this is not true of $\Re(\mathbf{E})$. Considering the final expression for the electric field

$$\mathbf{E} = \mathbf{E}_0 \, e^{i(\mathbf{k}\cdot\mathbf{r} - \omega t)} = (a_1 e^{i\delta_1}\hat{\mathbf{t}}_1 + a_2 e^{i\delta_2}\hat{\mathbf{t}}_2) e^{i(\mathbf{k}\cdot\mathbf{r} - \omega t)}. \tag{2.5}$$

The corresponding real electric field is given by

$$\mathbf{E}_{real} = \frac{1}{2}(a_1 \cos(\mathbf{k}\cdot\mathbf{r} - \omega t + \delta_1)\hat{\mathbf{t}}_1 + a_2 \cos(\mathbf{k}\cdot\mathbf{r} - \omega t + \delta_2)\hat{\mathbf{t}}_2). \tag{2.6}$$

Defining the components of $\mathbf{E}_{real}$ with respect to $\hat{\mathbf{t}}_1$ and $\hat{\mathbf{t}}_2$ as $x = \mathbf{E}_{real} \cdot \hat{\mathbf{t}}_1$ and $y = \mathbf{E}_{real} \cdot \hat{\mathbf{t}}_2$, they are related through an ellipse equation:

$$a_1^2 a_2^2 \sin^2(\delta_2 - \delta_1) = a_2^2 x^2 + a_1^2 y^2 - 2a_1 a_2 xy \cos(\delta_2 - \delta_1) \quad [53]. \tag{2.7}$$

This implies that the tip of the vector $\mathbf{E}_{real}$ always lies on an ellipse, the shape of which is determined by a_1, a_2, and $\delta_2 - \delta_1$. The exact position of $\mathbf{E}_{real}$ on this ellipse depends on the phase argument $\mathbf{k}\cdot\mathbf{r} - \omega t$. This is known as the *polarization ellipse* [19, 53, 58]. If $\delta_2 - \delta_1 = n\pi$ for integer n, then it follows from equation 2.7 that

$$\begin{aligned} 0 &= (a_2 x - a_1 y)^2 \implies \\ y &= \frac{a_2}{a_1} x \end{aligned}$$

so the ellipse collapses into a straight line passing through the origin. In this case the wave is said to be *linearly polarized* [19]. If $\delta_2 - \delta_1 = n\pi + \pi/2$ and $a_1 = a_2$,

$$a_1^2 = x^2 + y^2$$

so the ellipse reduces to a circle and the wave is said to be *circularly polarized* [19]. In all other cases, the wave at $\mathbf{r}$ is said to be *elliptically polarized* [19]. For circular and elliptical polarization, one can distinguish the direction in which $\mathbf{E}_{real}$ traces out the ellipse. If, with increasing t, $\mathbf{E}_{real}$ traces the ellipse in anti-clockwise direction in the $(\hat{\mathbf{t}}_1, \hat{\mathbf{t}}_2)$ plane the polarization is called right handed; otherwise, it is called left handed [41].

The choice of $\hat{\mathbf{t}}_1$ and $\hat{\mathbf{t}}_2$ is not unique. However, with respect to a new basis $\hat{\mathbf{t}}_1'$ and $\hat{\mathbf{t}}_2'$ obeying $\hat{\mathbf{t}}_1' \times \hat{\mathbf{t}}_2' = \hat{\mathbf{n}}$, linear polarization will remain linear, circular polarization will remain circular, and handedness will be preserved.

2.1.3 Jones Vectors and Stokes Vectors

The polarization state of a wave at a given point can be written as a 2×1 vector

$$\mathbf{j} \equiv \begin{bmatrix} a_1 e^{i\delta_1} \\ a_2 e^{i\delta_2} \end{bmatrix} \tag{2.8}$$

known as a *Jones vector* [53]. Note that this definition assumes a particular choice of $\hat{\mathbf{t}}_1$ and $\hat{\mathbf{t}}_2$.

Jones vectors are a useful theoretical tool, but cannot be directly measured. This is because the temporal frequencies of visible light are extremely rapid in comparison to the response time of a typical detector [53, 58], meaning $\mathbf{E}$ is not measured directly. Detectors instead measure the irradiance, which is the average energy deposited in the detector per unit area per unit time [40, 58]. Typically, it is assumed that $\mathbf{E}$ is sufficiently close to a plane wave that the irradiance is constant spatially across the relevant portion of the detector. Then irradiance is proportional to $\langle |\mathbf{E}|^2 \rangle$ [58], where $\langle f(\mathbf{r}, t) \rangle$ represents the average of f over the measurement time. The *Stokes parameters* represent a set of irradiance measurements from which the polarization ellipse of a plane wave can be inferred. These are

$$s_0 \equiv \left\langle a_1^2 + a_2^2 \right\rangle \tag{2.9}$$

$$s_1 \equiv \left\langle a_1^2 - a_2^2 \right\rangle \tag{2.10}$$

$$s_2 \equiv \langle 2a_1 a_2 \cos(\delta_2 - \delta_1) \rangle \tag{2.11}$$

$$s_3 \equiv \langle 2a_1 a_2 \sin(\delta_2 - \delta_1) \rangle \quad [66]. \tag{2.12}$$

The Stokes parameter s_0 is the irradiance of the wave. The component $s_1 = \pm 1$ for linearly polarized light aligned with the $\hat{\mathbf{t}}_1$ or $\hat{\mathbf{t}_1}$ directions respectively. The next component $s_2 = \pm 1$ for linearly polarized light aligned with the $\hat{\mathbf{t}}_1 + \hat{\mathbf{t}}_2$ or $\hat{\mathbf{t}}_1 - \hat{\mathbf{t}}_2$ directions. Lastly, $s_3 = \pm 1$ for right or left-handed circularly polarized light. If a_1, a_2, and $\delta_2 - \delta_1$ are constant across the pixel size and measurement time, and these parameters obey

$$s_0^2 = s_1^2 + s_2^2 + s_3^2. \tag{2.13}$$

The Stokes parameters can be arranged into a 4x1 *Stokes vector*

$$\mathbf{s} \equiv \begin{bmatrix} s_0 \\ s_1 \\ s_2 \\ s_3 \end{bmatrix}. \tag{2.14}$$

Stokes vectors have the advantage of being directly measurable quantities (irradiances) and can also describe partially polarized light, discussed in the next section. For every Jones vector $\mathbf{j}$, there is a corresponding Stokes vector $\mathbf{s}$ equal to

$$\mathbf{s} = \mathcal{L} \langle \mathbf{j} \otimes \mathbf{j}^* \rangle \quad [53] \tag{2.15}$$

where

$$\mathcal{L} = \begin{bmatrix} 1 & 0 & 0 & 1 \\ 1 & 0 & 0 & -1 \\ 0 & 1 & 1 & 0 \\ 0 & i & -i & 0 \end{bmatrix},$$

* is the complex conjugate, and $\otimes$ is the Kronecker product [60].

2.1.4 Unpolarized and Partially Polarized Light

The monochromatic plane waves treated so far exist at all points $\mathbf{r}$ in space and t in time. This would not be the case for a real wave. For any physical wave, a source started emitting the wave at some point in time and will stop emitting it at a later time, and so the wave is actually a wave pulse [19, 58]. It can still be described by the sum of 2.5 for a range of frequencies ω. For a long enough wave pulse, the range of frequencies will be narrow and the wave is called quasimonochromatic [58].

A nonlaser light source will in fact emit wave pulses at random, overlapping with one another such that the light emission appears continuous [58, 131]. This leads to fluctuations in time of the polarization parameters a_1, a_2, δ_1, and δ_2, causing the shape and handedness of the polarization ellipse to vary with time. If it varies slowly enough to be constant over the measurement time, then the Stokes parameters will still obey equation 2.13. If however they are not constant during the measurement time, restriction 2.13 is no longer true, although the Stokes parameters must always obey the inequality

$$s_0^2 \geq s_1^2 + s_2^2 + s_3^2 \quad [53]. \tag{2.16}$$

If $s_1^2 + s_2^2 + s_3^2 = 0$, the light is said to be *unpolarized* [58]. *Fully polarized* light on the other hand is light for which $s_1^2 + s_2^2 + s_3^2 = s_0^2$, and *partially polarized* light lies between these two extremes.

If a_1/a_2 and $\delta_1 - \delta_2$ stay constant in time, then the Jones vector can be written as a scalar multiplied by a time independent vector:

$$\mathbf{j} = a(t)e^{i\delta(t)} \begin{bmatrix} a_{c1}e^{i\delta_{c1}} \\ a_{c2}e^{i\delta_{c2}} \end{bmatrix}. \tag{2.17}$$

This wave is fully polarized despite the time dependence, because the associated Stokes parameters obey 2.13. It can be shown that the shape and handedness of the polarization ellipse are constant, although the amplitude and phase may fluctuate. However, the time dependence will matter once again if two such waves are added together. Even if both are of the form 2.17, the sum may or not be, depending on the relationships between the two time dependent prefactors. The different possibilities are described by the concepts of coherent and incoherent superposition of waves [53].

2.1.5 Coherence

Consider the sum of two plane waves $\mathbf{E}_{real}$ and $\mathbf{E}'_{real}$: $\mathbf{E}_{real,sum} \equiv \mathbf{E}_{real} + \mathbf{E}'_{real} = \Re(\mathbf{E} + \mathbf{E}')$, with their complex fields each described by 2.5 and having the same $\mathbf{k}$ and ω. The Jones vector of the sum is

$$\mathbf{j}_{sum} \equiv \mathbf{j} + \mathbf{j}' = a(t)e^{i\delta(t)} \left(\begin{bmatrix} a_{c1}e^{i\delta_{c1}} \\ a_{c2}e^{i\delta_{c2}} \end{bmatrix} + \frac{a'(t)}{a(t)} e^{i(\delta'(t)-\delta(t))} \begin{bmatrix} a'_{c1}e^{i\delta'_{c1}} \\ a'_{c2}e^{i\delta'_{c2}} \end{bmatrix} \right). \tag{2.18}$$

If the factor

$$\frac{a'(t)}{a(t)} e^{i(\delta'(t)-\delta(t))}$$

is constant over the measurement time, then $\mathbf{j}_{sum}$ has the form of 2.17 and the wave is fully polarized. The two waves are said to be *coherent* [58]. As an example, consider a single wave that is split into two components that travel along different paths. The polarization state of each wave will change in different ways along its path. If the two paths then come back together and the waves are recombined, and if the total path length that each has travelled is similar enough, then the two waves will add coherently.

If $\delta_i' - \delta_i$ is not constant over the measurement time, consider the Stokes parameter

$$\begin{aligned} s_{0,sum} &= \left\langle a_1^2 + a_1'^2 + 2a_1 a_1' \cos(\delta_1' - \delta_1) + a_2^2 + a_2'^2 + 2a_2 a_2' \cos(\delta_2' - \delta_2) \right\rangle \\ &= s_0 + s_0' + \left\langle 2a_1 a_1' \cos(\delta_1' - \delta_1) + 2a_2 a_2' \cos(\delta_2' - \delta_2) \right\rangle . \end{aligned}$$

If $\delta_i' - \delta_i$ for $i = 1, 2$ varies at random during the measurement time then the interference term

$$\left\langle 2a_1 a_1' \cos(\delta_1' - \delta_1) + 2a_2 a_2' \cos(\delta_2' - \delta_2) \right\rangle$$

averages to zero. In this case, the two waves are said to add *incoherently* [53]. By considering the other Stokes parameters, it can be shown that in this case the Stokes vector $\mathbf{s}_{sum} = \mathbf{s} + \mathbf{s}'$. Therefore, while adding Jones vectors represents coherent sum of plane waves, adding Stokes vectors represents incoherent sum [53]. In the intermediate case in which $\delta_i' - \delta_i$ varies in time but the interference terms do not vanish, the two waves are partially coherent. They can be split into fully coherent components that are added as Jones vectors and fully incoherent components that are added as Stokes vectors [53].

2.2 Light in Matter

2.2.1 Electromagnetic Waves in Matter

The wave equations that were the starting point of the previous section were only strictly valid in vacuum. In matter, the complicated distribution of charges within atoms and molecules makes the microscopic Maxwell equations impractical to use [66]. The macroscopic Maxwell equations can be introduced by taking the spatial average over small volumes (of the order $\approx 10^{-24} m^3$ [66]), smoothing out these microscopic fluctuations. In addition to the electric and magnetic fields, these equations involve the additional fields $\mathbf{D}$ and $\mathbf{H}$ [19, 66]. Different types of materials are characterized by different *constitutive relations* which identify the relationship between $(\mathbf{D}, \mathbf{H})$ and $(\mathbf{E}, \mathbf{B})$ [19]. These constitutive relations lead to different behaviors of elecromagnetic waves in those materials. A few

important examples of constitutive relations will be discussed in this section, to show how these materials modify the polarization state of light.

In the case of a linear, nonmagnetic, isotropic material,

$$\mathbf{D} = \epsilon \mathbf{E} \tag{2.19}$$

$$\mathbf{H} = \frac{1}{\mu_0}\mathbf{B} \tag{2.20}$$

where ϵ is a scalar known as the dielectric constant [19]. Assuming that there are no charges or currents, it can be shown that

$$\nabla^2 \mathbf{E} - \epsilon\mu_0 \frac{\partial^2 \mathbf{E}}{\partial t^2} = 0 \quad [41]. \tag{2.21}$$

This is identical to the wave equation in the previous section, with the substitution $\epsilon_0 \longrightarrow \epsilon$. Waves of the form of 2.3 propagate just as they would in the vacuum, but at a different speed. An absorbing isotropic medium can be represented using a complex ϵ, which results in an exponential decaying factor in the amplitude of the wave [19]. Light can propagate through this type of material without altering the shape of its polarization ellipse [41].

A second important example is that of a linear, nonmagnetic, electrically anisotropic material, for which

$$\mathbf{D} = \boldsymbol{\epsilon} \mathbf{E} \tag{2.22}$$

$$\mathbf{H} = \frac{1}{\mu_0}\mathbf{B} \tag{2.23}$$

$$\boldsymbol{\epsilon} \equiv \mathbf{U}^T \begin{bmatrix} \epsilon_{x'} & 0 & 0 \\ 0 & \epsilon_{y'} & 0 \\ 0 & 0 & \epsilon_{z'} \end{bmatrix} \mathbf{U} \tag{2.24}$$

where $\boldsymbol{\epsilon}$ is the 3×3 dielectric tensor, T means transpose, and $\mathbf{U}$ is a real orthogonal[1] matrix [19, 41]. In this form, the strength of the response of the material depends on the direction of $\mathbf{E}$ [19]. $\mathbf{U}$ is a change-of-basis matrix into a new coordinate system x', y', z', known as the principle coordinates of the material [19]. Wave propagation in such a material is significantly more complicated than in a vacuum. Assuming plane wave harmonic solutions it can be shown that for a given wave normal $\hat{\mathbf{n}}$, the only plane waves that can propagate in the medium are those that are linearly polarized along one of two orthogonal directions [19, 41]. Each direction has a different effective dielectric constant, determining the speed

[1] That is, a matrix for which $\mathbf{U}^T\mathbf{U} = \mathbf{U}\mathbf{U}^T = \mathbb{I}$, where $\mathbb{I}$ is the identity matrix.

at which the wave travels and how much it is absorbed. The difference in speeds means that at an interface, Snell's law will cause the each wave to refract in different directions [19]. As well, in general the waves are not transverse, that is, $\mathbf{E}$ is not perpendicular to $\hat{\mathbf{n}}$. A consequence of this is that the energy of the wave proceeds in a different direction than $\hat{\mathbf{n}}$ [19, 58]. This "ray vector" direction is also different between the two possible linearly polarized waves [19].

Consider the situation in which a plane wave in vacuum passes through a slab of an anisotropic material. Combining the requirements of Snell's law for entry into the medium with those of the Maxwell equations for propagation within the medium, there are in general two linearly polarized states that are permissible [19]. The incident plane wave, whatever its polarization, can be written as a coherent sum of these two states [53]. These two waves propagate through the medium, and then upon exiting can in general be added coherently to obtain again a single waves [53]. Within the medium, each travels at a different speed and is absorbed at a different rate. The difference in speeds means that there is a phase difference between the two waves that accumulates as they traverse the slab. The total phase difference is known as *linear retardance*, and the polarization of the wave that travelled fastest is known as the *linear fast axis* [39]. The amount of retardance per unit thickness is known as the *birefringence* [19]. The phase difference affects the degree to which the component waves add destructively or constructively upon exiting the medium, and therefore changes the polarization ellipse of the output wave.

If the two component waves are absorbed at different rates, this is known as *linear dichroism*. *Linear diattenuation* is a measure of the total difference between the absorption of the two waves, while the polarization that is absorbed less is known as the *linear diattenuation orientation* [39]. Like retardance, this also changes the polarization ellipse as the wave propagates through the medium. Reflections at the interface between two materials can also cause retardance and diattenuation [53], even though the materials may not be birefringent or dichroic.

Next, a chiral material can be described using the constitutive relations

$$\mathbf{D} = \epsilon(\mathbf{E} + \beta\nabla \times \mathbf{E}) \tag{2.25}$$

$$\mathbf{B} = \mu(\mathbf{H} + \beta\nabla \times \mathbf{H}) \quad [46,\ 77]. \tag{2.26}$$

In this type of media, the permitted plane waves are those with left and right handed circular polarization states [41, 77]. Similar to the effect anisotropic materials have on linear polarization states, chiral materials can impose phase differences between left and right handed circularly polarized light (circular birefringence) and/or absorb one preferentially (circular dichroism) [39]. This will also have the effect of changing the polarization ellipse as a wave propagates through the material.

For each of these types of materials, the change in polarization ellipse due to propagation can be represented using the Jones calculus [65]. If the incident wave is represented by a Jones vector $\mathbf{j}_{IN}$, then transmission through the material has the effect of transforming this into a different Jones vector $\mathbf{j}_{OUT}$. These can always be related to one another by a complex 2×2 *Jones matrix*:

$$\mathbf{j}_{OUT} = \mathbf{J}\,\mathbf{j}_{IN} \quad [41,\ 53,\ 58]. \tag{2.27}$$

The Jones matrix can be used to predict the output Jones vector given any input Jones vector. Any process in which the input and output fields are linearly related, and both have a well defined Jones vector, can be represented using a Jones matrix [53]. The concepts of retardance and diattenuation can be extended to describe the phase difference and absorption difference between elliptical states of polarization. In fact, any 2×2 complex matrix is a valid Jones matrix and its effects can always be understood as a combination of retardance and diattenuation [8, 53]. While these concepts have been introduced by considering transmission through birefringent and dichroic materials, retardance and diattenuation can be caused by other processes, such as the Fresnel equations for reflection and transmission at an interface [66]. Jones matrices for various types of retarders and diattenuators can be found in standard textbooks; *e.g.* [53, 58].

Linear diattenuation and linear retardance are indicators of the anisotropy of the sample. While they were defined by considering the dielectric tensor (indicating anisotropy on the molecular level), they can also occur due to anisotropy on larger scales [70, 94]. For example, linear retardance and linear retardance fast axis have been used to visualize the thickness and orientation of bundles of fibres in biological tissue [49, 50, 57, 70, 142]. Likewise, circular diattenuation and circular retardance are indicators of the chirality of the sample. They can be used to test for the presence of chiral molecules, such as glucose [18, 107].

2.2.2 Non-depolarizing Mueller Matrices

Similar to the Jones matrix, the *Mueller matrix* (MM) represents transformations between input and output Stokes vectors. Starting from equation 2.27 and using equation 2.15 to convert both Jones vectors to Stokes vectors, it can be shown that

$$\mathbf{s}_{OUT} = \mathcal{L}(\mathbf{J} \otimes \mathbf{J}^*)\mathcal{L}^{-1}\mathbf{s}_{IN} \quad [53].$$

The real 4×4 matrix

$$\mathbf{M}_J = \mathcal{L}(\mathbf{J} \otimes \mathbf{J}^*)\mathcal{L}^{-1} \quad [53] \tag{2.28}$$

is a non-depolarizing MM. "Non-depolarizing" refers the the fact that given a fully polarized $\mathbf{s}_{IN}$, the output Stokes vector $\mathbf{s}_{OUT}$ will always also be fully polarized. In subsection 2.2.3, it will be shown that MMs can also describe processes that introduce depolarization into the output Stokes vector. This is not possible using Jones matrices, and is the reason why MMs are often preferred for the study of biological tissues [1, 57] and particularly retinal amyloid deposits [45, 106]. A product of MMs $\mathbf{M}_{J2}\,\mathbf{M}_{J1}$ is equivalent to a system in which light experiences first $\mathbf{M}_{J1}$, and then $\mathbf{M}_{J2}$ [53].

The concepts of diattenuation and retardance can also be represented using MMs. A *diattenuator* MM, which has diattenuation but no retardance, can be written (using matrix block notation) as

$$\begin{aligned} \mathbf{M}_D &= \frac{1}{1+D}\begin{bmatrix} 1 & \mathbf{D}^T \\ \mathbf{D} & \mathbf{m}_D \end{bmatrix} \\ \mathbf{m}_D &= \sqrt{1-D^2}\mathbb{I} + \frac{1-\sqrt{1-D^2}}{D^2}\mathbf{D}\mathbf{D}^T \end{aligned} \tag{2.29}$$

where $\mathbf{D}$ is a 3×1 vector known as the *diattenuation vector*[2] [39, 53, 83]. Lower case $\mathbf{m}_D$ is the lower right 3×3 submatrix of $\mathbf{M}_D$. It is symmetric, and has the property $\mathbf{m}_D\,\mathbf{D} = \mathbf{D}$. The matrix $\mathbf{M}_D$ is specified entirely by the diattenuation vector $\mathbf{D}$.

Any diattenuator has two *eigenpolarizations* for which the shape of the polarization ellipse is unchanged by $\mathbf{M}_D$ [83]. For an anisotropic material with the constitutive relations 2.22, these are the two linear polarization states that are permitted inside the material, as described in the previous subsection. The Stokes vectors of the two eigenpolarizations are given by $[1,\,\hat{\mathbf{D}}]^T$ and $[1,\,-\hat{\mathbf{D}}]^T$ respectively:

$$\mathbf{M}_D\,[1,\,\hat{\mathbf{D}}]^T = T_{max}[1,\,\hat{\mathbf{D}}]^T \tag{2.30}$$

$$\mathbf{M}_D\,[1,\,-\hat{\mathbf{D}}]^T = T_{min}[1,\,-\hat{\mathbf{D}}]^T \tag{2.31}$$

where T_{max} and T_{min} are scalars with $T_{max} > T_{min} > 0$, indicating that one eigenpolarization is transmitted more strongly than the other [39, 83]. The diattenuation magnitude $|\mathbf{D}| = D$ is bounded by zero and one and is related to the difference in transmittance between the eigenpolarizations:

$$D = \frac{T_{max} - T_{min}}{T_{max} + T_{min}} \quad [39]. \tag{2.32}$$

[2] $\mathbf{D}$ shares a symbol with the displacement vector in the macroscopic Maxwell equations. From this point on in the thesis, $\mathbf{D}$ will always refer to diattenuation vector.

Equation 2.29 is normalized such that $T_{max} = 1$. The diattenuation vector $\mathbf{D}$ indicates both the eigenpolarizations of the diattenuator and the difference in transmittance between those eigenpolarizations.

$\mathbf{D}$ can be separated into three scalar components:

$$\mathbf{D} = \begin{bmatrix} D_H \\ D_{45} \\ D_C \end{bmatrix} \tag{2.33}$$

which represent horizontal diattenuation, forty-five degree diattenuation and circular diattenuation respectively [83]. The first two components can instead be represented by a linear diattenuation magnitude,

$$D_L = \sqrt{D_H^2 + D_{45}^2} \quad [127] \tag{2.34}$$

and linear diattenuation orientation[3]

$$D_\theta = (1/2)\text{arctan2}(D_{45}, D_H) \quad [127]. \tag{2.35}$$

D_L and D_θ are indicative of the strength and orientation of the optical anisotropy of the sample respectively.

Note that diattenuators also exhibit *polarizance*, which is the property of turning incident unpolarized light into partially or fully polarized light [53]. The polarizance vector $\mathbf{P}$ of any MM $\mathbf{M}$ is defined as

$$c' \, [1, \, \mathbf{P}]^T \equiv \mathbf{M}[1, \, 0, \, 0, \, 0]^T \tag{2.36}$$

for some scalar c'. Any diattenuator $\mathbf{M}_D$ has $\mathbf{P} = \mathbf{D}$. A polarizer (or partial polarizer) with zero retardance is the same as a diattenuator, given by equation 2.29.

In turn, a retarder with zero diattenuation can be written

$$\mathbf{M}_R \equiv \begin{bmatrix} 1 & \mathbf{0}^T \\ \mathbf{0} & \mathbf{m}_R \end{bmatrix} \quad [53] \tag{2.37}$$

where $\mathbf{0}$ is the 3×1 zero vector. Mathematically, $\mathbf{m}_R$ is a 3D proper rotation matrix in the space of the last three Stokes parameters $[s_1, \, s_2, \, s_3]$ [53]. In order to be a rotation matrix, $\mathbf{m}_R$ must obey

$$\mathbf{m}_R \, \mathbf{m}_R^T = \mathbb{I}$$
$$\det(\mathbf{m}_R) = +1.$$

[3] $\text{arctan2}(Y, X)$ is the four quadrant arctangent function, which is equal to $\arctan(Y/X)$ if X is positive, and $\arctan(Y/X) + \pi$ if it is negative [89].

$\mathbf{m}_R$ can be specified entirely by a rotation axis $\hat{\mathbf{R}}$ and an angular rotation distance R [53]. Together these make up the *retardance vector* $\mathbf{R} = R\hat{\mathbf{R}}$ [83]. The 3×1 vector $\mathbf{R}$ completely specifies $\mathbf{M}_R$. Physically speaking, the direction $\hat{\mathbf{R}}$ gives the two eigenpolarizations of $\mathbf{M}_R$, $[1,\, \hat{\mathbf{R}}]^T$ and $[1,\, -\hat{\mathbf{R}}]^T$. A wave with Stokes vector $[1,\, \hat{\mathbf{R}}]^T$ is advanced in phase relative to a wave with Stokes vector $[1,\, -\hat{\mathbf{R}}]^T$, hence $\hat{\mathbf{R}}$ is known as the *fast axis* [83]. The magnitude of the retardance vector R is the retardance, *i.e.* the phase difference between the two waves [83].

$\mathbf{R}$ can be written in terms of three components

$$\mathbf{R} = \begin{bmatrix} R_H \\ R_{45} \\ R_C \end{bmatrix} \quad [83]$$

which can be calculated using[4]

$$\begin{aligned} R &= \arccos\left(\frac{\text{trace}(\mathbf{m}_R) - 1}{2}\right) \\ R_H &= \frac{R}{2\sin R}(\mathbf{m}_R(2,3) - \mathbf{m}_R(3,2)) \\ R_{45} &= \frac{R}{2\sin R}(\mathbf{m}_R(3,1) - \mathbf{m}_R(1,3)) \\ R_C &= \frac{R}{2\sin R}(\mathbf{m}_R(1,2) - \mathbf{m}_R(2,1)) \end{aligned} \quad [83]. \tag{2.38}$$

Similar to the diattenuation, these components represent horizontal, forty-five degree, and circular retardance respectively. Define the linear retardance $R_L \equiv \sqrt{R_H^2 + R_{45}^2}$ and linear fast axis $\theta \equiv (1/2)\text{arctan2}(R_{45}, R_H)$ [127]. A linear retarder is a retarder for which $R_C = 0$, and can always be written as

$$\mathbf{M}_{LR}(R_L, \theta) = \begin{bmatrix} 1 & \mathbf{0}^T \\ \mathbf{0} & \mathbf{m}_{LR}(R_L, \theta) \end{bmatrix}$$

$$\mathbf{m}_{LR}(R_L, \theta) =$$

$$\begin{bmatrix} \cos^2(2\theta) + \cos(R_L)\sin^2(2\theta) & (1-\cos(R_L))\cos(2\theta)\sin(2\theta) & -\sin(R_L)\sin(2\theta) \\ (1-\cos(R_L))\cos(2\theta)\sin(2\theta) & \cos(R_L)\cos^2(2\theta) + \sin^2(2\theta) & \cos(2\theta)\sin(R_L) \\ \sin(R_L)\sin(2\theta) & -\cos(2\theta)\sin(R_L) & \cos(R_L) \end{bmatrix} \quad [39]. \tag{2.39}$$

[4]Strictly speaking, equations 2.38 fail for $R = 0$ or $R = \pi$ [53]. In the $R = \pi$ case, other equations can be derived to determine the three components R_H, R_{45}, and R_C. If $R = 0$, then $\mathbf{M}_R = \mathbb{I}$.

Note that $R_C = 0$ implies that the eigenpolarizations $[1, \hat{\mathbf{R}}]^T$ and $[1, -\hat{\mathbf{R}}]^T$ both represent linearly polarized light.

A circular retarder on the other hand has circularly polarized eigenpolarizations. This implies $R_L = 0$, and

$$\mathbf{M}_{CR}(R_C) = \begin{bmatrix} 1 & 0 & 0 & 0 \\ 0 & \cos(R_C) & \sin(R_C) & 0 \\ 0 & -\sin(R_C) & \cos(R_C) & 0 \\ 0 & 0 & 0 & 1 \end{bmatrix} \quad [53]. \tag{2.40}$$

A retarder with $R_L \neq 0$ and $R_C \neq 0$ is known as an elliptical retarder, and has elliptically polarized eigenpolarizations.

Because of the periodic nature of waves, a retardance of 2π radians has no effect on the polarization state of a wave. This leads to an ambiguity in the retardance vector: the vectors

$$\mathbf{R} = R\hat{\mathbf{R}} \longrightarrow (R + 2\pi n)\hat{\mathbf{R}} \qquad n \in \mathbb{Z} \tag{2.41}$$

all give the same MM $\mathbf{M}_R$ [39]. Equations 2.38 return the unique retardance vector for which $0 < R < \pi$.

Any non-depolarizing MM can constructed (up to a scalar constant) by multiplying together $\mathbf{M}_D$ and $\mathbf{M}_R$ [53, 83]. Non-depolarizing MMs are always equivalent to a Jones matrix [53]. They are more convenient than Jones matrices for some types of analyses due to their connection with Stokes vectors, which are more directly measurable than Jones vectors [40]. However, one can also consider depolarizing MMs, which may output partially or unpolarized Stokes vectors even given fully polarized input. This type of process cannot be represented with Jones matrices [53].

2.2.3 Depolarizing Mueller Matrices

Depolarizing MMs are those that can output partially polarized or unpolarized light for fully polarized input light [53]. This occurs when the beam that is recorded at the detector is made up of two or more incoherent components $\mathbf{s}_{OUT,i}$ that have experienced different polarimetric effects [53]. These components could be contributions from different light paths through the optical system, due to scattering, multiple reflections, or spatial heterogeneity of the sample [53]. For polychromatic light, they could be different spectral components

that experience different polarimetric effects as a consequence of dispersion [53]. The total Stokes vector at the detector can be written

$$\mathbf{s}_{OUT} = \sum_i \rho_i \mathbf{s}_{OUT,i}$$
$$\mathbf{s}_{OUT,i} = \mathbf{M}_{J_i}\, \mathbf{s}_{IN} \quad [53].$$

where ρ_i are scalar values indicating the strength of the contribution $\mathbf{s}_{OUT,i}$, and $\mathbf{M}_{J_i}$ are non-depolarizing MMs that represent the polarimetric effects experienced by that component of the beam. Then the total output Stokes vector is related to the input Stokes vector via

$$\mathbf{s}_{OUT} = \sum_i \rho_i \mathbf{M}_{J_i} \mathbf{s}_{IN} \implies$$
$$\mathbf{M} = \sum_i \rho_i \mathbf{M}_{J_i} \quad [53]. \tag{2.42}$$

$\mathbf{M}$ defined by equation 2.42 has in general sixteen degrees of freedom, and can cause retardance, diattenuation, and polarizance in addition to depolarization. This equation defines what it means to be a MM: every valid MM is either non-depolarizing or is equal to a weighted sum of non-depolarizing MMs [42, 53], as in equation 2.42. 4×4 matrices that cannot be written in this form are not MMs at all [42, 53].

An example of a MM that contains only depolarization is the diagonal matrix

$$\mathbf{M}_\Delta = \begin{bmatrix} 1 & 0 & 0 & 0 \\ 0 & e_1 & 0 & 0 \\ 0 & 0 & e_2 & 0 \\ 0 & 0 & 0 & e_3 \end{bmatrix} \quad [83] \tag{2.43}$$
$$0 \leq e_1, e_2, e_3 \leq 1. \tag{2.44}$$

If $e_1 = e_2 = e_3 = 0$, then $\mathbf{M}_\Delta$ is a total depolarizer and always outputs unpolarized light regardless of the input polarization.

The strength of a depolarizer can be assessed using its *depolarization power* Δ:

$$\Delta = 1 - \frac{\text{trace}(\text{abs}(\mathbf{M}_\Delta)) - 1}{3} \quad [83]. \tag{2.45}$$

Δ ranges from zero for nondepolarizing MMs to one for a total depolarizer.

2.3 Polarimetry

2.3.1 Mueller Matrix-Measuring Devices

MM polarimetry (usually shortened to "polarimetry" in this thesis) is the process of measuring the MM of a sample. Once the MM is determined, it is known how the sample will transform any Stokes vector. The MM provides detailed information about the sample that can be used for testing optical elements [138], determining the dielectric tensor under some assumptions [13, 14], and improving contrast between different types of samples, including biological tissue [29, 41, 57].

The operation of a MM polarimeter is governed by the *polarimetric measurement equation*, which will be derived in this section, following the derivation by by Chipman [40]. Other approaches for calculating the MM exist (*e.g.* [29, 128, 137]) but are less general.

A MM polarimeter must be equipped with both a Polarization State Generator (PSG) and a Polarization State Analyzer (PSA). These are sequences of optical elements with the ability to modulate their polarimetric properties. One simple PSG design consists of a horizontal linear polarizer (equation 2.29 with $\mathbf{D} = [1,\, 0,\, 0]^T$) followed by a Quarter Wave Plate (QWP) (equation 2.39 with $R_L = \pi/2$) [4, 29]. The linear fast axis direction θ_G can be varied by rotating the QWP. The MMs of these two components can be multiplied together to obtain the net MM of the PSG:

$$\mathbf{M}_{PSG,i} = \frac{1}{2}\begin{bmatrix} 1 & 1 & 0 & 0 \\ \cos^2(2\theta_{G,i}) & \cos^2(2\theta_{G,i}) & 0 & 0 \\ \cos(2\theta_{G,i})\sin(2\theta_{G,i}) & \cos(2\theta_{G,i})\sin(2\theta_{G,i}) & 0 & 0 \\ \sin(2\theta_{G,i}) & \sin(2\theta_{G,i}) & 0 & 0 \end{bmatrix}.$$

The subscript i has been introduced to represent the fact that $\theta_{G,i}$ may change for each of i irradiance measurements. The same optical elements in the reverse order can be used for the PSA [29], giving

$$\mathbf{M}_{PSA,i} = \frac{1}{2}\begin{bmatrix} 1 & \cos^2(2\theta_{A,i}) & \cos(2\theta_{A,i})\sin(2\theta_{A,i}) & -\sin(2\theta_{A,i}) \\ 1 & \cos^2(2\theta_{A,i}) & \cos(2\theta_{A,i})\sin(2\theta_{A,i}) & -\sin(2\theta_{A,i}) \\ 0 & 0 & 0 & 0 \\ 0 & 0 & 0 & 0 \end{bmatrix}.$$

The PSG is situated before the sample, while the PSA is placed after the sample. The net MM of the entire polarimeter during measurement i is therefore $\mathbf{M}_{PSA,i}\,\mathbf{M}\,\mathbf{M}_{PSG,i}$,

where $\mathbf{M}$ is the MM of the sample itself. Then, the ith irradiance measurement I_i is given by

$$\begin{aligned} I_i &= c\,[1,\,0,\,0,\,0]\,\mathbf{M}_{PSA,i}\,\mathbf{M}\,\mathbf{M}_{PSG,i}\,[1,\,0,\,0,\,0]^T \\ &= c\,\mathbf{s}_{A,i}^T\,\mathbf{M}\,\mathbf{s}_{G,i} \end{aligned} \tag{2.46}$$

where, in the case of the rotating QWP design,

$$\mathbf{s}_{G,i} \equiv (1/2)\,[1,\,\cos^2(2\theta_{G,i}),\,\cos(2\theta_{G,i})\sin(2\theta_{G,i}),\,\sin(2\theta_{G,i})]^T \tag{2.47}$$

$$\mathbf{s}_{A,i} \equiv (1/2)\,[1,\,\cos^2(2\theta_{A,i}),\,\cos(2\theta_{A,i})\sin(2\theta_{A,i}),\,-\sin(2\theta_{A,i})]^T. \tag{2.48}$$

Equation 2.46 assumes that that the light generated by the source, prior to reaching the PSG, is unpolarized. Likewise, it assumes that after the PSA, the detector measures irradiance without any polarization bias. These assumptions may not be completely accurate, but it can be shown that equation 2.46 holds regardless if the first element of the PSG and the last element of the PSA are both polarizers. The scalar constant c depends on many factors such as the intensity of illumination, sensitivity of the detector, losses within the instrument, and so on. Equation 2.46 can be rewritten in the form

$$I_i = \mathbf{W}_i^T\,\vec{\mathbf{M}} \quad [40] \tag{2.49}$$

where

$$\mathbf{W}_i \equiv c(\mathbf{s}_{A,i} \otimes \mathbf{s}_{G,i}) \tag{2.50}$$

is known as the ith *measurement vector* and $\vec{\mathbf{M}}$ is the *Mueller vector* consisting of rows of

$\mathbf{M}$ stacked into a 16×1 vector; *i.e.*

$$\vec{\mathbf{M}} \equiv \begin{bmatrix} M(1,1) \\ M(1,2) \\ M(1,3) \\ M(1,4) \\ M(2,1) \\ M(2,2) \\ M(2,3) \\ M(2,4) \\ M(3,1) \\ M(3,2) \\ M(3,3) \\ M(3,4) \\ M(4,1) \\ M(4,2) \\ M(4,3) \\ M(4,4) \end{bmatrix}. \tag{2.51}$$

Equation 2.49 relates an irradiance measurement to a linear combination of Mueller matrix elements, with coefficients that are given by $\mathbf{W}_i$. If n irradiance measurements are made, these can be grouped into a single matrix equation

$$\vec{\mathbf{I}} = \mathbf{W}\,\vec{\mathbf{M}} \quad [40] \tag{2.52}$$

$$\vec{\mathbf{I}} \equiv [I_1,\ I_2,\ ...,\ I_n]^T \tag{2.53}$$

$$\mathbf{W} \equiv [\mathbf{W}_1,\ \mathbf{W}_2,\ ...,\ \mathbf{W}_n]^T. \tag{2.54}$$

$\mathbf{W}$ has dimensions $n \times 16$ and is known as the *measurement matrix*. It can be constructed if the MMs of the PSG and PSA are known for all n measurements. The constant c is not usually known, and furthermore is a dimensionful quantity with the same units as $\vec{\mathbf{I}}$. The final MM is usually normalized to remove the influence of c [53]. Equation 2.52 is the polarimetric measurement equation [40, 125] and is useful for understanding many different aspects of MM polarimetry. Primarily, it is used for the purpose of calculating the MM, by solving the equation

$$\vec{\mathbf{I}}_{EST} = \mathbf{W}\,\vec{\mathbf{M}}_{EST} \tag{2.55}$$

for $\vec{\mathbf{M}}_{EST}$ [40]. $\vec{\mathbf{I}}_{EST}$ is the estimated irradiance; it differs from the idealized irradiance $\vec{\mathbf{I}}$ due to errors in the PSG, PSA, and detector. This leads to an estimated Mueller vector

$\vec{\mathbf{M}}_{EST}$ that may differ from the true Mueller vector of the sample. Calculating $\vec{\mathbf{M}}_{EST}$ requires that $\mathbf{W}$ is invertible. If $n < 16$, then no inverse exists and there are an infinite number of possible $\vec{\mathbf{M}}_{EST}$ that can satisfy equation 2.52. If $n = 16$, then $\mathbf{W}$ is square so unless it is singular it has an inverse and a unique $\vec{\mathbf{M}}_{EST}$ can be calculated. If $n > 16$, then the system of equations is overdetermined. Due to the error in $\vec{\mathbf{I}}_{EST}$, it is very likely that the system will be inconsistent- that is, there will be no $\vec{\mathbf{M}}_{EST}$ that perfectly satisfies equation 2.55. In this case, the pseudoinverse of $\mathbf{W}$ given by

$$\mathbf{W}^{-1} = (\mathbf{W}^T \mathbf{W})^{-1} \mathbf{W}^T \tag{2.56}$$

is used in place of the regular inverse [40, 102]. The pseudoinverse has the property that the Mueller vector estimate $\vec{\mathbf{M}}_{EST} = \mathbf{W}^{-1} \vec{\mathbf{I}}_{EST} = (\mathbf{W}^T \mathbf{W})^{-1} \mathbf{W}^T \vec{\mathbf{I}}_{EST}$ minimizes the quantity

$$\|\vec{\mathbf{I}}_{EST} - \mathbf{W} \vec{\mathbf{M}}_{EST}\|_2$$

where $\|\cdot\|_2$ is the Euclidean vector norm:

$$\|\vec{\mathbf{x}}\|_2 = (\sum_{i=1}^{n} x(i)^2)^{1/2} = \vec{\mathbf{x}}^T \vec{\mathbf{x}} \tag{2.57}$$

for any $n \times 1$ vector $\vec{\mathbf{x}}$ [102].

In conclusion, at least sixteen measurements are necessary in order to fully determine the MM. Each of these measurements is described by a PSG state $\mathbf{s}_{G,i}$ and a PSA state $\mathbf{s}_{A,i}$. The PSG and the PSA each have a range of states available to it, depending on the optical elements it consists of and their modulation method. *Polarimeter optimization* (e.g. [4, 81, 125, 128, 139]) is the process of choosing the n PSG and PSA state combinations to use for the n irradiance measurements, in order to decrease the error $\mathbf{M} - \mathbf{M}_{EST}$. For a rotating QWP polarimeter design, this amounts to choosing the angles $(\theta_{G,i}, \theta_{A,i})$. Optimization guarantees firstly that $\mathbf{W}^T \mathbf{W}$ is nonsingular, allowing calculation of the pseudoinverse or inverse. Additionally, it maximizes the resilience of the polarimeter to experimental errors. This topic will be discussed in more detail in chapter 4.

2.3.2 Interpretation of Mueller Matrices

Once a MM is measured, a number of different techniques exist for calculating polarimetric properties such as diattenuation, retardance, and depolarization. These give insight into

the physical structure of the sample, and in imaging applications can provide additional contrast, such as between retinal amyloid deposits and the background retina [68].

One method of extracting these properties that is popular for the study of many materials including biological tissues (e.g. [43, 50, 101, 119]) is the Lu-Chipman decomposition [83]. This is an example of a serial decomposition [53], meaning that it interprets the sample as a sequence of discrete elements, each of which have easy to understand polarimetric properties. The Lu-Chipman decomposition writes the MM as the product of a diattenuator, a retarder, and a depolarizer:

$$\mathbf{M} = c' \, \mathbf{M}_{\Delta P} \, \mathbf{M}_R \, \mathbf{M}_D \quad [83]. \tag{2.58}$$

The scalar c' is usually ignored due to $\mathbf{M}$ being normalized. While $\mathbf{M}_{\Delta P}$ is generally referred to as a depolarizer MM, it contains both depolarization and polarizance. It has the form

$$\mathbf{M}_{\Delta P} = \begin{bmatrix} 1 & \mathbf{0}^T \\ \mathbf{P}_{\Delta P} & \mathbf{m}_{\Delta P} \end{bmatrix} \tag{2.59}$$

where $\mathbf{m}_{\Delta P}$ is a 3×3 symmetric matrix, and $\mathbf{P}_{\Delta P}$ is the *depolarizer-polarizance vector* [83].

Combining the expressions for the three component matrices 2.29, 2.37, and 2.59,

$$\begin{aligned} \mathbf{M} &= c \, \mathbf{M}_{\Delta P} \, \mathbf{M}_R \, \mathbf{M}_D \\ &= \frac{c}{1+D} \begin{bmatrix} 1 & \mathbf{D}^T \\ \mathbf{P} & \mathbf{m} \end{bmatrix} \end{aligned} \tag{2.60}$$

$$\begin{aligned} \mathbf{P} &\equiv \mathbf{P}_{\Delta P} + \mathbf{m}_{\Delta P} \, \mathbf{m}_R \, \mathbf{D} \\ \mathbf{m} &\equiv \mathbf{P}_{\Delta P} \, \mathbf{D}^T + \mathbf{m}_{\Delta P} \, \mathbf{m}_R \, \mathbf{m}_D. \end{aligned} \tag{2.61}$$

The diattenuation $\mathbf{D}$ can be read directly off the first row of $\mathbf{M}$, allowing one to calculate $\mathbf{m}_D$ using 2.29. Likewise, the $\mathbf{P}$ and $\mathbf{m}$ can be read from $\mathbf{M}$. Lu and Chipman developed an algorithm for using equations 2.61 and $\mathbf{D}$, $\mathbf{m}_D$, $\mathbf{P}$, and $\mathbf{m}$ in order to determine the remaining unknowns $\mathbf{P}_{\Delta P}$, $\mathbf{m}_{\Delta P}$, and $\mathbf{m}_R$ [83]. These components can be assembled using equations 2.29, 2.37, and 2.59 in order to obtain the matrices $\mathbf{M}_D$, $\mathbf{M}_R$, and $\mathbf{M}_{\Delta P}$ such that $\mathbf{M} = c' \, \mathbf{M}_{\Delta P} \, \mathbf{M}_R \, \mathbf{M}_D$. The retardance $\mathbf{R}$ is then calculated by applying equations 2.38 to $\mathbf{M}_R$, and the depolarization power Δ is calculated applying equation 2.45 to $\mathbf{M}_{\Delta P}$. This technique results in two different but related polarizance vectors $\mathbf{P}$ and $\mathbf{P}_{\Delta P}$.

Chapter 3

Reciprocal Invariance and *In Vivo* Retinal Polarimetry

3.1 Introduction

In *in vivo* retinal polarimetry, incident light passes through the cornea, pupil, and lens prior to reaching the retina. Light reflects at some depth in the retina before passing through those same structures in the reverse direction and reaching the detector. Some previous authors have used a *double pass model* to describe the interaction of the eye with polarized light, so called because the beam must pass twice through ocular tissue [24, 26, 64, 74, 100]. This model assigns a specific mathematical structure to the MM, namely, that it is the product (right to left) of individual MMs of the cornea, lens, and upper layers of the retina, followed by the MM of the reflection, followed by the MMs of the upper retina, lens, and cornea for light traversing in the opposite direction. To the best of the author's knowledge, this has always been combined with the assumption that each of the cornea, lens, and retina is either polarimetrically inert, acts as a linear retarder, or acts as a linear retarder times an isotropic depolarizer[1].

While the retinal amyloid deposits studied by Campbell Labs have strong linear retardance [68, 106], for future *in vivo* measurements it is preferred not to ignore their other polarimetric properties. However, it was observed that even without assuming that the retina (or retinal deposit) acts as a linear retarder, the double pass model implies a set of restrictions on the total MM. These restrictions stem from the fact that if the direction of

[1] That is, a depolarizer of the form $\mathbf{M}_{i\Delta} \equiv \mathrm{diag}(1, e, e, e)$ for $0 < e \leq 1$.

light propagation is reversed (or equivalently, if the source and detector are switched) then the beam will pass through the same structures in the same order as before. A MM that is unchanged upon reversal of the direction of light propagation is known in this thesis as *reciprocal invariant*. The purpose of this chapter is to define the double pass model and reciprocal invariance in terms of MMs, and to justify why these concepts are applicable to *in vivo* retinal polarimetry.

Section 3.2 discusses the Helmholtz reciprocity theorem, its representation using Jones and Mueller matrices, and the concept of reciprocal invariance. These concepts are not novel, but are helpful for understanding the remainder of this thesis. Section 3.3 applies them to *in vivo* retinal polarimetry. The reciprocity theorem is used to write an expression for a double pass MM in terms of the single pass MM for transmission once through ocular tissue, similar to previous work by Bueno [24]. It is observed that regardless of the form of the single pass MM, the double pass MM must be RI. In addition to the double pass model, a new ray tracing model is used to reinforce the claim that the MM measured by *in vivo* retinal polarimetry should be RI, and to identify some of the conditions necessary for this claim to be accurate. The idea that the MM should be RI, and the relationship between single and double pass polarimetry properties implied by the double pass model, are fundamental to subsequent chapters of this thesis.

3.2 The Reciprocity Theorem

The *Helmholtz reciprocity theorem* describes how an optical system behaves when the direction of light propagation through the system is reversed. The original statement of the reciprocity theorem for vector waves was given by Helmholtz in 1867 (English translation by J. P. C. Southall):

> Suppose light proceeds by any path whatever from a point A to another point B, undergoing any number of reflections or refractions en route.... Now suppose that a certain amount of light J leaving the point A in the given direction is polarised in the plane a_1, and that of this light the amount K arrives at the point B polarised in the plane b_1; then it can be proved that, when the light returns over the same path, and the quantity of light J polarised in the plane b_1 proceeds from the point B, the amount of this light that arrives at the point A polarised in the plane a_1 will be equal to K.
>
> Apparently the above proposition is true no matter what happens to the light in the way of single or double refraction, reflection, absorption, ordinary dis-

> persion, and diffraction, provided there is no change of its refrangibility, and provided it does not traverse any magnetic medium that affects the position of the plane of polarisation, as Faraday found to be the case. [134]

As an example, imagine that between points A and B there is a slab of an isotropic, absorbing material. The reciprocity theorem states that light will be attenuated by an equal amount if it travels from A to B as if it travels from B to A. Note that the reciprocity theorem is different from the concept of *time reversal* [6, 104]: the time reversed wave travelling from B to A would be amplified, not absorbed, which is unphysical. When the polarization state changes between A and B, the behaviour implied by the reciprocity theorem is more complicated. Later in this section, it will be seen that the reciprocity theorem leads to a relationship between the Jones and Mueller matrices for propagation from A to B and those for propagation from B to A.

Helmholtz stated his theorem without giving any proof[2] [134]. A less general reciprocity theorem has been shown rigorously in scattering theory by Saxon [114] and de Hoop [44], and appears in light scattering textbooks (*e.g.* [46, 76]). To summarize their result, suppose that there is an object embedded in an otherwise uniform, isotropic, nonabsorbing medium. A plane wave propagating through the medium will be disturbed or *scattered* by the object or scatterer. It can be shown that far enough away from the scatterer, the total wave is given by the sum of the original plane wave with a spherical wave emitting from the scatterer [66, 76]. Let A and B be two points that are both a large distance R from the scatterer. Let $\mathbf{E}_A$ be a plane wave of arbitrary polarization that approaches the scatterer from the direction of point A, evaluated at point A. Let $\mathbf{E}_B$ be the resulting scattered spherical wave evaluated at point B. Likewise, let $\mathbf{E}'_B$ be a plane wave of arbitrary polarization that approaches the scatterer from the direction of point B evaluated at point B, and $\mathbf{E}'_A$ be the resulting scattered spherical wave evaluated at point A. Saxon [114] and de Hoop [44] use Maxwell's equations to derive

$$\mathbf{E}_A \cdot \mathbf{E}'_A = \mathbf{E}_B \cdot \mathbf{E}'_B. \tag{3.1}$$

Equation 3.1 is a mathematical statement of Helmholtz's reciprocity theorem, with the following modifications: equation 3.1 implies also that the phase accumulated for the trip from A to B is the same as that for the trip from B to A, it allows the incident plane waves to be elliptically polarized, and it is so far restricted to single scattering. The proof of

[2] In fact, he claimed that "anybody who is at all familiar with the laws of optics can easily prove it for himself" [134]. Proofs that the author has found (*e.g.* [54, 114]) seem fairly involved and are less general than Helmholtz's original statement, so it is unclear what proof Helmholtz had in mind.

equation 3.1 requires several assumptions about the constitutive relations of the scatterer (see section 2.2) [76, 114]. These assumptions apply to the linear isotropic, anisotropic, and chiral materials described in section 2.2 [41]. They fail for nonlinear materials and gyrotropic materials in the presence of an external magnetic field [41, 44]. It will be assumed in this thesis that matter in the eye obeys the necessary conditions.

Next, equation 3.1 can be written in terms of Jones matrices. The result is well known [53, 131, 116], but the details of the derivation are provided here in order to make explicit the coordinate system choices involved. $\mathbf{E}_A$ is a plane wave travelling in the $\hat{\mathbf{k}}$ direction, where $\hat{\mathbf{k}}$ is a unit vector pointing from point A towards the scatterer. Let $(\hat{\mathbf{t}}_1, \hat{\mathbf{t}}_2, \hat{\mathbf{k}})$ be a righthanded orthonormal set of unit vectors, so that one can write[3] $\mathbf{E}_A = E_{A,\hat{\mathbf{t_1}}}\hat{\mathbf{t}}_1 + E_{A,\hat{\mathbf{t}}_2}\hat{\mathbf{t}}_2$, and express its polarization state using the Jones vector

$$\mathbf{j}_A = \begin{bmatrix} E_{A,\hat{\mathbf{t_1}}} \\ E_{A,\hat{\mathbf{t_2}}} \end{bmatrix}.$$

At point A, the spherical wave $\mathbf{E}'_A$ is approximated by a plane wave traveling in the $-\hat{\mathbf{k}}$ direction. If one wishes to always write Jones vectors in terms of right handed coordinate systems, it is necessary to write $\mathbf{E}'_A$ in terms of a different basis than $\mathbf{E}_A$. A convenient choice is to use $(\hat{\mathbf{t}}_1, -\hat{\mathbf{t}}_2, -\hat{\mathbf{k}})$. Then $\mathbf{E}'_A$ can be written in terms of the components $\mathbf{E}'_A = E'_{A,\hat{\mathbf{t_1}}}\hat{\mathbf{t}}_1 + E'_{A,-\hat{\mathbf{t}}_2}(-\hat{\mathbf{t}}_2)$. The Jones vector of $\mathbf{E}'_A$ with respect to this basis is

$$\mathbf{j}'_A = \begin{bmatrix} E'_{A,\hat{\mathbf{t_1}}} \\ E'_{A,-\hat{\mathbf{t_2}}} \end{bmatrix}.$$

Using these Jones vectors, the left side of equation 3.1 can be rewritten as

$$\begin{aligned} \mathbf{E}_A \cdot \mathbf{E}'_A &= (E_{A,\hat{\mathbf{t_1}}}\hat{\mathbf{t}}_1 + E_{A,\hat{\mathbf{t}}_2}\hat{\mathbf{t}}_2) \cdot (E'_{A,\hat{\mathbf{t_1}}}\hat{\mathbf{t}}_1 + E'_{A,-\hat{\mathbf{t}}_2}(-\hat{\mathbf{t}}_2)) \\ &= E_{A,\hat{\mathbf{t_1}}}\, E'_{A,\hat{\mathbf{t_1}}} - E_{A,\hat{\mathbf{t}}_2}\, E'_{A,-\hat{\mathbf{t}}_2} \\ &= \begin{bmatrix} E_{A,\hat{\mathbf{t}}_1} & E_{A,\hat{\mathbf{t}}_2} \end{bmatrix} \begin{bmatrix} E'_{A,\hat{\mathbf{t}}_1} \\ -E'_{A,-\hat{\mathbf{t}}_2} \end{bmatrix} \\ &= \mathbf{j}_A^T \begin{bmatrix} 1 & 0 \\ 0 & -1 \end{bmatrix} \mathbf{j}'_A. \end{aligned} \tag{3.2}$$

[3] A time dependent phase term $e^{i(kR-\omega t)}$ has been dropped for simplicity, because these terms cancel from equation 3.1.

The same coordinate convention can be applied at point B to describe the plane wave $\mathbf{E}'_B$ and the spherical wave $\mathbf{E}_B$, resulting in the equation

$$\mathbf{E}_B \cdot \mathbf{E}'_B = \mathbf{j}_B^T \begin{bmatrix} 1 & 0 \\ 0 & -1 \end{bmatrix} \mathbf{j}'_B. \tag{3.3}$$

Finally, because the scatterer is linear, incident and scattered Jones vectors can be related to one another using Jones matrices:

$$\mathbf{j}_B = \mathbf{J}_{A\to B}\, \mathbf{j}_A \tag{3.4}$$
$$\mathbf{j}'_A = \mathbf{J}_{B\to A}\, \mathbf{j}'_B. \tag{3.5}$$

$\mathbf{J}_{A\to B}$ and $\mathbf{J}_{B\to A}$ depend on the makeup and orientation of the scatterer, as well as the relative positions of A and B. They could have any amounts of retardance and diattenuation, but it will be shown that they must be related to each other in a specific way. Assembling equations 3.1, 3.2, 3.3, 3.4, and 3.5,

$$\mathbf{j}_A^T \begin{bmatrix} 1 & 0 \\ 0 & -1 \end{bmatrix} \mathbf{J}_{B\to A}\, \mathbf{j}'_B = \mathbf{j}_A^T\, \mathbf{J}_{A\to B}^T \begin{bmatrix} 1 & 0 \\ 0 & -1 \end{bmatrix} \mathbf{j}'_B. \tag{3.6}$$

The polarization states of the two plane waves are arbitrary, so equation 3.6 holds for any combination of complex vectors $\mathbf{j}_A$ and $\mathbf{j}'_B$. Therefore, it follows that

$$\begin{bmatrix} 1 & 0 \\ 0 & -1 \end{bmatrix} \mathbf{J}_{B\to A} = \mathbf{J}_{A\to B}^T \begin{bmatrix} 1 & 0 \\ 0 & -1 \end{bmatrix}$$
$$\mathbf{J}_{B\to A} = \begin{bmatrix} 1 & 0 \\ 0 & -1 \end{bmatrix} \mathbf{J}_{A\to B}^T \begin{bmatrix} 1 & 0 \\ 0 & -1 \end{bmatrix}. \tag{3.7}$$

The final result 3.7 is the reciprocity theorem for Jones matrices [53, 116, 131]. It can be extended to non-depolarizing MMs using equation 2.28, resulting in

$$\mathbf{M}_{J,B\to A} = \mathbf{X}\mathbf{M}_{J,A\to B}^T\mathbf{X} \tag{3.8}$$
$$\mathbf{X} \equiv \begin{bmatrix} 1 & 0 & 0 & 0 \\ 0 & 1 & 0 & 0 \\ 0 & 0 & -1 & 0 \\ 0 & 0 & 0 & 1 \end{bmatrix} \quad [53,\ 115,\ 116]. \tag{3.9}$$

Equations 3.7 and 3.8 depend on the convention used to represent Jones vectors of waves travelling in opposite directions. If a wave travelling in the $\hat{\mathbf{k}}$ direction uses the basis

$(\hat{\mathbf{t}}_1, \hat{\mathbf{t}}_2, \hat{\mathbf{k}})$, then it was chosen to use $(\hat{\mathbf{t}}_1, -\hat{\mathbf{t}}_2, -\hat{\mathbf{k}})$ for a wave travelling in the $-\hat{\mathbf{k}}$ direction. It can be shown that the choice $(-\hat{\mathbf{t}}_1, \hat{\mathbf{t}}_2, -\hat{\mathbf{k}})$ leads to the same Mueller reciprocity equation 3.8. Another option is to use the *left*-handed basis $(\hat{\mathbf{t}}_1, \hat{\mathbf{t}}_2, -\hat{\mathbf{k}})$ for the second wave, representing both waves using the same coordinate frame. This leads to a different form of the Jones and Mueller reciprocity equations, used by some authors:

$$\begin{aligned} \mathbf{J}_{B\to A} &= \mathbf{J}^T_{A\to B} \quad [69,\ 132] \\ \mathbf{M}_{J,B\to A} &= \mathbf{Q}\mathbf{M}^T_{J,A\to B}\mathbf{Q} \quad [24] \\ \mathbf{Q} &\equiv \begin{bmatrix} 1 & 0 & 0 & 0 \\ 0 & 1 & 0 & 0 \\ 0 & 0 & 1 & 0 \\ 0 & 0 & 0 & -1 \end{bmatrix}. \end{aligned} \tag{3.10}$$

The difference in coordinate system choices has no impact of the physical meaning of reciprocity, but can be a source of confusion. This topic is discussed further in Appendix C.

Equations 3.7 and 3.8 are commonly used in situations other than single scattering (*e.g.* [15, 24, 20, 65, 104]). Schönhofer and Kuball have derived equation 3.8 directly using the language of quantum mechanics, with minimal assumptions about the optical system [115]. As well, many types of light-matter interactions can be described using the coherent sum, incoherent sum, or product of single scattering matrices. Accordingly, Greffet and Nieto-Vesperinas have proven the reciprocity theorem for reflections from flat surfaces [54]. Chandrasekhar has shown the reciprocity of diffuse reflections and transmission [36]. For a wave that propagates from A to B through an optical system while experiencing any sequence of reflection, transmission, or scattering, the total MM is the product of individual MMs representing each process. By applying the reciprocity theorem to each MM in the product, the MM for propagation from B to A is

$$\mathbf{M}_{B\to A} = \mathbf{X}\,\mathbf{M}^T_{A\to B}\,\mathbf{X}. \tag{3.11}$$

Likewise, as described in section 2.2.3, any MM is the weighted sum of nondepolarizing MMs. Applying 3.11 to each of these component matrices, it follows that 3.11 holds true for all MMs, even those that contain depolarization [53].

These reciprocity equations describe how the Jones or Mueller matrix changes when the direction of light propagation is reversed, which will be referred to as *motion reversal*. Equivalently, if the MM is measured using a source at point A and a detector at point B, they allow one to calculate the MM that would be measured if the locations of the source and the detector were switched. Some optical systems are symmetric upon motion

reversal. This is the case if the system is symmetric upon reflection through the plane that bisects the line between A and B [131]. It follows that for such a system,

$$\begin{aligned} \mathbf{M}_{B\to A} &= \mathbf{M}_{A\to B} = \mathbf{M} \\ \mathbf{M} &= \mathbf{X}\,\mathbf{M}^T\,\mathbf{X} \quad [41,\ 131,\ 118]. \end{aligned} \tag{3.12}$$

MMs that obey equation 3.12 will be referred to in this thesis as *reciprocal invariant*[4] (RI). Unlike time reversal symmetry, this does not preclude the existence of absorption in $\mathbf{M}$. It states that a wave generated at A and detected at B will experience the same MM as a wave generated at B and detected at A[5]. The simplest example of this is when point A and B coincide, and the output light returns along the same path as the incident light. The MM in this case is known as a *backscattering* MM [41, 91, 118].

Equation 3.12 is equivalent to six linear relationships between the off diagonal elements of $\mathbf{M}$:

$$\begin{aligned} 0 &= M(2,1) - M(1,2) \\ 0 &= M(3,1) + M(1,3) \\ 0 &= M(4,1) - M(1,4) \\ 0 &= M(3,2) + M(2,3) \\ 0 &= M(4,2) - M(2,4) \\ 0 &= M(4,3) + M(3,4) \end{aligned} \tag{3.13}$$

Suppose $\mathbf{M}$ is written as the sum of non-depolarizing component MMs (perhaps representing different paths through the system, multiple scattering, *etc.*). If each of these components individually satisfies equation 3.12, then it can be shown that the total MM will obey not only the six restrictions 3.13, but also the *trace condition*

$$0 = M(1,1) - M(2,2) + M(3,3) - M(4,4) \quad [41,\ 91]. \tag{3.14}$$

MMs that obey only equations 3.13 will be called *ten parameter RI MMs*, while those that also obey equation 3.14 will be called *nine parameter RI MMs*. Many of the results in this thesis apply to both types, and in these contexts "RI MM" will be used without specifying nine or ten parameter.

[4] To clarify this terminology, an optical system for which any MM and its motion reversed version are related by equation 3.11 is known as *reciprocal* [76]. A MM that is equal to its motion reversed version, and for which the optical system is reciprocal, is reciprocal invariant.

[5] Time reversal symmetry would instead state that the two are inverses, which is impossible if the medium is absorbing, or when the energy of the incident wave is split into more than one output wave.

3.3 Modelling *In Vivo* Retinal Polarimetry

The reciprocity theorem and the concept of reciprocal invariance are useful for modelling *in vivo* retinal polarimetry. It will be assumed that the instrument used for this is a Confocal Scanning Laser Opthalmoscope (cSLO) [136] equipped with a PSG and PSA (*e.g.* [29]). In this imaging modality, light of a known polarization state is focused by the optics of the eye onto a finite spot on the retina. This light is reflected, scattered, or absorbed by structures within the eye. Some of it exits through the pupil, passes through the PSA and reaches the detector. In order to reduce the amount of multiply scattered light, the detector only accepts light that originated from a small part of the retina, which should overlap with the illumination spot [136]. Then both the illumination spot and the detected spot are scanned over the retina in order to generate a 2D image. This process is then repeated with different PSG and PSA configurations, until enough images have been collected to calculate a pixel-by-pixel MM for each point on the retina.

The double pass model is based on the observation that the beam transmits through the cornea, lens, and the upper layers of the retina, before reflecting and passing through the same layers of the retina, the lens, and the cornea in the opposite direction. It is assumed either that the input and output cones of light coincide in space, or that polarimetric properties of the ocular tissue vary slowly enough spatially that any difference between the two can be ignored. The total MM is then assumed to be the product of MMs representing each of these stages, resulting in

$$\begin{aligned}\mathbf{M} &= \mathbf{X}\,\mathbf{M}_{SP}^{T}\,\mathbf{X}\,\mathbf{M}_{ref}\,\mathbf{M}_{SP} \\ \mathbf{M}_{SP} &\equiv \mathbf{M}_{retina}\,\mathbf{M}_{lens}\,\mathbf{M}_{cornea}.\end{aligned}$$

The reciprocity theorem has been used to write the MM of the second pass through ocular structures on the way out of the eye. This sort of model has been used commonly in *in vivo* retinal polarimetry [24, 26, 64, 74, 100]. However, to the author's knowledge, it has always been used in conjunction with additional assumptions about the polarimetric properties of the retina. In the present analysis, $\mathbf{M}_{SP}$ is instead permitted to be any MM. Following these previous authors (*i.e.* [24, 26, 64, 74, 100]), assume that the reflection matrix $\mathbf{M}_{ref}$ acts as a perfect reflector, which in the current coordinate system conventions is given by

$$\mathbf{M}_{ref} = \mathbf{Y} \equiv \begin{bmatrix} 1 & 0 & 0 & 0 \\ 0 & 1 & 0 & 0 \\ 0 & 0 & -1 & 0 \\ 0 & 0 & 0 & -1 \end{bmatrix} \quad [39,\ 53]. \tag{3.15}$$

Using this expression,

$$\mathbf{M} = \mathbf{X}\,\mathbf{M}_{SP}^{T}\,\mathbf{X}\,\mathbf{Y}\,\mathbf{M}_{SP}. \tag{3.16}$$

Equation 3.16 is the *double pass model*. Observe that

$$\begin{aligned}\mathbf{X}\,\mathbf{M}^{T}\,\mathbf{X} &= \mathbf{X}\,(\mathbf{X}\,\mathbf{M}_{SP}^{T}\,\mathbf{X}\,\mathbf{Y}\,\mathbf{M}_{SP})^{T}\,\mathbf{X} \\ &= \mathbf{X}\,\mathbf{M}_{SP}^{T}\,\mathbf{Y}^{T}\,\mathbf{X}^{T}\,\mathbf{M}_{SP}\,\mathbf{X}^{T}\,\mathbf{X} \\ &= \mathbf{X}\,\mathbf{M}_{SP}^{T}\,\mathbf{X}\,\mathbf{Y}\,\mathbf{M}_{SP} = \mathbf{M}.\end{aligned}$$

Therefore, the double pass model implies that[6] $\mathbf{M} = \mathbf{X}\,\mathbf{M}^{T}\,\mathbf{X}$ is ten parameter RI (it does not guarantee that $\mathbf{M}$ obeys the trace condition 3.14, so $\mathbf{M}$ may or may not be nine parameter RI). This result is due to the fact that the double pass model has motion-reversal symmetry: it was assumed that the input and output beams traverse identical tissue, therefore they can be switched without changing the MM.

The same result can be obtained by modelling the total irradiance at the detector as the sum (coherent or incoherent) of a finite number of individual rays that have returned from the eye. Each ray is assumed to have a well-defined Jones vector that is transformed as it traverses different optical elements and ocular structures. This technique is inspired by the polarization ray tracing that has been used to study polarization aberrations of optical systems [37, 38, 90], as well as backscattering from large particles [20]. It also bears similarity to a much more detailed model used by Huang and Knighton [63] to examine scattering from the RNFL. The current section ignores important effects such as diffraction and the optical aberrations of the human eye [47, 103]. Despite these shortcomings, this polarization ray tracing approach provides a useful picture of how reciprocal invariance may manifest in *in vivo* retinal polarimetry, complementary to the double pass model.

Figure 3.1 shows a schematic of the human eye, illuminated by the cSLO at a fixed scanning position. The central ray in the diagram is exactly backscattered, returning along exactly the same path as it came down. However another ray path is shown, which approaches the retina in the direction $\hat{\mathbf{n}}$, is scattered or reflected in the retina at position $\mathbf{x}$, and travels away from the retina in the direction $-\hat{\mathbf{n}}'$. The example ray is singly scattered, but the arguments presented in this section apply to multiple scattering as well. Even for a fixed scanning position there are a collection of nearby locations $\mathbf{x}$ that contribute

[6] Note that the exact expression depends on the relationship between the coordinates used to express the input and output Stokes vectors, as discussed in the previous section. If the same coordinates are used for both input and output Stokes vectors, then the double pass model has the form $\mathbf{M} = \mathbf{Q}\,\mathbf{M}_{SP}^{T}\,\mathbf{Q}\,\mathbf{M}_{SP}$. This is the expression used by Bueno [24]. This version of the double pass model implies that $\mathbf{M} = \mathbf{Q}\,\mathbf{M}^{T}\,\mathbf{Q}$.

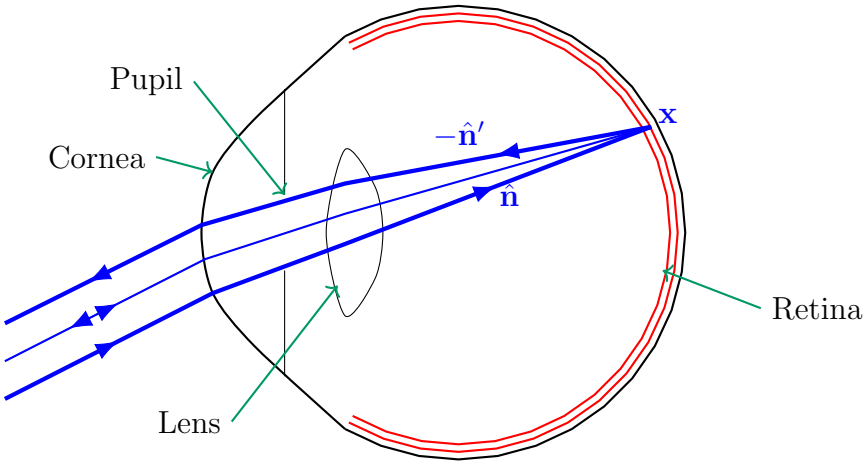

Figure 3.1: The human eye and a possible ray path for an *in vivo* retinal polarimetry experiment.

to the measurement. The directions $\hat{\mathbf{n}}$ and $-\hat{\mathbf{n}}'$ are not necessarily related by the law of reflection, and for a fixed $\hat{\mathbf{n}}$ and $\mathbf{x}$ there are permitted to be many different output rays that represent the field scattered in all directions. For example, there is also a ray that approaches the retina in the $\hat{\mathbf{n}}$ direction but returns along the central ray path. The Jones vector associated with each ray is transformed as it transmits through different structures in the eye, and scatters at the location $\mathbf{x}$. This can be represented by a Jones matrix[7] $\mathbf{J}(-\hat{\mathbf{n}}', \mathbf{x}, \hat{\mathbf{n}})$. This Jones matrix accounts for the polarimetric effects on the ray of transmitting through the cornea, lens, and upper retina, as well as scattering at $\mathbf{x}$. The scalar amplitude and phase of this matrix are important- for example, if the retina only scatters a small amount of light in the $-\hat{\mathbf{n}}'$ direction, the associated Jones matrix will have small entries. It is assumed that prior to entering the eye, each ray has the same Jones vector $\mathbf{j}_{in}$ up to a scalar multiplier. Label this scalar multiplier as $a_G(\mathbf{x}, \hat{\mathbf{n}})$ which specifies the amplitude of the input ray segment uniquely defined by coordinates $(\mathbf{x}, \hat{\mathbf{n}})$, prior to it entering the eye. This function accounts for the size of the entrance pupil and any variations in amplitude across the entrance pupil. Additionally, introduce the function $a_A(-\hat{\mathbf{n}}', \mathbf{x})$, which represents the sensitivity of the detector to the output ray segment uniquely defined by $(-\hat{\mathbf{n}}', \mathbf{x})$. This function accounts for the size of the exit pupil, the size and angular acceptance of the detector, and any variation in detector response for off-axis rays.

[7]Multiply scattered rays could be notated as $\mathbf{J}(-\hat{\mathbf{n}}', \mathbf{x}_n, ..., \mathbf{x}_0\, \hat{\mathbf{n}})$ for any number of scattering locations $\mathbf{x}_0, ..., \mathbf{x}_n$. The argument in the following paragraph applies to these paths but single scattering is used as the example for simplicity.

The effective Jones vector at the PSA due to any individual ray is equal to

$$\mathbf{j}_{out}(-\hat{\mathbf{n}}',\, \mathbf{x},\, \hat{\mathbf{n}}) = a_G(\mathbf{x},\, \hat{\mathbf{n}})\, a_A(-\hat{\mathbf{n}}',\, \mathbf{x})\, \mathbf{J}(-\hat{\mathbf{n}}',\, \mathbf{x},\, \hat{\mathbf{n}})\, \mathbf{j}_{in}.$$

Consider the sum of this ray with the ray that travels in the opposite path, approaching the retina in the $\hat{\mathbf{n}}'$ direction and leaving it in the $-\hat{\mathbf{n}}$ direction. The Jones matrix experienced by this ray can be related to the Jones matrix of the original ray using the reciprocity theorem 3.7:

$$\mathbf{J}(-\hat{\mathbf{n}},\, \mathbf{x},\, \hat{\mathbf{n}}') = \begin{bmatrix} 1 & 0 \\ 0 & -1 \end{bmatrix} \mathbf{J}(-\hat{\mathbf{n}}',\, \mathbf{x},\, \hat{\mathbf{n}})^T \begin{bmatrix} 1 & 0 \\ 0 & -1 \end{bmatrix}.$$

Under the current approximations, it will be shown that the total MM is RI if the instrument measures each ray and its opposite ray with equal sensitivity. This requirement can be expressed mathematically as $a_A(-\hat{\mathbf{n}},\, \mathbf{x}) = a_G(\mathbf{x},\, \hat{\mathbf{n}})$. This assumption requires symmetry between the illumination and detection branches of the instrument. It implies that the entrance and exit pupils are equal, and also that if there is nonuniform illumination over the entrance pupil, then the rays passing through the exit pupil are also detected with a matching nonuniform sensitivity.

A ray and its opposite have identical total path length, and so are expected to add coherently. Then the sum of their Jones vectors at the PSA is given by

$$\begin{aligned} \mathbf{j}_{out}(\hat{\mathbf{n}} \leftrightarrow \hat{\mathbf{n}}', \mathbf{x}) &\equiv \mathbf{j}_{out}(-\hat{\mathbf{n}}',\, \mathbf{x},\, \hat{\mathbf{n}}) + \mathbf{j}_{out}(-\hat{\mathbf{n}},\, \mathbf{x},\, \hat{\mathbf{n}}') \\ &= \Big(a_G(\mathbf{x},\, \hat{\mathbf{n}})\, a_A(-\hat{\mathbf{n}}',\, \mathbf{x})\, \mathbf{J}(-\hat{\mathbf{n}}',\, \mathbf{x},\, \hat{\mathbf{n}}) + \ldots \\ &\qquad a_G(\mathbf{x},\, \hat{\mathbf{n}}')\, a_A(-\hat{\mathbf{n}},\, \mathbf{x})\, \mathbf{J}(-\hat{\mathbf{n}},\, \mathbf{x},\, \hat{\mathbf{n}}') \Big)\, \mathbf{j}_{in}. \end{aligned} \tag{3.17}$$

Using the assumption of the last paragraph, $a_G(\mathbf{x},\, \hat{\mathbf{n}})\, a_A(-\hat{\mathbf{n}}',\, \mathbf{x}) = a_G(\mathbf{x},\, \hat{\mathbf{n}}')\, a_A(-\hat{\mathbf{n}},\, \mathbf{x})$. From equation 3.17, it can be seen that the two Jones vectors $\mathbf{j}_{in}$ and $\mathbf{j}_{out}(\hat{\mathbf{n}} \leftrightarrow \hat{\mathbf{n}}', \mathbf{x})$ are related through the Jones matrix

$$\mathbf{J}(\hat{\mathbf{n}} \leftrightarrow \hat{\mathbf{n}}', \mathbf{x}) \equiv a_G(\mathbf{x}, \hat{\mathbf{n}})\, a_A(-\hat{\mathbf{n}}', \mathbf{x}) \Big(\mathbf{J}(-\hat{\mathbf{n}}', \mathbf{x}, \hat{\mathbf{n}}) + \begin{bmatrix} 1 & 0 \\ 0 & -1 \end{bmatrix} \mathbf{J}(-\hat{\mathbf{n}}', \mathbf{x}, \hat{\mathbf{n}})^T \begin{bmatrix} 1 & 0 \\ 0 & -1 \end{bmatrix} \Big).$$

It can be observed that

$$\mathbf{J}(\hat{\mathbf{n}} \leftrightarrow \hat{\mathbf{n}}', \mathbf{x}) = \begin{bmatrix} 1 & 0 \\ 0 & -1 \end{bmatrix} \mathbf{J}(\hat{\mathbf{n}} \leftrightarrow \hat{\mathbf{n}}', \mathbf{x})^T \begin{bmatrix} 1 & 0 \\ 0 & -1 \end{bmatrix}.$$

This shows that $\mathbf{J}(\hat{\mathbf{n}} \leftrightarrow \hat{\mathbf{n}}', \mathbf{x})$ is an RI Jones matrix, that is, the non-depolarizing MM calculated from $\mathbf{J}(\hat{\mathbf{n}} \leftrightarrow \hat{\mathbf{n}}', \mathbf{x})$ using equation 2.28 is RI. It was implicitly assumed that

$\hat{\mathbf{n}} \neq \hat{\mathbf{n}}'$, because otherwise equation 3.17 is double counting the same ray. However, rays for which $\hat{\mathbf{n}} = \hat{\mathbf{n}}'$ are exactly backscattered rays and so are also described by RI Jones matrices.

At the detector, some rays are expected to add coherently, such as those due to single scattering from the same location $\mathbf{x}$, or multiple scattering paths of the same path length. This means that they add as Jones vectors. The Jones matrix relating $\mathbf{j}_{in}$ to the total Jones vector for such a collection of rays is the sum of the effective Jones matrices for each ray [53]. This sum can be grouped into backscattering rays for which $\hat{\mathbf{n}} = \hat{\mathbf{n}}'$, which are RI, and path plus opposite path pairs, which are together also RI as found in the previous paragraph. Therefore, the total Jones matrix for that collection of rays is the sum of RI Jones matrices and it follows that it must be RI itself. This Jones matrix can then be written as a RI MM using equation 2.28.

These collections of rays will be then assumed to add incoherently with one another, such as single scattering from different locations and multiple scattering paths of different path lengths. Therefore, they add rather as Stokes vectors. The MM relating $\mathbf{s}_{in}$ to the total Stokes vector is the sum of the MMs for each Stokes vector in the sum. These individual MMs are all non-depolarizing and RI, because each is associated with a single RI Jones matrix. It follows that the total MM, which may be depolarizing, is also RI. Unlike the double pass model 3.16, this model also implies that the MM should obey the trace condition 3.14 because every component non-depolarizing MM is RI (see section 3.2). Future chapters will therefore consider both the possibilities that the MM does or does not obey the trace condition.

The reciprocal invariance of the MM in this ray tracing model is the result not only of the presence of backscattered rays that return exactly along their incident path, but also of the balance between every non-backscattered ray and its opposite path ray. It was required to assume that the illumination and detection branches of the instrument are symmetric, or mathematically speaking $a_A(-\hat{\mathbf{n}}, \mathbf{x}) = a_G(\mathbf{x}, \hat{\mathbf{n}})$. Additionally, it was assumed that the rays could be grouped into collections of rays that were completely mutually coherent (adding as Jones matrices), and completely incoherent with all other rays outside the group (adding as MMs). This is an approximation, and describing complicated partial coherence behaviour is beyond the scope of this thesis. Lastly, this polarization ray tracing approach is also of limited validity, especially within the eye where the effects of diffraction are significant [47]. However, it shows some of the conditions under which the total MM from *in vivo* retinal polarimetry is RI.

Past experimental *in vivo* retinal polarimetry measurements were examined to see if the resulting MM was RI as predicted by the current section. For many publications

this was impossible to tell because of assumptions made in that paper about the MM (*e.g.* [34, 48, 142], or because not enough of the MM was included in the paper (*e.g.* [26, 33, 31, 28, 49, 72, 100]). Bueno has reported a numerical 3×3 MM submatrix measured using a partial *in vivo* retinal polarimeter [25]. The result is consistent within the reported errors with $\mathbf{M} = \mathbf{Q}\,\mathbf{M}^T\,\mathbf{Q}$, which is the expression for reciprocal invariance if the input and output Stokes vectors are represented in the same coordinate system. Note that a MM obeying $\mathbf{M} = \mathbf{Q}\,\mathbf{M}^T\,\mathbf{Q}$ has the general form

$$\mathbf{M} = \begin{bmatrix} M(1,1) & M(1,2) & M(1,3) & M(1,4) \\ M(1,2) & M(2,2) & M(2,3) & M(2,4) \\ M(1,3) & M(2,3) & M(3,3) & M(3,4) \\ -M(1,4) & -M(2,4) & -M(3,4) & M(4,4) \end{bmatrix}.$$

Bueno [21, 22, 23] and Bueno and Artal [27] have published sets of sixteen MM images of the eye. The instrument used in each paper did not scan the incident beam, but instead had a CCD camera array that captured an image for a fixed beam location. This design may have less symmetry between the illumination and detection branches of the instrument than the scanning design modelled in this section. While it is difficult to tell from MM images, their results seem to be approximately RI with $\mathbf{M} = \mathbf{Q}\,\mathbf{M}^T\,\mathbf{Q}$. However a noticeable deviation from reciprocal invariance can be observed in the $M(4,1)$ element, which is not similar to $-M(1,4)$. Bueno noted that the results from this instrument were not "totally symmetric", by which it was meant that $M(i,j)^2 \neq M(j,i)^2$ [23]. Lastly, Twietmeyer [127] and Twietmeyer *et al.* [126] have also published full sets of sixteen MM images, measured using a scanning *in vivo* retinal polarimeter. Several off-diagonal elements show the expected RI relationships, but others, specifically $M(4,1)$ and $M(3,2)$, do not.

There could be several reasons for the disagreement between these published MMs and the prediction of reciprocal invariance. One possibility is the presence of experimental errors, which may obscure the underlying RI behaviour of the MM. More likely however is that the discrepancies are due to a lack of symmetry between the illumination and detection branches of these instruments, leading to non-RI components of the measured MM. For a future *in vivo* retinal polarimeter for detecting amyloid deposits, it may be beneficial to maximize this symmetry so that the MM is more exactly RI. The advantages of this are that it allows the MM to be calculated from a reduced number of measurements, as will be explained in chapter 4. As well, it means that the MM can be interpreted through the lens of the double pass model, which will be explored in chapter 5. Future work should test this idea experimentally to confirm if it is beneficial for the purpose of identifying retinal amyloid deposits.

3.4 Conclusion

This chapter has introduced and explained two important ideas about the mathematical structure of the MM that is measured in *in vivo* retinal polarimetry. The first is that the MM should be RI, obeying a set of linear relationships between MM elements. As will be seen in Chapter 4, this has major implications for how to most efficiently measure these MMs. The second is the double pass model, which relates the MM to the single pass MM for transmission through the structures of the eye. This idea aids in the interpretation of the MM, and is the baseline for the discussions of Chapter 5.

Chapter 4

Measurement of Reciprocal Invariant Mueller Matrices

4.1 Introduction

As described in section 2.3.1, determining a general MM requires at least sixteen independent irradiance measurements [40]. In a real polarimeter, these are subject to experimental error. The way in which error propagates into the final MM estimate strongly depends on the choice of PSG and PSA states for each measurement [125]. Polarimeter optimization (e.g. [4, 81, 120, 125, 129, 133, 139]), is the process of choosing which PSG and PSA states to use, usually on the basis of making the estimated MM more resistant to error. Error performance can be further improved by increasing the number of measurements [120, 125], but this increases the total time required to determine the MM.

Partial MM polarimeters are those that cannot determine a general MM [40, 112, 130]. These may provide enough information to completely determine some polarimetry properties of the sample, or to determine the entire MM if it is assumed to have a particular form [25, 40, 73, 82, 113]. Partial MM polarimeters may have simpler PSG and PSA designs than full MM polarimeters, and/or use fewer than sixteen total measurements [25, 112, 130]. Additionally, if the form of the MM is well known, restricting the measured MM to fit that form may remove deviations due to error.

For *in vivo* retinal polarimetry, speed is a priority in order to reduce discomfort for the patient as well as disruptions such as blinks, involuntary eye movements [88], and tear film drying [62]. Based on section 3.3, this chapter proposes novel partial polarimeter designs

that utilize the assumption of reciprocal invariance[1] in order to determine all sixteen MM elements from as few as nine or ten measurements.

To accomplish this, the first objective is to efficiently solve the linear system of equations consisting of the RI symmetry restrictions 3.13 (and possibly 3.14) combined with the polarimetric measurement equation 2.52. This problem has been considered for nine parameter RI MMs by Arteaga and Ossikovski [9, 96]. Their approach assumes a polarimeter that completely determines either nine [96] or twelve [9] MM elements. Tyo *et al.* state that symmetry restrictions on an MM (such as equations 3.13) can be treated in the same way as additional measurements [130], however it is shown in section 4.2 that this can lead to a non-RI MM estimate if the system is overdetermined. In section 4.2, a method is demonstrated that allows for the calculation of the MM using any number of measurements (over the minimum of nine or ten) and any kind of polarimeter. Late in the development of this thesis, it was observed that an equivalent method has been used before by Hayman *et al.* for polarimetric lidar [55].

The second objective is to decide which PSG and PSA states to use for measuring RI MMs. Section 4.3 shows derivations for polarimeter optimization metrics used for full polarimeters, based especially on the work of Twietmeyer and Chipman [125] and Zallat *et al.* [139]. Then, a novel extension of these metrics to partial polarimeters is shown. The new metrics can be minimized in order to choose the PSG and PSA states that will give the best error performance for determining RI MMs.

This method was developed based on existing methods for full MM polarimeters [81, 125, 139]. A few other works have treated the optimization of partial MM polarimeters. Savenkov [112, 113] has discussed the optimization of polarimeters that fully determine some number of rows or columns of the MM. Tyo *et al.* [130] and Anna *et al.* [5] have described techniques for optimizing a partial polarimeter for a specific classification or discrimination task. Alenin and Tyo [2, 3] have extensively analyzed the design of some types of partial polarimeters. The method in this chapter, which was developed independently of these references, has the advantages of simplicity and applicability to any type of PSG and PSA. Additionally, it is based on reducing the total error in the RI MM, rather than having to define a specific classification or discrimination task. Finally, the suggestion by Tyo *et al.* [130] that symmetry relations are treated as if they were additional measurements is considered in section 4.3, but is found to create ambiguities in the optimization metrics used in this chapter.

Sections 4.4 and 4.5 apply the methods of section 4.3 to find several rotating QWP par-

[1] Both nine and ten parameter RI MMs are considered throughout. Separate designs are shown for each case.

tial polarimeter designs capable of measuring RI MMs in fewer than sixteen measurements. Each design consists of a sequence of angles for both QWPs in the polarimeter. These are chosen based both on error performance and on other practical considerations for *in vivo* retinal polarimetry, such as the time required to rotate the QWPs. A simulation is used to compare the performance of each design in the presence of errors, using standard sixteen measurement full polarimeter QWP designs as a baseline.

The sets of QWP angles obtained in this chapter, and the equations developed in section 4.2, can be used directly to measure RI MMs in as few as nine or ten measurements. For a future *in vivo* retinal polarimeter intended to detect amyloid-β in the retina, it may be decided to use other modulating elements than rotating QWPs, or a different number of measurements. In that case, the methodology exhibited in this chapter should serve as a template for how to choose the PSG and PSA states for each measurement.

4.2 The Polarimetric Measurement Equation and Reciprocal Invariance

As derived in section 2.3.1, typical Mueller matrix measuring devices involving n measurements are governed by the polarimetric measurement equation

$$\vec{\mathbf{I}} = \mathbf{W}\vec{\mathbf{M}} \tag{4.1}$$

where $\vec{\mathbf{I}}$ is a $n \times 1$ vector containing the measured irradiance data, $\vec{\mathbf{M}}$ is the MM reshaped into a 16×1 Mueller vector (equation 2.51), and $\mathbf{W}$ is a $n \times 16$ matrix relating the two [40]. Arrows have been added to vectors in order to prevent confusion between matrix and vector forms of $\mathbf{I}$ and $\mathbf{M}$. Each row of $\mathbf{W}$ is constructed from the elements of the MMs of the PSG and PSA during the corresponding measurement (equation 2.50). Vector equation 4.1 is the same as n scalar equations, all of which are linear in elements of $\mathbf{M}$. For $\mathbf{M}$ to be determined, n must be at least 16. The reciprocal invariance restrictions 3.13 and 3.14 are likewise scalar equations and are linear in elements of $\mathbf{M}$. They can be represented by a matrix equation analogous to equation 2.52:

$$\vec{\mathbf{0}} = \mathbf{W}_r\vec{\mathbf{M}} \tag{4.2}$$

where $\mathbf{W}_r$ is a matrix encoding the restrictions on RI MMs. $\mathbf{W}_r$ is of dimension $a \times 16$ where $a = 7$ or $a = 6$ for nine or ten parameter RI MMs respectively. This is because for ten parameter RI MMs there are six linear relationships between MM elements (equations 3.13)

while nine parameter RI MMs obey also a seventh restriction (equation 3.14). By inspection of equations 3.13 and 3.14, an expression for $\mathbf{W}_r$ in the nine parameter case can be obtained:

$$\mathbf{W}_r \equiv \left[\begin{array}{cccc|cccc|cccc|cccc} 1 & 0 & 0 & 0 & 0 & -1 & 0 & 0 & 0 & 0 & 1 & 0 & 0 & 0 & 0 & -1 \\ 0 & 1 & 0 & 0 & -1 & 0 & 0 & 0 & 0 & 0 & 0 & 0 & 0 & 0 & 0 & 0 \\ 0 & 0 & 1 & 0 & 0 & 0 & 0 & 0 & 1 & 0 & 0 & 0 & 0 & 0 & 0 & 0 \\ 0 & 0 & 0 & 1 & 0 & 0 & 0 & 0 & 0 & 0 & 0 & 0 & -1 & 0 & 0 & 0 \\ 0 & 0 & 0 & 0 & 0 & 0 & 1 & 0 & 0 & 1 & 0 & 0 & 0 & 0 & 0 & 0 \\ 0 & 0 & 0 & 0 & 0 & 0 & 0 & 1 & 0 & 0 & 0 & 0 & 0 & -1 & 0 & 0 \\ 0 & 0 & 0 & 0 & 0 & 0 & 0 & 0 & 0 & 0 & 0 & 1 & 0 & 0 & 1 & 0 \end{array}\right]. \tag{4.3}$$

The ten parameter case can be obtained by dropping the first row of $\mathbf{W}_r$, which corresponds to the trace condition 3.14. However, in either case, $\mathbf{W}_r$ is not unique. The matrix $\mathbf{W}'_r \equiv \mathbf{B}\mathbf{W}_r$, where $\mathbf{B}$ is any nonsingular $a \times a$ matrix, imposes the same restrictions on $\vec{\mathbf{M}}$.

One way to incorporate this symmetry information into the measurement equation 4.1 is by appending the rows of $\mathbf{W}_r$ to $\mathbf{W}$, and correspondingly the zero vector $\vec{\mathbf{0}}$ to $\vec{\mathbf{I}}$:

$$\left[\begin{array}{c} \vec{\mathbf{I}} \\ \vec{\mathbf{0}} \end{array}\right] = \left[\begin{array}{c} \mathbf{W} \\ \mathbf{B}\mathbf{W}_r \end{array}\right] \vec{\mathbf{M}}. \tag{4.4}$$

This scheme treats the restrictions on RI MMs as though they were additional measurements, which is what was suggested by Tyo *et al.* [130]. The estimated Mueller vector can be reconstructed using

$$\vec{\mathbf{M}}_{EST} = \left[\begin{array}{c} \mathbf{W} \\ \mathbf{B}\,\mathbf{W}_r \end{array}\right]^{-1} \left[\begin{array}{c} \vec{\mathbf{I}}_{EST} \\ \vec{\mathbf{0}} \end{array}\right]. \tag{4.5}$$

The elements of $\mathbf{W}$ are dimensionful quantities, and as seen in section 2.3.1 contain the unknown scalar factor c. This causes a problem regarding the relative scaling of $\mathbf{W}$ and $\mathbf{W}_r$. If an experiment uses exactly the minimum number of measurements (*i.e.* $n+a = 16$), then this problem has no effect on the calculation of $\vec{\mathbf{M}}_{EST}$ (although it will be seen in section 4.3 that it causes ambiguities in the optimization of the polarimeter). However, if $n + a > 16$ the pseudoinverse must be used to calculate $\vec{\mathbf{M}}_{EST}$ [40], as discussed in section 2.3.1. The system of equations is overdetermined in this case, and it will usually be inconsistent due to errors in $\vec{\mathbf{I}}_{EST}$. In general there will be no $\vec{\mathbf{M}}_{EST}$ that perfectly satisfies equation 4.4, but the use of the pseudoinverse returns $\vec{\mathbf{M}}_{EST}$ that minimizes the quantity

$$\left\| \left[\begin{array}{c} \vec{\mathbf{I}}_{EST} \\ \vec{\mathbf{0}} \end{array}\right] - \left[\begin{array}{c} \mathbf{W} \\ \mathbf{B}\mathbf{W}_r \end{array}\right] \vec{\mathbf{M}}_{EST} \right\|_2 \quad [102] \tag{4.6}$$

where $\|\cdot\|_2$ is the Euclidean vector norm defined in equation 2.57. Minimizing this quantity does not guarantee that $\mathbf{W}_r \vec{\mathbf{M}}_{EST} = \vec{\mathbf{0}}$, that is, the estimated Mueller vector may not be perfectly RI. Furthermore, $\vec{\mathbf{M}}_{EST}$ will depend on the choice of $\mathbf{B}$.

A different approach will be proposed that always returns the same estimate $\vec{\mathbf{M}}_{EST}$, and guarantees that $\vec{\mathbf{M}}_{EST}$ is always RI. This method rewrites equation 4.1 in terms of the nine (or ten) dimensional space of RI MMs, rather than the sixteen dimensional space of general MMs. The null space of $\mathbf{W}_r$ is the set of vectors $\vec{\mathbf{M}}$ that satisfy equation 4.2 [61], meaning it is the space of RI Mueller vectors. Because equations 3.13 and 3.14 are linearly independent, the dimension of the row space of $\mathbf{W}_r$ is a and so the dimension of the null space is $b \equiv 16 - a$ [61]. Therefore any vector in the null space of $\mathbf{W}_r$, *i.e.* any RI $\vec{\mathbf{M}}$, can be built from a linear combination of b basis vectors. This is expressed by the equation $\vec{\mathbf{M}} = \mathbf{z}\vec{\mathbf{R}}$, where $\vec{\mathbf{R}}$ is an arbitrary real $b \times 1$ vector[2] and $\mathbf{z}$ is a $16 \times b$ matrix, the columns of which are a set of basis vectors for the null space of $\mathbf{W}_r$. In MATLAB, $\mathbf{z}$ can be calculated using the built-in command `z = null(Wr)` [89]. $\vec{\mathbf{R}}$ is a reparameterization of $\vec{\mathbf{M}}$ under the assumption of reciprocal invariance, with $\mathbf{z}$ being the set of instructions on how to return from $\vec{\mathbf{R}}$ to MM elements. Combining this with equation 4.1,

$$\begin{aligned} \vec{\mathbf{I}} &= \mathbf{W}\,\vec{\mathbf{M}} \\ &= \mathbf{W}\,\mathbf{z}\,\vec{\mathbf{R}} \\ &= \mathbf{W}_{RI}\,\vec{\mathbf{R}} \end{aligned} \tag{4.7}$$

where $\mathbf{W}_{RI} \equiv \mathbf{W}\,\mathbf{z}$ is the $n \times b$ *reciprocal invariant measurement matrix*. To obtain $\vec{\mathbf{M}}_{EST}$, first calculate $\vec{\mathbf{R}}_{EST} \equiv \mathbf{W}_{RI}^{-1}\,\vec{\mathbf{I}}_{EST}$, using the pseudoinverse[3] $\mathbf{W}_{RI}^{-1} \equiv (\mathbf{z}^T\,\mathbf{W}^T\,\mathbf{W}\mathbf{z})^{-1}\,\mathbf{z}^T\,\mathbf{W}^T$ (see equation 2.56). Due to the reduced dimensions of $\mathbf{W}_{RI}$ compared to $\mathbf{W}$, this requires a minimum of nine or ten measurements instead of sixteen. Then take $\vec{\mathbf{M}}_{EST} = \mathbf{z}\,\vec{\mathbf{R}}_{EST}$. This estimate is RI, because by definition, $\mathbf{W}_r\,\mathbf{z} = \mathbf{0}$:

$$\begin{aligned} \mathbf{W}_r\,\vec{\mathbf{M}}_{EST} &= \mathbf{W}_r\,\mathbf{z}\,\vec{\mathbf{R}}_{EST} \\ &= \vec{\mathbf{0}} \end{aligned}$$

Like $\mathbf{W}_r$, the matrix $\mathbf{z}$ is not unique. The matrix $\mathbf{z}' \equiv \mathbf{z}\mathbf{C}$, where $\mathbf{C}$ is any $b \times b$ nonsingular matrix, is an equally valid representation of the null space of $\mathbf{W}_r$. The

[2] This $\vec{\mathbf{R}}$ is unrelated to the retardance vector $\mathbf{R}$ defined in section 2.2.2.

[3] If $\mathbf{W}_{RI}$ is square ($n = b$), then this expression is the same as normal inverse.

estimated Mueller vector calculated using $\mathbf{z}'$ instead of $\mathbf{z}$ is given by

$$\begin{aligned}
\vec{\mathbf{M}}'_{EST} &= \mathbf{z}'\,\vec{\mathbf{R}}'_{EST} \\
&= \mathbf{z}'\,\mathbf{W}'^{-1}_{RI}\,\vec{\mathbf{I}}_{EST} \\
&= \mathbf{z}'\,(\mathbf{z}'^{T}\,\mathbf{W}^{T}\,\mathbf{W}\,\mathbf{z}')^{-1}\,\mathbf{z}'^{T}\,\mathbf{W}^{T}\,\vec{\mathbf{I}}_{EST} \\
&= \mathbf{z}\,\mathbf{C}\,(\mathbf{C}^{T}\,\mathbf{z}^{T}\,\mathbf{W}^{T}\,\mathbf{W}\,\mathbf{z}\,\mathbf{C})^{-1}\,\mathbf{C}^{T}\,\mathbf{z}^{T}\,\mathbf{W}^{T}\,\vec{\mathbf{I}}_{EST} \\
&= \mathbf{z}\,\mathbf{C}\,\mathbf{C}^{-1}\,(\mathbf{z}^{T}\,\mathbf{W}^{T}\,\mathbf{W}\,\mathbf{z})^{-1}\,(\mathbf{C}^{T})^{-1}\,\mathbf{C}^{T}\,\mathbf{z}^{T}\,\mathbf{W}^{T}\,\vec{\mathbf{I}}_{EST} \\
&= \mathbf{z}\,(\mathbf{z}^{T}\,\mathbf{W}^{T}\,\mathbf{W}\mathbf{z})^{-1}\,\mathbf{z}^{T}\,\mathbf{W}^{T}\,\vec{\mathbf{I}}_{EST} \\
&= \mathbf{z}\mathbf{W}^{-1}_{RI}\vec{\mathbf{I}}_{EST} \\
&= \vec{\mathbf{M}}_{EST}.
\end{aligned}$$

Therefore, all possible versions of $\mathbf{z}$ give the same reconstructed MM.

4.3 Polarimeter Optimization Metrics

As introduced in section 2.3.1, the performance of a polarimeter in the presence of errors can be improved through polarimeter optimization (e.g. [4, 81, 125, 129, 139]). Typically, the measurement matrix $\mathbf{W}(\boldsymbol{\psi})$ is written as a function of some number of parameters $\boldsymbol{\psi} = [\psi_1, \psi_2, ...\psi_m]$ which represent modifiable aspects the PSG and PSA [139]. For example, in the rotating QWP polarimeter described in section 2.3.1, these could be the QWP angles $\theta_{G,i}$ and $\theta_{A,i}$ for each of the n measurements. Polarimeter optimization metrics are scalar functions of $\mathbf{W}$ that characterize how resistant the polarimeter is to error. The parameters $\boldsymbol{\psi}$ are chosen in such a way as to maximize or minimize an optimization metric. This section will provide a mathematical treatment of errors in polarimetry, and derive a few optimization metrics, mostly following the work of Twietmeyer and Chipman [125]. Then, these results will be extended for the first time to the modified polarimetric measurement equation 4.7.

Error in a polarimetry experiment can arise due to errors in the PSG and PSA, and errors in the irradiance measurements[4]. Suppose that the MMs of the PSG and PSA are differ slightly from their idealized values during some or all of the n measurements, such that the true measurement matrix of the polarimeter is $\mathbf{W} + \delta\mathbf{W}$. Let the nonsubscripted

[4]It will be assumed that computational errors due to calculating the inverse or pseudoinverse are small relative to these sources of error.

symbols $\vec{\mathbf{I}} = \mathbf{W}\,\vec{\mathbf{M}}$ represent the idealized system in the presence of zero errors. The true irradiance that reaches the detector differs from $\vec{\mathbf{I}}$ because of the error $\delta\mathbf{W}$:

$$\vec{\mathbf{I}}_{Detector} = (\mathbf{W} + \delta\mathbf{W})\,\vec{\mathbf{M}} \tag{4.8}$$

$$= \vec{\mathbf{I}} + \delta\mathbf{W}\,\vec{\mathbf{M}}. \tag{4.9}$$

The detector does not perfectly record $\vec{\mathbf{I}}_{Detector}$, but is assumed to contain an additive error $\delta\vec{\mathbf{I}}$:

$$\vec{\mathbf{I}}_{EST} = \vec{\mathbf{I}}_{Detector} + \delta\vec{\mathbf{I}} \tag{4.10}$$

$$= \mathbf{W}\,\vec{\mathbf{M}} + \delta\mathbf{W}\,\vec{\mathbf{M}} + \delta\vec{\mathbf{I}}. \tag{4.11}$$

The experimenter only has access to $\vec{\mathbf{I}}_{EST}$ and the idealized measurement matrix $\mathbf{W}$. These are used to calculate the Mueller vector estimate, given by

$$\vec{\mathbf{M}}_{EST} = \mathbf{W}^{-1}\,\vec{\mathbf{I}}_{EST} \tag{4.12}$$

$$= \vec{\mathbf{M}} + \mathbf{W}^{-1}\,(\delta\mathbf{W}\,\vec{\mathbf{M}} + \delta\vec{\mathbf{I}}) \quad \Longrightarrow \tag{4.13}$$

$$\delta\vec{\mathbf{M}} = \mathbf{W}^{-1}\,(\delta\mathbf{W}\,\vec{\mathbf{M}} + \delta\vec{\mathbf{I}}), \tag{4.14}$$

where $\delta\vec{\mathbf{M}} \equiv \vec{\mathbf{M}}_{EST} - \vec{\mathbf{M}}$ is the error in the estimated Mueller vector. This is the same expression found by Twietmeyer and Chipman [125], but it differs from that of Zallat *et al.* [139], who used $\vec{\mathbf{M}}_{EST} = (\mathbf{W} + \delta\mathbf{W})^{-1}\,\vec{\mathbf{I}}_{EST}$ instead of equation 4.12. This assumes that $(\mathbf{W} + \delta\mathbf{W})^{-1}$ is known by the experimenter (and hence can be used to calculate $\vec{\mathbf{M}}_{EST}$), while in the above analysis it was assumed that only $\mathbf{W}$ is known. The assumption of Zallat *et al.* is appropriate if calibration is performed to obtain $(\mathbf{W} + \delta\mathbf{W})$, and/or if $\delta\mathbf{W}$ is due primarily to computational errors when calculating the inverse or pseudoinverse of $\mathbf{W}$ [61].

The single value decomposition of $\mathbf{W}$ can be used to understand how errors propagate into $\delta\vec{\mathbf{M}}$ [110, 125]. Any $\mathbf{W}$ can be decomposed into the product $\mathbf{W} = \mathbf{U}\mathbf{S}\mathbf{V}^T$, where $\mathbf{U}$ and $\mathbf{V}$ are orthogonal $n \times n$ and 16×16 matrices respectively, while $\mathbf{S}$ is $n \times 16$ and has the property $S(i,j) = 0$ for $i \neq j$ [61]. The diagonal entries $S(i,i)$ are known as the singular values of $\mathbf{W}$ [61]. Inserting this decomposition into the idealized equation 4.1,

$$\mathbf{U}^T\vec{\mathbf{I}} = \mathbf{S}\mathbf{V}^T\vec{\mathbf{M}} \quad \Longrightarrow$$

$$\vec{\mathbf{I}}' = \mathbf{S}\vec{\mathbf{M}}' \quad \Longrightarrow$$

$$\vec{I}'(i) = S(i,i)\vec{M}'(i)$$

where $i \leq \min(n, 16)$, and $\vec{\mathbf{I}}' \equiv \mathbf{U}^T\vec{\mathbf{I}}$ and $\vec{\mathbf{M}}' \equiv \mathbf{V}^T\vec{\mathbf{M}}$ are the irradiance and Mueller vectors expressed in new bases. As noted by Twietmeyer and Chipman [125], elements $\vec{\mathbf{M}}'(i)$ for which $S(i,i) = 0$ or $i > n$ represent linear combinations of MM elements to which the polarimeter is "blind". The reconstructed MM is undetermined, because any amount of $\vec{\mathbf{M}}'(i)$ could be added to or subtracted from the estimated Mueller vector to find a new estimate that also obeys equation 2.55. Therefore, to determine the full MM, $\mathbf{W}$ must have sixteen nonzero singular values. If $S(i,i)$ is small, then the corresponding irradiance signal $\vec{I}'(i)$ will be small relative to the error terms in 4.11. This suggests that the best error performance can be found by maximizing the sizes of the singular values of $\mathbf{W}$.

This simple argument aids in the understanding of several optimization metrics based on the singular values of $\mathbf{W}$:

$$\kappa_2 \equiv \frac{\max\{S(i,i) \,:\, i \leq df\}}{\min\{S(i,i) \,:\, i \leq df\}} \quad [61,\ 125] \tag{4.15}$$

$$\xi \equiv \left(\sum_{i=1}^{df} \frac{1}{(S(i,i))^2}\right)^{1/2} \quad [109,\ 139]. \tag{4.16}$$

where $df = 16$ is the number of degrees of freedom of $\vec{\mathbf{M}}$. Each of these optimization metrics is intended to be minimized to guarantee good error performance of the polarimeter. It can be shown that multiplying $\mathbf{W}$ by a positive scalar has no impact on κ_2, but the new ξ is divided by that scalar. This does not change the locations of minima of ξ, so the resulting optimized designs are unaffected.

κ_2 is known as the *condition number* based on the L_2 matrix norm[5]

$$|||\mathbf{A}|||_2 = \max\{\|\mathbf{A}\,\vec{\mathbf{x}}\|_2 : \|\vec{\mathbf{x}}\|_2 = 1\} \quad [52] \tag{4.17}$$

for any $i \times j$ matrix $\mathbf{A}$. Using equation 4.14 and the properties of the L_2 matrix norm [52], it can be shown that

$$\kappa_2 = \left|\left|\left|\mathbf{W}^{-1}\right|\right|\right|_2 |||\mathbf{W}|||_2 \quad [125] \tag{4.18}$$

$$\frac{\|\delta\vec{\mathbf{M}}\|_2}{\|\vec{\mathbf{M}}\|_2} \leq \kappa_2 \left(\frac{|||\delta\mathbf{W}|||_2}{|||\mathbf{W}|||_2} + \frac{\|\delta\vec{\mathbf{I}}\|_2}{\|\vec{\mathbf{I}}\|_2}\right). \tag{4.19}$$

[5]Notice the distinction between the vector norm $\|\cdot\|_2$ and the matrix norm $|||\cdot|||_2$.

A similar upper bound involving κ_2 was found by Zallat *et al.* [139], which differs trivially from relation 4.19 due to the different assumptions discussed above. In either case, minimizing κ_2 lowers an upper bound on the relative error in the Mueller vector, compared to the experimental errors $\delta\mathbf{W}$ and $\delta\vec{\mathbf{I}}$. Considering equation 4.15, minimizing κ_2 requires maximizing the lowest singular value. Therefore, κ_2 is representative of the "worst case scenario" error in the polarimeter. It is not however the best indicator of average error. For example, increasing the largest singular value improves the error performance of the polarimeter overall, but results in a higher or "worse" value of κ_2.

On the other hand, ξ considers all of the singular values of $\mathbf{W}$. It is related to the *equally weighted variance* as defined by Sabatke *et al.* [110] and Zallat *et al.* [139]. A concrete justification for ξ as an optimization metric (following Sabatke *et al.* [110]) can be given under the assumptions that $\delta\mathbf{W}$ is negligible and the expected value is $E(\delta\vec{\mathbf{I}}\,\delta\vec{\mathbf{I}}^T) = \sigma^2\mathbb{I}$ [110]. This is the case if the irradiance error $\delta\vec{\mathbf{I}}$ is uncorrelated between measurements and has variance σ for every measurement [110, 130]. Then, the expected value of $\|\delta\vec{\mathbf{M}}\|_2^2$ is given by

$$\begin{aligned} E(\|\delta\vec{\mathbf{M}}\|_2^2) &= E(\delta\vec{\mathbf{I}}^T\,(\mathbf{W}^{-1})^T\,\mathbf{W}^{-1}\,\delta\vec{\mathbf{I}}) \\ &= \mathrm{trace}((\mathbf{W}^{-1})^T\,\mathbf{W}^{-1}\,E(\delta\vec{\mathbf{I}}\,\delta\vec{\mathbf{I}}^T)) \\ &= \sigma^2\mathrm{trace}((\mathbf{W}^{-1})^T\,\mathbf{W}^{-1}), \end{aligned} \tag{4.20}$$

using the cyclical property of the trace. It can be shown that

$$\mathrm{trace}((\mathbf{W}^{-1})^T\,\mathbf{W}^{-1}) = \xi^2 \quad [110] \tag{4.21}$$

so

$$E(\|\delta\vec{\mathbf{M}}\|_2^2) = \sigma^2\xi^2. \tag{4.22}$$

Under these conditions, ξ is proportional to the expected value of the normed error in $\vec{\mathbf{M}}_{EST}$. Compared to κ_2, which indicates worst case error, minimizing ξ reduces the average error in the experiment.

A polarimeter design that is optimal for measuring general MMs is not necessarily optimal for measuring RI MMs. Additionally, both κ_2 and ξ approach ∞ for a polarimeter using fewer than sixteen measurements. In order to incorporate symmetry information into these optimization metrics, the symmetry restrictions $\mathbf{W}_r$ could be treated as if they were additional measurements, by calculating the singular values of

$$\begin{bmatrix} \mathbf{W} \\ \mathbf{B}\mathbf{W}_r \end{bmatrix} \tag{4.23}$$

instead of those of $\mathbf{W}$. Then, new versions of κ_2 and ξ could be calculated. However, these singular values depend on the relative scaling between $\mathbf{W}$ and $\mathbf{W}_r$. This is an unphysical ambiguity that would lead to multiple different "optimized" designs, as there is no clear way to know how to choose $\mathbf{B}$.

A better alternative is to use the modified measurement equation 4.7, and apply the singular value decomposition to $\mathbf{W}_{RI} = \mathbf{U}_{RI}\,\mathbf{S}_{RI}\,\mathbf{V}_{RI}^T$ instead of $\mathbf{W}$. The metrics $\kappa_{2,RI}$, ξ_{RI} can be calculated using

$$\kappa_{2,RI} \equiv \frac{\max\{S_{RI}(i,i) \,:\, i \leq df\}}{\min\{S_{RI}(i,i) \,:\, i \leq df\}} \tag{4.24}$$

$$\xi_{RI} \equiv \left(\sum_{i=1}^{df} \frac{1}{(S_{RI}(i,i))^2} \right)^{1/2} \tag{4.25}$$

where $df = 9$ or $df = 10$ for nine or ten parameter MMs respectively. Because of the parallelism between equations 4.7 and 4.1, the above error analysis can all be repeated while replacing $\mathbf{W}$ with $\mathbf{W}_{RI}$ and $\vec{\mathbf{M}}$ with $\vec{\mathbf{R}}$. This assumes that the true Mueller vector is RI; that is, that it can be written $\vec{\mathbf{M}} = \mathbf{z}\,\vec{\mathbf{R}}$ for some $\vec{\mathbf{R}}$. In the presence of errors $\delta\vec{\mathbf{I}}$ and $\delta\mathbf{W}_{RI}$ ($\equiv \delta\mathbf{W}\,\mathbf{z}$), it can be shown that

$$\delta\vec{\mathbf{R}} = \mathbf{W}_{RI}^{-1}(\delta\mathbf{W}_{RI}\,\vec{\mathbf{R}} + \delta\vec{\mathbf{I}}) \tag{4.26}$$

using an identical proof as that leading to equation 4.14. Similarly, it follows that

$$\frac{\|\delta\vec{\mathbf{R}}\|_2}{\|\vec{\mathbf{R}}\|_2} \leq \kappa_{2,RI} \left(\frac{|||\delta\mathbf{W}_{RI}|||_2}{|||\mathbf{W}_{RI}|||_2} + \frac{\|\delta\vec{\mathbf{I}}\|_2}{\|\vec{\mathbf{I}}\|_2} \right) \tag{4.27}$$

$$E(\|\delta\vec{\mathbf{R}}\|_2^2) = \sigma^2\xi_{RI}^2 \tag{4.28}$$

where equation 4.28 is true under the same assumptions as equation 4.22.

Equations 4.27 and 4.28 both involve the error in $\vec{\mathbf{R}}$, not $\vec{\mathbf{M}}$. However,

$$\vec{\mathbf{M}}_{EST} = \mathbf{z}\,\vec{\mathbf{R}}_{EST} \implies$$

$$\vec{\mathbf{M}} + \delta\vec{\mathbf{M}} = \mathbf{z}\,\vec{\mathbf{R}} + \mathbf{z}\,\delta\vec{\mathbf{R}} \implies \tag{4.29}$$

$$\delta\vec{\mathbf{M}} = \mathbf{z}\,\delta\vec{\mathbf{R}}. \tag{4.30}$$

The Euclidean norm of $\delta\vec{\mathbf{M}}$ is given by

$$\|\delta\vec{\mathbf{M}}\|_2 = \sqrt{\delta\vec{\mathbf{M}}^T\,\delta\vec{\mathbf{M}}} \tag{4.31}$$

$$= \sqrt{\delta\vec{\mathbf{R}}^T\,\mathbf{z}^T\,\mathbf{z}\,\delta\vec{\mathbf{R}}}. \tag{4.32}$$

Recall that $\mathbf{z}$ is not uniquely defined, but its columns must form a basis for the space of RI MMs (section 4.2). If it is now required that the columns form an orthonormal basis, then $\mathbf{z}^T\,\mathbf{z} = \mathbb{I}$ and $\|\delta\vec{\mathbf{M}}\|_2 = \|\delta\vec{\mathbf{R}}\|_2$. Such a choice must be possible because $\mathbf{z}$ is full rank [61]. This is favorable because it means that the optimization metrics $\kappa_{2,RI}$ and ξ_{RI} guarantee the best error performance not just of $\vec{\mathbf{R}}$ but also of $\vec{\mathbf{M}}$. Additionally, it implies that $|||\mathbf{W}_{RI}|||_2 = |||\mathbf{W}|||_2$ and $|||\delta\mathbf{W}_{RI}|||_2 = |||\delta\mathbf{W}|||_2$. Using these results in equations 4.27 and 4.28,

$$\frac{\|\delta\vec{\mathbf{M}}\|_2}{\|\vec{\mathbf{M}}\|_2} \leq \kappa_{2,RI}\left(\frac{|||\delta\mathbf{W}|||_2}{|||\mathbf{W}|||_2} + \frac{\|\delta\vec{\mathbf{I}}\|_2}{\|\vec{\mathbf{I}}\|_2}\right) \tag{4.33}$$

$$E(\|\delta\vec{\mathbf{M}}\|_2^2) = \sigma^2\xi_{RI}^2 \tag{4.34}$$

assuming the true Mueller vector is RI, and where equation 4.34 as before assumes that $\delta\mathbf{W} = 0$ and $E(\delta\vec{\mathbf{I}}\,\delta\vec{\mathbf{I}}^T) = \mathbb{I}$.

There is more than one orthonormal basis $\mathbf{z}$ that could be used. For a given $\mathbf{z}$, all other options can be written $\mathbf{z}' = \mathbf{z}\,\mathbf{C}$ where $\mathbf{C}$ is an orthogonal matrix. However, this choice has no impact on the final optimized designs. This can be seen by considering

$$\begin{aligned}\mathbf{W}'_{RI} &= \mathbf{W}_{RI}\,\mathbf{C}\\ &= \mathbf{U}_{RI}\,\mathbf{S}_{RI}\,\mathbf{V}_{RI}^T\,\mathbf{C}\\ &= \mathbf{U}_{RI}\,\mathbf{S}_{RI}\,\mathbf{V}_{RI}'^T,\end{aligned}$$

because the product of two orthogonal matrices is itself orthogonal. The last line of this is a valid singular value decomposition of $\mathbf{W}'_{RI}$, and the singular values of any matrix are unique [61]. Therefore the singular values of $\mathbf{W}'_{RI}$ are the same as those of $\mathbf{W}_{RI}$. $\kappa_{2,RI}$ and ξ_{RI} are both calculated from the singular values of the RI measurement matrix, so they will be the same regardless of which orthonormal basis is used for $\mathbf{z}$. In summary, $\kappa_{2,RI}$ and ξ_{RI} are both measures of the amount of error in a RI Mueller vector, when calculated using the approach described in section 4.2.

The methodology described in this chapter so far is applicable not only to RI MMs, but also in any situation in which there are constraints on the MM that can be written as

$$\vec{\mathbf{0}} = \mathbf{W}_r\vec{\mathbf{M}} \tag{4.35}$$

for some $\mathbf{W}_r$. For example, for independent scattering from a cloud of particles which have

a plane of symmetry and are randomly oriented, the MM has the form

$$\begin{bmatrix} a_1 & b_1 & 0 & 0 \\ b_1 & a_2 & 0 & 0 \\ 0 & 0 & a_3 & b_2 \\ 0 & 0 & -b_2 & a_4 \end{bmatrix} \tag{4.36}$$

for parameters a_1, a_2, a_3, a_4, b_1, and b_2 [131]. Every such MM obeys equation 4.35 with

$$\mathbf{W}_r \equiv \begin{bmatrix} 0 & 1 & 0 & 0 & -1 & 0 & 0 & 0 & 0 & 0 & 0 & 0 & 0 & 0 & 0 & 0 \\ 0 & 0 & 1 & 0 & 0 & 0 & 0 & 0 & 0 & 0 & 0 & 0 & 0 & 0 & 0 & 0 \\ 0 & 0 & 0 & 1 & 0 & 0 & 0 & 0 & 0 & 0 & 0 & 0 & 0 & 0 & 0 & 0 \\ 0 & 0 & 0 & 0 & 0 & 0 & 1 & 0 & 0 & 0 & 0 & 0 & 0 & 0 & 0 & 0 \\ 0 & 0 & 0 & 0 & 0 & 0 & 0 & 1 & 0 & 0 & 0 & 0 & 0 & 0 & 0 & 0 \\ 0 & 0 & 0 & 0 & 0 & 0 & 0 & 0 & 1 & 0 & 0 & 0 & 0 & 0 & 0 & 0 \\ 0 & 0 & 0 & 0 & 0 & 0 & 0 & 0 & 0 & 1 & 0 & 0 & 0 & 0 & 0 & 0 \\ 0 & 0 & 0 & 0 & 0 & 0 & 0 & 0 & 0 & 0 & 0 & 1 & 0 & 0 & 1 & 0 \\ 0 & 0 & 0 & 0 & 0 & 0 & 0 & 0 & 0 & 0 & 0 & 0 & 1 & 0 & 0 & 0 \\ 0 & 0 & 0 & 0 & 0 & 0 & 0 & 0 & 0 & 0 & 0 & 0 & 0 & 1 & 0 & 0 \end{bmatrix}. \tag{4.37}$$

This matrix can be used to calculate a 16×6 orthonormal basis $\mathbf{z}$ and a modified measurement matrix analogous to $\mathbf{W}_{RI}$.

4.4 Methods

The procedure of sections 4.2 and 4.3 was applied in order to find optimized PSG and PSA designs for determination of RI MMs with a rotating QWP polarimeter (section 2.3.1). These designs are applicable to *in vivo* retinal polarimetry assuming the double pass model. Optimization amounts to choosing the angles of the QWPs for each irradiance measurement. However, depending on the type of motors used to rotate the QWPs, the scanning method used to image the retina, the detector, and the data collection procedure, there may be many other practical considerations beyond sheer error performance (see *e.g.* [33, 126, 136]). These design elements may differ between different instruments, and a detailed analysis of them is beyond the scope of this thesis. For the purposes of this chapter, it was assumed that the time required to rotate the QWPs between each measurement is a non-negligible contribution to the total data acquisition time. Additionally, it was assumed that it would be favorable for the QWPs to rotate in one direction only. This reduces the potential for backlash in some motor systems. Finally, some designs were made under the

assumption that only one QWP should rotate at a time. This simplifies the control of the motors and minimizes the total number of rotations necessary during data acquisition. All three of these assumptions are true of the *ex vivo* retinal polarimeter currently used by Campbell Labs. Sections 4.4.1 and 4.4.2 show how these restrictions can be incorporated into the optimization process. Section 4.4.3 describes the numerical optimization itself, while section 4.4.4 describes simulations used to test the final designs.

For a future *in vivo* retinal polarimeter, there may be other practical considerations that are unforeseen by this chapter. As well, the PSG and PSA may consist of different optical elements than a rotating QWP and fixed linear polarizer. The methodology of this section could be adapted to choose PSG and PSA states that are practical while also having good error performance.

4.4.1 Parameterization of the Reciprocal Invariant Measurement Matrix

First, it is necessary to write $\mathbf{W}_{RI}$ as a function of the QWP angles. As described in subsection 2.3.1, the regular measurement matrix $\mathbf{W}$ consists of n rows each having the form

$$\mathbf{W}_i \equiv c(\mathbf{s}_{A,i} \otimes \mathbf{s}_{G,i}). \tag{2.50}$$

It was chosen to set $c = 1$. In general, $\mathbf{s}_{A,i}$ and $\mathbf{s}_{G,i}$ could take unique values for every measurement i. For a rotating QWP polarimeter design,

$$\mathbf{s}_{G,i} \equiv (1/2)\,[1,\, \cos^2(2\theta_{G,i}),\, \cos(2\theta_{G,i})\sin(2\theta_{G,i}),\, \sin(2\theta_{G,i})]^T \tag{2.47}$$

$$\mathbf{s}_{A,i} \equiv (1/2)\,[1,\, \cos^2(2\theta_{A,i}),\, \cos(2\theta_{A,i})\sin(2\theta_{A,i}),\, -\sin(2\theta_{A,i})]^T. \tag{2.48}$$

Define the vectors

$$\boldsymbol{\theta}_G \equiv [\theta_{G,1},\, \theta_{G,2}, ...\theta_{G,n}] \tag{4.38}$$

$$\boldsymbol{\theta}_A \equiv [\theta_{A,1},\, \theta_{A,2}, ...\theta_{A,n}], \tag{4.39}$$

which characterize the sequence of n positions for each QWP. It is assumed for simplicity that the irradiance measurements are taken in increasing order in i. The most general choice is to assign a unique parameter to every angle:

$$\begin{aligned} \boldsymbol{\theta}_G &= [\psi_1,\, \psi_2, ...\psi_n] \\ \boldsymbol{\theta}_A &= [\psi_{n+1},\, \psi_{n+2}, ...\psi_{2n}], \end{aligned} \tag{4.40}$$

resulting in $2n$ total parameters. The RI measurement matrix can be constructed as a function of $\boldsymbol{\psi}$:

$$\mathbf{W}_{RI}(\boldsymbol{\psi}) = \mathbf{W}(\boldsymbol{\psi})\mathbf{z}. \tag{4.41}$$

This "$2n$" design is the most general parameterization of the QWP angles, because it allows every angle to be chosen independently without restriction.

Other designs were obtained using different parameterizations of the angles $\boldsymbol{\theta}_G$ and $\boldsymbol{\theta}_A$. For example, consider a ten measurement "alternating" design with

$$\begin{aligned}
\boldsymbol{\psi}' &= [\text{sort}(\boldsymbol{\psi}(1:5), \text{sort}(\boldsymbol{\psi}(6:11)] \\
\boldsymbol{\theta}_G &= [\psi'_1, \psi'_1, \psi'_2, \psi'_2, \psi'_3, \psi'_3, \psi'_4, \psi'_4, \psi'_5, \psi'_5] \\
\boldsymbol{\theta}_A &= [\psi'_6, \psi'_7, \psi'_7, \psi'_8, \psi'_8, \psi'_9, \psi'_9, \psi'_{10}, \psi'_{10}, \psi'_{11}],
\end{aligned} \tag{4.42}$$

where the sort function places its arguments in ascending order. This parameterization has the properties that both QWPs only rotate in the positive theta direction, and that only one of them rotates at a time. These restrictions mean that the optimization metrics may be higher for this design than for a "$2n$" design with the same number of measurements. However, they may make it preferable for a real *in vivo* retinal polarimeter. Similar "alternating" parameterizations were used for $n = 9, 12$ and will be written explicitly in section 4.5.

A common pattern in MM polarimetry is for the PSG to have q unique states while the PSA has p different states, and then to measure the irradiance for all pq combinations of states [29, 81, 128, 129, 139]. This will be referred to in this thesis as a "p by q" design. For a sixteen measurement polarimeter with $p = q = 4$, this can be expressed through the parameterization

$$\begin{aligned}
\boldsymbol{\theta}_G &= [\psi_1, \psi_1, \psi_1, \psi_1, \psi_2, \psi_2, \psi_2, \psi_2, \psi_3, \psi_3, \psi_3, \psi_3, \psi_4, \psi_4, \psi_4, \psi_4] \\
\boldsymbol{\theta}_A &= [\psi_1, \psi_2, \psi_3, \psi_4, \psi_4, \psi_3, \psi_2, \psi_1, \psi_1, \psi_2, \psi_3, \psi_4, \psi_4, \psi_3, \psi_2, \psi_1].
\end{aligned} \tag{4.43}$$

When optimizing the ordinary measurement matrix $\mathbf{W}$, this type of design has several advantages, including that it allows the PSG and PSA to be optimized separately [125]. However, Appendix A demonstrates that this property does not extend to $\mathbf{W}_{RI}$. Additionally, it shows that no "p by q" design is capable of measuring an RI MM in the minimum number of measurements. Therefore, designs of other, more complicated forms are necessary, such as 4.40 and 4.42.

When the results are presented in section 4.5, each design will be labelled explicitly with the parameterization of $\boldsymbol{\theta}_G$ and $\boldsymbol{\theta}_A$ that was used.

4.4.2 Additional Optimization Objectives

The distance the QWPs must rotate between each measurement contributes to the total time necessary to determine the MM. It was observed that when optimizing using ξ_{RI} alone, there could be many sets of angles that gave similar minima. A secondary metric that characterizes the distance the QWPs must rotate was used to steer the result towards designs that are faster to operate in practice. When both wave plates move simultaneously (such as for the "$2n$" design 4.40), it is expected that the larger movement is the rate limiting factor. Therefore, a metric w was calculated as the sum of the largest angular distance in radians moved between each irradiance measurement. When faster designs were desired, a hybrid metric $\xi_{RI} + \alpha w$ was minimized. The weighting factor α is somewhat arbitrary, but a small value $\alpha = 0.25$ was chosen such that the contribution from ξ_{RI} is strongly emphasized. ξ_{RI} tended to be $6 - 10\times$ larger than $0.25w$ for the designs that will be shown in section 4.5.

As mentioned before, blinks and involuntary eye movements [88, 126] can disrupt *in vivo* retinal polarimetry. Twietmeyer *et al.* reported having to occasionally drop individual irradiance measurements from consideration due to these factors [126]. In practice, it may be possible for the instrument operator to check for these defects in the measured data immediately, so that the affected images can be retaken. However, a valuable degree of flexibility would be provided by a design that performs well even if an individual irradiance measurement is unusable. This requires that the polarimeter uses more than the minimum number of measurements.

Dropping a measurement from consideration amounts to removing a row from $\mathbf{W}_{RI}$. All of the optimization metrics that have been considered can be applied to the reduced $\mathbf{W}_{RI}$, although their values will depend on which row was removed. Therefore a new metric $\xi_{RI}(-1)$ was calculated by taking the average ξ_{RI} for the n different ways of dropping one row from $\mathbf{W}_{RI}$. Similarly, $\xi_{RI}(-2)$ is the average over the $n(n-1)/2$ ways of dropping two measurements from $\mathbf{W}_{RI}$, and so on. $\kappa_2(i)$ were defined in the same way. These metrics characterize the resilience of the polarimeter to discarded irradiance measurements. To generate designs that had good performance when a single measurement is dropped, the hybrid metric $\xi_{RI} + 0.25\xi_{RI}(-1) + 0.25w$ was used as the optimization objective. The weighting factor 0.25 was chosen semi-arbitrarily, but in the future it could be fine-tuned based on how frequently dropped measurements occur in practice.

In section 4.5, each design will be labeled with the metric that was optimized. Optimization using different metrics results in designs that reflect different combinations of priorities.

4.4.3 Numerical Optimization

Optimization of $\mathbf{W}_{RI}$ was performed in MATLAB [89]. For each design, $\mathbf{W}(\boldsymbol{\psi})$ was constructed using equations 2.50, 2.47, 2.48, and a specific parameterization of the QWP angles (*e.g.* equations 4.40, 4.42, 4.43). For nine parameter[6] RI MMs, the matrix W_r given by definition 4.3 was used. For ten parameter RI MMs, the first row of W_r (corresponding to the trace condition 3.14) was dropped. A matrix $\mathbf{z}$ obeying $\mathbf{z}^T\mathbf{z} = \mathbb{I}$ was obtained using the command `z = null(Wr)` [89]. This allowed $\mathbf{W}_{RI}(\boldsymbol{\psi}) = \mathbf{W}(\boldsymbol{\psi})\,\mathbf{z}$ to be written as a function of the parameters $\boldsymbol{\psi}$. A function was written to calculate the optimization metric for each design, whether it was $\kappa_{2,RI}$, ξ_{RI}, or a hybrid metric involving w or $\xi_{RI}(-1)$. The MATLAB function `lsqnonlin` [89] was used to find a local minimum of the optimization metric, with each parameter ψ having a randomized starting point. The function was run between 10^3 and 10^4 times (depending on the design) with new randomized starting points for each trial. The set of parameters corresponding to the lowest minimum among all trials was chosen. The exact settings varied between designs, and were adjusted based on the feedback provided by `lsqnonlin` to ensure that local minima were being reached.

4.4.4 Simulation

Lastly, simulations were used to compare the performance of these PSG and PSA designs in the presence of experimental errors. A set of 30 000 nine parameter RI MMs, and a second set of the same number of ten parameter RI MMs, were randomly generated using the method described in Appendix B.2. For each polarimeter design $\mathbf{W}_{RI}$ and for each MM in the relevant set, the "true" measurement matrix $\mathbf{W} + \delta\mathbf{W}$ was generated assuming a small amount of random rotational error in the QWPs. Each position $\boldsymbol{\theta}_G$ and $\boldsymbol{\theta}_G$ was taken to have an error term $\delta\theta$ taken from a zero mean normal distribution with standard deviation 0.5°. When the angle of a QWP remained fixed between two measurements, $\delta\theta$ remained fixed as well.

The resulting measurement matrix was used to calculate the simulated irradiance at the detector $\vec{\mathbf{I}}_{Detector}$ using equation 4.9. Because of the scaling of the set of MMs (Appendix B.2), the irradiance values all lay between zero and one half. Then each element of the irradiance error $\delta\vec{\mathbf{I}}$ was taken independently from a normal distribution with zero mean and standard deviation 0.005. The reconstructed Mueller vectors $\vec{\mathbf{M}}_{EST}$ were calculated

[6] "Nine parameter" refers to the number of degrees of freedom of this type of RI MMs, not to the number of parameters $\boldsymbol{\psi}$ in the design.

using

$$\vec{\mathbf{M}}_{EST} = \mathbf{z}\,\mathbf{W}_{RI}^{-1}\,\vec{\mathbf{I}}_{EST}. \tag{4.44}$$

As well, a standard filtering procedure was applied to check if each $\vec{\mathbf{M}}_{EST}$ was a valid Mueller vector, and replace unphysical $\vec{\mathbf{M}}_{EST}$ with a nearby physical version (see [40, 42, 53] for more details on this process). It can be shown that this preserves the reciprocal invariance of an MM (including the trace condition 3.14) so the final $\vec{\mathbf{M}}_{EST}$ was always perfectly RI. For each $\vec{\mathbf{M}}$, the relative error

$$\frac{\|\delta\vec{\mathbf{M}}\|_2}{\|\vec{\mathbf{M}}\|_2} = \frac{\|\vec{\mathbf{M}}_{EST} - \vec{\mathbf{M}}\|_2}{\|\vec{\mathbf{M}}\|_2} \tag{4.45}$$

was recorded. This value was then averaged across across all 3×10^4 MMs in the simulation.

For designs using more than the minimum number of measurements, additional values of mean$\{\|\delta\vec{\mathbf{M}}\|_2/\|\vec{\mathbf{M}}\|_2\}$ were simulated in the case that one, two, or three of the irradiance measurements prove to be unusable. This was done for each MM in the simulation by randomly discarding the appropriate number of elements from $\vec{\mathbf{I}}_{EST}$, and discarding the associated rows of $\mathbf{W}$ before calculating $\mathbf{W}_{RI}$.

The value of mean$\{\|\delta\vec{\mathbf{M}}\|_2/\|\vec{\mathbf{M}}\|_2\}$ depends significantly on the amount and types of errors included in $\mathbf{W}$ and $\vec{\mathbf{I}}$, as well as the properties of the set of MMs (Appendix B.2). The simulations in this chapter are intended as a mode of comparison between different sets of angles for the PSG and PSA, and not as an absolute predictor of the level of error in a real *in vivo* retinal polarimeter. The resulting values of mean$\{\|\delta\vec{\mathbf{M}}\|_2/\|\vec{\mathbf{M}}\|_2\}$ are similar to those found to identity matrix images taken by the *ex vivo* retinal polarimeter used currently by Campbell Labs.

4.5 Results

To provide a point of comparison for the novel designs that will be shown in this section, a full sixteen measurement "4 by 4" design was optimized without assuming reciprocal invariance. To accomplish this, $\mathbf{W}$ was optimized instead of $\mathbf{W}_{RI}$, using ξ as the objective metric. Additionally, a simulation was performed as described in section 4.4.4, but the ordinary measurement equation 4.12 was used to generate the MM estimate instead of RI equation 4.44. The resulting metrics and the QWP angles are shown in Table 4.1, under "Four by Four Design 1". Sets of angles for rotating wave plate polarimeters have

already been reported by several authors [4, 109, 128, 133, 139]. The optimized design is in agreement with the result of Zallat *et al.* [139], and is close to designs listed by Ambirajan and Look [4] and Vaughn and Hoover [133]. Very similar angles have been found for wave plates with higher than quarter wave retardance by Sabatke *et al.* [109] and Tyo [128]. This provides a validation of the optimization code used by the present author, and will also be used for comparison with the RI designs optimized later in this section. A second design ("Four by Four Design 2"), proposed by Ambirajan and Look [4], is also shown in Table 4.1 alongside its optimization metrics and simulation results. This set of angles was not obtained by the optimization procedure, but was analyzed for comparison because it is the angle set currently used by Campbell Labs for *ex vivo* retinal polarimetry.

For clarity, the parameters $\boldsymbol{\psi} = [\psi_1, \psi_2, \psi_3, \psi_4]$ are written using only their numeral subscripts in Table 4.1. The metric w gives the total angular distance that both QWPs must move during the sequence of positions specified by $\boldsymbol{\theta}_G$ and $\boldsymbol{\theta}_A$. The simulation was performed for both nine parameter and ten parameter MM data sets. The nine parameter sample group consistently gave lower relative error mean$\{\|\delta\vec{\mathbf{M}}\|_2/\|\vec{\mathbf{M}}\|_2\}$ throughout this section. This difference is indicative only of the different statistical properties of the two generated sets of matrices, due to the fact that different methods are necessary to randomly generate nine and ten parameter RI MMs (see Appendix B.2).

Next, table 4.2 shows two designs that use the assumption that the sample MMs are ten parameter RI to determine them in ten measurements. For the first of these, labelled "$2n$ Design Ascending, Fast" each QWP angle for each measurement was chosen independently, resulting in twenty parameters. However, the angles were constrained such that each QWP could only rotate in the positive θ direction. Additionally, it was optimized by minimizing the objective function $\xi_{RI} + 0.25w$, in order to reduce the distance the QWPs must rotate. Recall that when both QWPs move between two measurements, w only counts the larger movement. Another "$2n$ Design" (not shown) was optimized without these constraints, and achieved only marginally better error performance at the cost of requiring large back and forth movements for both QWPs, which could significantly increase the total measurement time. This demonstrates that the inclusion of a secondary objective such as w can result in much more practical optimized designs.

A second design, labelled "Alternating Design", used these constraints in addition to the requirement that only one QWP move at a time. As can be seen in table 4.2, this comes at a modest cost to the error performance of the polarimeter, as well as an increase in the metric w. Therefore the first design can be expected to perform better in terms of both speed and accuracy, if the polarimeter is capable of rotating both QWPs at the same time.

Design	Properties		
Four by Four Design 1	Assumptions	None	
	Measurements	16	
	Objective	ξ	
	$\boldsymbol{\psi}$	{1-4} = {-51.8°, -14.4°, 14.4°, 51.8°}	
	$\boldsymbol{\theta}_G$	{1, 1, 1, 1, 2, 2, 2, 2, 3, 3, 3, 3, 4, 4, 4, 4}	
	$\boldsymbol{\theta}_A$	{1, 2, 3, 4, 4, 3, 2, 1, 1, 2, 3, 4, 4, 3, 2, 1}	
	κ_2	11.17	
	ξ	20.60	
	w	9.04 rad (= 518.0°)	
		Nine Param. RI Sample	Ten Param. RI Sample
	mean$\{\|\delta\vec{\mathbf{M}}\|_2/\|\vec{\mathbf{M}}\|_2\}$	0.096	0.102
Four by Four Design 2	Assumptions	None	
	Measurements	16	
	$\boldsymbol{\psi}$	{1-4} = {-45°, 0°, 30°, 60°}	
	$\boldsymbol{\theta}_G$	{1, 1, 1, 1, 2, 2, 2, 2, 3, 3, 3, 3, 4, 4, 4, 4}	
	$\boldsymbol{\theta}_A$	{1, 2, 3, 4, 4, 3, 2, 1, 1, 2, 3, 4, 4, 3, 2, 1}	
	κ_2	13.15	
	ξ	21.65	
	w	9.16 rad (= 525.0°)	
		Nine Param. RI Sample	Ten Param. RI Sample
	mean$\{\|\delta\vec{\mathbf{M}}\|_2/\|\vec{\mathbf{M}}\|_2\}$	0.100	0.106

Table 4.1: Examples of sixteen measurement polarimeter designs and their corresponding metrics.

When applied to the ten parameter RI MM sample set, the ten measurement designs have a simulated relative error mean$\{\|\delta\vec{\mathbf{M}}\|_2/\|\vec{\mathbf{M}}\|_2\} = 0.103$ and 0.109, while the sixteen measurement designs in table 4.1 have 0.102 and 0.106 respectively. Therefore, the designs shown in table 4.2 are capable of measuring ten parameter RI MMs with comparable accuracy to standard sixteen measurement designs, despite only having ten measurements. The reasons for this are twofold. Firstly, they were optimized using ξ_{RI} instead of ξ, which means that the found angles are specialized for covering the space of RI MMs. Secondly, the reconstructed MMs was generated using equation 4.7 instead of equation 4.1, which forces them to be RI and thus removes non-RI errors. Therefore, this result relies on the sample MMs being RI. Naturally, a sixteen measurement design that uses the assumption of reciprocal invariance could achieve better error performance in these simulations that any of the designs in tables 4.1 and 4.2.

Finally, the total angular distance w is significantly lower for the ten measurement designs than for the sixteen measurement designs, reflecting a decrease in the waiting time between measurements. This is in addition to the time savings due to only capturing ten images instead of sixteen.

Table 4.3 shows the same two types of designs, this time optimized to measure nine parameter RI MMs in nine measurements. The resulting designs similarly outperform the standard sixteen measurement designs when applied to nine parameter RI MMs, having lower relative error mean$\{\|\delta\vec{\mathbf{M}}\|_2/\|\vec{\mathbf{M}}\|_2\}$ and total movement distance w.

Lastly, other designs were tested that use more than the minimum number of measurements. This improves the error performance of the polarimeter, and it also means that it is possible to calculate the MM even if a measurement has to be discarded due to eye movement or blinking.

Two twelve measurement designs are presented in table 4.4, for nine and ten parameter RI designs respectively. The expected values of all metrics are given when zero, one, two, and three measurements are dropped. These designs were optimized under the constraints that each QWP rotate only in the positive theta direction, and that only one QWP rotates at a time. The objective $\xi_{RI} + 0.25\xi_{RI}(-1) + 0.25w$ was minimized so that the polarimeter would perform well even if one measurement is dropped. If more images are unusable however, the accuracy falls drastically. For ten parameter RI MMs, the -3 column is indeterminate due to having fewer than the minimum number of measurements. The -3 column of the nine parameter design highlights the importance of polarimeter optimization: the $\mathbf{W}_{RI}$ used to calculate this column involve the same number of measurements as the designs in table 4.3, but perform dramatically worse in the presence of error.

There are far more designs that can be obtained involving different numbers of measure-

Design	Properties	
$2n$ Design Ascending, Fast	Assumptions	Ten Parameter Reciprocal Invariance
	Measurements	10
	Objective	$\xi_{RI} + 0.25w$
	$\boldsymbol{\psi}$	{1-20} = {-154.1°, -120.1°, -77.7°, -64.1°, -58.8°, -45.0°, -40.1°, -7.1°, 45.2°, 86.7°, -155.1°, -148.3°, -102.3°, -70.3°, -33.7°, 45.0°, 84.9°, 100.3°, 134.8°, 136.6°}
	$\boldsymbol{\theta}_G$	{1, 2, 3, 4, 5, 6, 7, 8, 9, 10}
	$\boldsymbol{\theta}_A$	{11, 12, 13, 14, 15, 16, 17, 18, 19, 20}
	$\kappa_{2,RI}$	11.57
	ξ_{RI}	20.89
	w	6.87 rad (= 393.9°)
		Ten Param. RI Sample
	mean$\{\|\delta\vec{\mathbf{M}}\|_2/\|\vec{\mathbf{M}}\|_2\}$	0.103
Alternating Design	Assumptions	Ten Parameter Reciprocal Invariance
	Measurements	10
	Objective	$\xi_{RI} + 0.25w$
	$\boldsymbol{\psi}$	{1-11} = {-56.5°, 47.7°, 110.0°, 141.9°, 167.4°, -117.8°, -49.3°, -9.8°, 24.0°, 96.0°, 144.7°}
	$\boldsymbol{\theta}_G$	{1, 1, 2, 2, 3, 3, 4, 4, 5, 5}
	$\boldsymbol{\theta}_A$	{6, 7, 7, 8, 8, 9, 9, 10, 10, 11}
	$\kappa_{2,RI}$	13.13
	ξ_{RI}	22.47
	w	8.49 rad (= 486.3°)
		Ten Param. RI Sample
	mean$\{\|\delta\vec{\mathbf{M}}\|_2/\|\vec{\mathbf{M}}\|_2\}$	0.109

Table 4.2: Optimized designs for ten measurement determination of ten parameter RI MMs.

Design	Properties	
$2n$ Design Ascending, Fast	Assumptions	Nine Parameter Reciprocal Invariance
	Measurements	9
	Objective	$\xi_{RI} + 0.25w$
	$\boldsymbol{\psi}$	{1-18} = {-140.8°, -140.0°, -140.0°, -101.9°, -101.9°, -74.6°, -35.3°, 5.4°, 49.5°, -138.3°, -98.9°, -37.6°, 7.0°, 42.6°, 45.3°, 45.3°, 80.4°, 112.5°‘}
	$\boldsymbol{\theta}_G$	{1, 2, 3, 4, 5, 6, 7, 8, 9}
	$\boldsymbol{\theta}_A$	{10, 11, 12, 13, 14, 15, 16, 17, 18}
	$\kappa_{2,RI}$	10.43
	ξ_{RI}	19.55
	w	5.80 rad (= 332.4°)
		Nine Param. RI Sample
	mean$\{\|\delta\vec{\mathbf{M}}\|_2/\|\vec{\mathbf{M}}\|_2\}$	0.095
Alternating Design	Assumptions	Nine Parameter Reciprocal Invariance
	Measurements	9
	Objective	$\xi_{RI} + 0.25w$
	$\boldsymbol{\psi}$	{1-10} = {-117.9°, -87.2°, -44.1°, 45.0°, 129.7°, -89.5°, -33.3°, -1.5°, 26.0°, 57.1°}
	$\boldsymbol{\theta}_G$	{1, 1, 2, 2, 3, 3, 4, 4, 5}
	$\boldsymbol{\theta}_A$	{6, 7, 7, 8, 8, 9, 9, 10, 10}
	$\kappa_{2,RI}$	10.73
	ξ_{RI}	20.47
	w	6.88 rad (= 394.2°)
		Nine Param. RI Sample
	mean$\{\|\delta\vec{\mathbf{M}}\|_2/\|\vec{\mathbf{M}}\|_2\}$	0.098

Table 4.3: Optimized designs for nine measurement determination of nine parameter RI MMs.

Design	Properties				
Extra Measurements Ten Parameter	Assumptions	Ten Parameter Reciprocal Invariance			
	Measurements	12			
	$\boldsymbol{\psi}$	{1-13} = {-128.6°, -73.4°, -42.7°, -3.9°, 122.0°, 157.3°, -230.2°, -195.2°, -140.9°, -86.4°, -38.0°, 111.7°, 153.3°}			
	$\boldsymbol{\theta}_G$	{1, 1, 2, 2, 3, 3, 4, 4, 5, 5, 6, 6}			
	$\boldsymbol{\theta}_A$	{7, 8, 8, 9, 9, 10, 10, 11, 11, 12, 12, 13}			
	w	11.68 rad (= 669.4°)			
		(0)	(-1)	(-2)	(-3)
	κ_2	11.22	18.33	50.70	∞
	ξ	19.07	24.81	58.29	∞
		Ten Param. RI Sample			
	mean$\{\|\delta\vec{\mathbf{M}}\|_2/\|\vec{\mathbf{M}}\|_2\}$	0.092	0.118	0.239	n/a
Extra Measurements Nine Parameter	Assumptions	Nine Parameter Reciprocal Invariance			
	Measurements	12			
	$\boldsymbol{\psi}$	{1-13} = {-134.0°, -48.7°, -6.0°, -44.7°, -95.6°, 138.2°, -145.1°, -121.4°, -84.0°, -58.4°, -31.9°, -7.0°, 28.9°}			
	$\boldsymbol{\theta}_G$	{1, 1, 2, 2, 3, 3, 4, 4, 5, 5, 6, 6}			
	$\boldsymbol{\theta}_A$	{7, 8, 8, 9, 9, 10, 10, 11, 11, 12, 12, 13}			
	w	7.79 rad (= 446.1°)			
		(0)	(-1)	(-2)	(-3)
	$\kappa_{2,RI}$	10.64	13.65	71.19	1242.2
	ξ_{RI}	17.01	20.04	81.39	1359.2
		Nine Param. RI Sample			
	mean$\{\|\delta\vec{\mathbf{M}}\|_2/\|\vec{\mathbf{M}}\|_2\}$	0.081	0.094	0.282	3.244

Table 4.4: Optimized designs for twelve measurement determination of reciprocal invariant Mueller matrices, considering the possibility of dropped measurements.

ments, different parameterization of wave plate angles, and different weighting of optimization objectives. The presented designs were chosen to represent an assortment of possible priorities for *in vivo* retinal polarimeter design, and demonstrate how those priorities may be incorporated into the optimization process.

4.6 Conclusion

In this section, optimal sets of angles have been reported for a rotating QWP partial polarimeter that measures RI MMs. These designs could be of practical use for a polarimeter making in vivo measurements of the human retina. Using simulations, it has been shown that if the sample is truly RI, a nine or ten measurement partial polarimeter can obtain similar error performance to a sixteen measurement full polarimeter that does not use the assumption of reciprocal invariance.

The analysis was based on a novel extension of existing full polarimeter optimization methods to partial polarimeters in the presence of symmetries. The methodology used in this chapter could be applied when the PSG and PSA consist of different optical elements than linear polarizers and QWPs, and for different symmetries than reciprocal invariance.

Chapter 5

Interpretation of Double Pass Mueller Matrices

5.1 Introduction

Once a set of MMs have been measured in an *in vivo* retinal polarimetry experiment, they must be interpreted in order to give insight into the nature of the sample. The double pass model described in chapter 3 writes the MM as a product

$$\mathbf{M}_{DP} = \mathbf{X}\,\mathbf{M}_{SP}^{T}\,\mathbf{X}\,\mathbf{Y}\,\mathbf{M}_{SP} \tag{3.16}$$

where $\mathbf{M}_{SP}$ is the *single pass MM*, and $\mathbf{X} \equiv \mathrm{diag}(1,\ 1,\ -1,\ 1)$ and $\mathbf{Y} \equiv \mathrm{diag}(1,\ 1,\ -1,\ -1)$ as defined in chapter 3[1]. It will be assumed that the MM measured in *in vivo* retinal polarimetry has this form, which is a stronger assumption than simply taking the MM to be RI as in the previous chapter. In the model, $\mathbf{M}_{SP}$ is representative of the properties of the cornea, lens, and retina in transmission[2]. $\mathbf{M}_{DP}$ is called the *double pass MM*, because it arises from two passes through the structures of the eye. $\mathbf{M}_{DP}$ can be interpreted by

[1] $\mathrm{diag}(a,\ b,\ c,\ d)$ refers to the 4×4 matrix with elements a, b, c, and d along the diagonal, and with all other entries equal to zero.

[2] A few methods exist for isolating the MM of the retina, known as *anterior segment compensation* [74, 100, 142, 141]. These methods assume that the cornea and lens together act as a linear retarder which is uniform with scanning position, and also require an assumption about the MM of part of the retinal image. In the idealized case of perfect anterior segment compensation, $\mathbf{M}_{SP}$ in equation 3.16 would represent the retina alone. More realistically, $\mathbf{M}_{SP}$ is always influenced by the cornea and lens, but this influence may be decreased using anterior segment compensation.

using the Lu-Chipman decomposition to extract polarimetric properties such as retardance, diattenuation, and depolarization [83] (see section 2.3.2). However, these properties are influenced by the reflection geometry of the model. Double pass polarimetry values are not equal to what would be measured for the same ocular structures in transmission. For example, it is possible for the double pass MM to have nonzero circular retardance even if the single pass MM contains no circular retardance, and vice versa. Therefore, it is important to understand the relationship between the single pass polarimetric properties, obtained from $\mathbf{M}_{SP}$, and the double pass properties obtained from $\mathbf{M}_{DP}$. This is especially relevant to the AD diagnosis project of Campbell Labs, because polarimetric data for retinal amyloid deposits has so far been collected in single pass transmission *ex vivo* retinal measurements, while future *in vivo* measurements will be double pass.

A number of authors have analyzed the properties of some MMs in double pass. In the field of *in vivo* retinal polarimetry, Hunter *et al.* [64], Bueno [24], and Knighton *et al.* [74] have each described cases in which $\mathbf{M}_{SP}$ is a sequence of linear retarders. Bueno also examined linear diattenuators in double pass, as well as the combination of a horizontal linear polarizer followed by a QWP oriented at 45° (which is essentially a circular polarizer) [24]. The behaviour of a circular polarizer in double pass was also shown by Azzam [13]. Lara discussed features of linear polarizers, circular retarders, and depolarization produced by scattering in double pass [80]. Vansteenkiste *et al.* and Wolfe and Chipman have described what happens to an elliptical retarder in double pass [132, 138]. Schönhofer and Kuball discussed samples with weak, non-depolarizing polarimetric properties in double pass [115]. Sheppard *et al.* derived equations relating the "c-vectors" of non-depolarizing single and double pass MMs, which contain information about retardance and diattenuation [117].

This chapter endeavors to show the relationship between single and double pass polarimetric properties as assessed using the Lu-Chipman decomposition, for general $\mathbf{M}_{SP}$ containing any amounts of retardance, diattenuation, and depolarization. This is attempted first algebraically and later using simulated $\mathbf{M}_{DP}$. A particular focus is placed on the inverse problem of inferring $\mathbf{M}_{SP}$ from $\mathbf{M}_{DP}$ (the forwards problem of calculating $\mathbf{M}_{DP}$ from $\mathbf{M}_{SP}$ is trivial using equation 3.16). However $\mathbf{M}_{DP}$ is RI and so has fewer degrees of freedom than $\mathbf{M}_{SP}$, meaning some of the polarimetry information in $\mathbf{M}_{SP}$ must "cancel out" and become unavailable in double pass. There is therefore more than one single pass MM $\mathbf{M}_{SP}$ that corresponds to any given $\mathbf{M}_{DP}$. This chapter shows how to calculate a full or partial set of solutions for $\mathbf{M}_{SP}$ in some conditions, and considers the range of single pass polarimetric properties that can lead to the same $\mathbf{M}_{DP}$. This aids in the interpretation of $\mathbf{M}_{DP}$ and also identifies which single pass polarimetric properties can be reliably inferred from $\mathbf{M}_{DP}$. Compared to the work of previous authors, these efforts are believed

to be unique in their focus on the inverse problem of inferring the Lu-Chipman form of $\mathbf{M}_{SP}$ from $\mathbf{M}_{DP}$.

Subsections 5.2.1 and 5.2.2 treat the relationship between $\mathbf{M}_{DP}$ and $\mathbf{M}_{SP}$ when $\mathbf{M}_{SP}$ is a retarder or is non-depolarizing (*i.e.* may contain both retardance and diattenuation but no depolarization) respectively. While the goal of this chapter is to address this relationship for general $\mathbf{M}_{SP}$ with any combination of polarimetric properties, these simpler cases are more tractable and lead to conclusions that can be extended to general $\mathbf{M}_{SP}$. It is shown in both situations how to calculate all possible $\mathbf{M}_{SP}$ that correspond to a given double pass MM. Sets of polarimetric properties that lead to the same double pass MM are visualized in 3D space. This study shows the ambiguity in $\mathbf{M}_{SP}$ and specifies which information "cancels out" in double pass. In contrast to the work of Sheppard *et al.* [117], this is done using polarimetric properties as given by Lu-Chipman decomposition, rather than c-vectors. The derivation in subsection 5.2.2 is independent of the results of Sheppard *et al.* [117], and provides a different perspective on the relationship between single and double pass non-depolarizing MMs. Most importantly, using the Lu-Chipman approach facilitates the extension of the results to the case of general, depolarizing $\mathbf{M}_{SP}$. This is done in subsection 5.2.3, showing that several of the conclusions of subsections 5.2.1 and 5.2.2 apply even when depolarization is present.

The relationship between single and double pass MMs in the presence of depolarization is more complex, and it was not found how to calculate all possible $\mathbf{M}_{SP}$ for a given $\mathbf{M}_{DP}$. Section 5.3 and Appendix E instead develop a "double pass decomposition" that finds a set of possible $\mathbf{M}_{SP}$, by assuming that the depolarization matrix is diagonal. Ossikovski *et al.* have stated that many important types of depolarizing media can be written in terms of diagonal depolarization matrices [97]. This new decomposition is an adaptation of the symmetric decomposition of Ossikovski [95]. This provides a novel way of interpreting a depolarizing $\mathbf{M}_{DP}$ by calculating possible single pass polarimetric properties.

The double pass decomposition can be applied to any RI MM, not only to double pass MMs. The measurement equations described in chapter 4 are guaranteed to return RI MMs. It is conceivable that, due to experimental errors or a failure of the double pass model to represent the sample, the experimental RI MM may not be mathematically consistent with the double pass model. The double pass decomposition algorithm can detect such cases. Applied to experimental RI MMs obtained from *in vivo* retinal polarimetry, it could be used as a test of the validity of the double pass model 3.16.

Finally, in section 5.4 simulations are used to compare single and double pass polarimetric properties, as assessed using Lu-Chipman decomposition. These simulations are also used to test methods of predicting single pass properties from the double pass MM.

The work of this chapter has several applications to the work of the Campbell Labs Alzheimer's diagnosis project. It highlights which single pass polarimetry properties can be reliably inferred from $\mathbf{M}_{DP}$, and which cannot. This is important for other lab members analyzing *ex vivo* retinal MMs in transmission (*e.g.* [106]), so that their work can be based on polarimetric properties that are accessible to *in vivo* retinal polarimetry. Applied to a RI MM measured in *in vivo* retinal polarimetry, the novel double pass decomposition can test if it is mathematically consistent with the double pass model, and provide possible single pass polarimetric properties. This may be used alongside or instead of the Lu-Chipman decomposition of $\mathbf{M}_{DP}$ to better understand the results of *in vivo* retinal polarimetry.

5.2 Algebraic Relationships Between Single and Double Pass Mueller Matrices

This section explores algebraically the relationship between the Lu-Chipman decomposed forms of the double pass and single pass MMs. However, the double pass MM defined by equation 3.16 uses a different coordinate frame for the input and output Stokes vectors as a consequence of the conventions used in section 3.2. Several authors suggest that in reflection-type measurements, the same coordinate frame should be used for both input and output Stokes vectors [24, 78, 105]. This choice does not appear to be universal (see *e.g.* [17] and its use as an example in [53]). Representing the input and output Stokes vectors in the same coordinate frame gives a new MM

$$\overline{\mathbf{M}}_{DP} = \mathbf{Y}\,\mathbf{M}_{DP}. \tag{5.1}$$

$\overline{\mathbf{M}}_{DP}$ and $\mathbf{M}_{DP}$ in general have very different Lu-Chipman properties. Appendix C provides an explicit argument for why the Lu-Chipman decomposition of $\overline{\mathbf{M}}_{DP}$ is expected to provide more physically meaningful values than that of $\mathbf{M}_{DP}$.

Incorporating this coordinate change into the double pass model,

$$\begin{aligned}
\mathbf{M}_{DP} &\equiv \mathbf{X}\,\mathbf{M}_{SP}^{T}\,\mathbf{X}\,\mathbf{Y}\,\mathbf{M}_{SP} \quad \Longrightarrow \\
\overline{\mathbf{M}}_{DP} &\equiv \mathbf{Y}\,\mathbf{X}\,\mathbf{M}_{SP}^{T}\,\mathbf{X}\,\mathbf{Y}\,\mathbf{M}_{SP} \\
&= \mathbf{Q}\,\mathbf{M}_{SP}^{T}\,\mathbf{Q}\,\mathbf{M}_{SP}.
\end{aligned} \tag{5.2}$$

In this section, the relationship between the polarimetric properties of $\mathbf{M}_{SP}$ and $\overline{\mathbf{M}}_{DP}$ is investigated algebraically. This is done for three types of single pass MMs of increasing generality. Subsection 5.2.1 is focused on retarders. Several of the results are well known

in the literature [24, 41, 132, 138], but to the author's knowledge it has not been shown explicitly before how to calculate all possible retarder $\mathbf{M}_{SP}$ that give the same $\overline{\mathbf{M}}_{DP}$.

This result is applied in subsection 5.2.2 (augmented by Appendix D), which finds every possible non-depolarizing $\mathbf{M}_{SP}$ corresponding to a non-depolarizing $\overline{\mathbf{M}}_{DP}$. This is done while applying the Lu-Chipman decomposition to both $\mathbf{M}_{SP}$ and $\overline{\mathbf{M}}_{DP}$. The set of possible single pass polarimetric properties that lead to the same $\overline{\mathbf{M}}_{DP}$ are visualized in 3D space. The results can be summarized as a set of transformations of $\mathbf{M}_{SP}$ that can be performed without altering $\overline{\mathbf{M}}_{DP}$.

These results are partially extended to general $\mathbf{M}_{SP}$ (including any amounts of retardance, diattenuation, and depolarization) in subsection 5.2.3. However, the problem of finding all possible $\mathbf{M}_{SP}$ in this case is too complex for this thesis. Sections 5.3 and 5.4 will further address the relationship between single and double pass MMs in the presence of depolarization using other methods.

5.2.1 Retarder Mueller Matrices in Double Pass

It is well known that if the sample is a linear retarder, its retardance doubles in double pass [24, 49, 74, 78, 138]. Mathematically, this can be seen by inserting $\mathbf{M}_{SP} = \mathbf{M}_{LR}(R_L, \theta)$ (equation 2.39) into equation 5.2, from which it follows that $\overline{\mathbf{M}}_{DP} = \mathbf{M}_{LR}(2R_L, \theta)$. On the other hand, an ordinary[3] circular retarder cancels itself out in double pass [41, 80, 138]. The reflection MM $\mathbf{Y}$ reverses the handedness of incident light, and so the effects of the first pass are reversed by the second. Accordingly, using $\mathbf{M}_{SP} = \mathbf{M}_{CR}(R_C)$, equation 5.2 results in $\overline{\mathbf{M}}_{DP} = \mathbb{I}$. Lastly, as noted by Vansteenkiste *et al.* [132], any half wave linear retarder will contribute a full wave of retardance in double pass. A full wave of retardance has no effect on an input Stokes vector: $\overline{\mathbf{M}}_{DP} = \mathbf{M}_{LR}(2\pi, \theta) = \mathbb{I}$. Mathematically speaking, a half wave linear retarder will cancel itself out in double pass, just like a circular retarder.

In the most general case, if $\mathbf{M}_{SP}$ is an elliptical retarder, then it is always possible to write it as the product of a linear retarder and a circular retarder:

$$\begin{aligned}\mathbf{M}_{SP} &= \mathbf{M}_R(R_H, R_{45}, R_C) \\ &= \mathbf{M}_{CR}(R'_C)\mathbf{M}_{LR}(R'_L, \theta') \quad [86,\ 65].\end{aligned}$$

[3]Faraday rotation is circular retardance that occurs in gyrotropic media in an external magnetic field [41, 87]. Faraday rotators disobey the reciprocity theorem 3.11 and so have different properties in double pass than other types of circular retarders, such as a medium consisting of chiral molecules [41]. In this thesis it is assumed that all single pass MMs are related to their direction-reversed versions by equation 3.11.

The inner circular retarder will cancel in double pass, resulting in $\overline{\mathbf{M}}_{DP} = \mathbf{M}_{LR}(2R'_L, \theta')$. Therefore, regardless of the amount of circular retardance in $\mathbf{M}_{SP}$, $\overline{\mathbf{M}}_{DP}$ will be a linear retarder. However, generally $R_L \neq R'_L$, $\theta \neq \theta'$, and $R_C \neq R'_C$. Instead, they are related by the set of equations[4]

$$\begin{aligned} R'_L &= 2\arccos\left(\sqrt{\frac{R_C^2}{R^2}\sin^2(R/2) + \cos^2(R/2)}\right) \quad [86] \\ R'_C &= \text{sign}(R_C)\arccos\left(\frac{2\cos^2(R/2)}{\cos^2(R'_L/2)} - 1\right) \\ \theta' &= \theta + \frac{R'_C}{4} \end{aligned} \tag{5.3}$$

where as usual

$$R = \sqrt{R_L^2 + R_C^2}.$$

In the following sections it will be important to distinguish between the retardance parameters that treat $\mathbf{M}_R$ as a single elliptical retarder (equations 2.38), and those that treat it as a *compound* retarder consisting of a linear retarder followed by a circular retarder (equations 5.3). Primed R'_L, θ', and R'_C will always refer to the compound version, while the unprimed versions are the ordinary retardance parameters.

Recall from section 2.2 that there are multiple values of retardance that can give the same retardance matrix. Equations 2.38 always return a value that is in the range $0 < R < \pi$. Likewise, equation 5.3 implies that $R'_L < \pi$, so the true double pass retardance is $2R'_L < 2\pi$. However, the retardance $R_{L,DP}$ that is calculated from $\overline{\mathbf{M}}_{DP}$ using equations 2.38 is always in the range $0 < R_{L,DP} < \pi$. It can be shown that the single pass (R'_L, θ') and double pass $(R_{L,DP}, \theta_{DP})$ are related by

$$\begin{aligned} R'_L < \pi/2 &\implies R_{L,DP} = 2R'_L \quad \text{and} \quad \theta_{DP} = \theta' \\ R'_L > \pi/2 &\implies R_{L,DP} = 2\pi - 2R'_L \quad \text{and} \quad \theta_{DP} = \theta' - \pi/2. \end{aligned} \tag{5.4}$$

These results can be used to find all possible retarder $\mathbf{M}_{SP}$ given a retarder $\overline{\mathbf{M}}_{DP}$. It has already been shown that $\overline{\mathbf{M}}_{DP}$ must be a linear retarder. Inverting the inequalities 5.4,

[4]The expressions for R'_C and θ' given here have been altered from those found in [86]. The expression for R'_C is equivalent apart from the addition of the sign function, which assures the correct handedness. The correctness of equations 5.3 was confirmed algebraically and numerically using Matlab.

all possible retarder $\mathbf{M}_{SP}$ can be written

$$\mathbf{M}_{SP} = \mathbf{M}_{CR}(R'_C)\,\mathbf{M}_{LR}(R_{L,DP}/2, \theta_{DP}) \tag{5.5}$$

or

$$\mathbf{M}_{SP} = \mathbf{M}_{CR}(R'_C)\,\mathbf{M}_{LR}(\pi - R_{L,DP}/2, \theta_{DP} + \pi/2) \tag{5.6}$$

for $0 < R'_C < \pi$.

Because a circular retarder cancels itself out in double pass, any $\mathbf{M}_{SP}$ can be left multiplied by any circular retarder without changing $\overline{\mathbf{M}}_{DP}$. For a $\mathbf{M}_{SP}$ of the form of equation 5.5, clearly all other $\mathbf{M}_{SP}$ obeying equation 5.5 can be calculated through left multiplication by a circular retarder. A halfwave linear retarder $\mathbf{M}_{HLR}$ also cancels itself out in double pass. A halfwave linear retarder with azimuth α can be written

$$\mathbf{M}_{HLR}(\alpha) = \begin{bmatrix} 1 & 0 & 0 & 0 \\ 0 & \cos 4\alpha & \sin 4\alpha & 0 \\ 0 & \sin 4\alpha & -\cos 4\alpha & 0 \\ 0 & 0 & 0 & -1 \end{bmatrix} \quad [39] \tag{5.7}$$

$$= \begin{bmatrix} 1 & 0 & 0 & 0 \\ 0 & \cos 4\alpha & -\sin 4\alpha & 0 \\ 0 & \sin 4\alpha & \cos 4\alpha & 0 \\ 0 & 0 & 0 & 1 \end{bmatrix} \begin{bmatrix} 1 & 0 & 0 & 0 \\ 0 & 1 & 0 & 0 \\ 0 & 0 & -1 & 0 \\ 0 & 0 & 0 & -1 \end{bmatrix} \tag{5.8}$$

$$= \mathbf{M}_{CR}(4\alpha)\,\mathbf{Y}. \tag{5.9}$$

The action of the $\mathbf{Y}$ on a linear retarder was analyzed algebraically using MATLAB, and it was found that

$$\begin{aligned} &\mathbf{M}_{HLR}(\alpha)\,\mathbf{M}_{CR}(R'_C)\,\mathbf{M}_{LR}(R_{L,DP}/2, \theta_{DP}) \\ =&\mathbf{M}_{CR}(4\alpha)\,\mathbf{Y}\,\mathbf{M}_{CR}(R'_C)\,\mathbf{M}_{LR}(R_{L,DP}/2, \theta_{DP}) \\ =&\mathbf{M}_{CR}(4\alpha)\,\mathbf{Y}\,\mathbf{M}_{CR}(R'_C)\,(\mathbf{Y}\,\mathbf{Y})\,\mathbf{M}_{LR}(R_{L,DP}/2, \theta_{DP}) \\ =&\mathbf{M}_{CR}(4\alpha)\,\mathbf{M}_{CR}(-R'_C)\,\mathbf{M}_{CR}(4\theta)\,\mathbf{M}_{LR}(\pi - R_L, \theta + \pi/2) \\ =&\mathbf{M}_{CR}(4\alpha - R'_C + 4\theta)\,\mathbf{M}_{LR}(\pi - R_L, \theta + \pi/2). \end{aligned}$$

That is, left multiplying equation 5.5 by a half wave linear retarder gives a new $\mathbf{M}_{SP}$ with a form equivalent to equation 5.6. Similarly, it can be shown that left multiplying equation 5.6 by a half wave linear retarder gives a new $\mathbf{M}_{SP}$ with a form equivalent to equation 5.5. Therefore, given any retarder $\mathbf{M}_{SP}$, all other possible single pass retarders that lead to the same $\overline{\mathbf{M}}_{DP}$ are related to $\mathbf{M}_{SP}$ through left multiplication by either a

circular retarder or a half wave linear retarder. Therefore equations 5.5 and 5.6 can be summarized as

$$\mathbf{M}_{SP} = \mathbf{M}_{CR/HLR}\,\mathbf{M}_{LR}(R_{L,DP}/2, \theta_{DP}) \tag{5.10}$$

where $\mathbf{M}_{CR/HLR}$ is any circular retarder or half wave linear retarder. Explicitly,

$$\begin{aligned}
\mathbf{Q}\,\mathbf{M}_{SP}^T\,\mathbf{Q}\,\mathbf{M}_{SP} &= \mathbf{Q}\,\mathbf{M}_{LR}(R_{L,DP}/2, \theta_{DP})^T\,\mathbf{M}_{CR/HLR}^T\mathbf{Q}\,\mathbf{M}_{CR/HLR}\,\mathbf{M}_{LR}(R_{L,DP}/2, \theta_{DP}) \\
&= \mathbf{Q}\,\mathbf{M}_{LR}(R_{L,DP}/2, \theta_{DP})^T\,\mathbf{Q}(\mathbf{Q}\,\mathbf{M}_{CR/HLR}^T\mathbf{Q}\,\mathbf{M}_{CR/HLR})\mathbf{M}_{LR}(R_{L,DP}/2, \theta_{DP}) \\
&= \mathbf{Q}\,\mathbf{M}_{LR}(R_{L,DP}/2, \theta_{DP})^T\,\mathbf{Q}\,\mathbf{M}_{LR}(R_{L,DP}/2, \theta_{DP}) \\
&= \mathbf{M}_{LR}(R_{L,DP}, \theta_{DP}) = \overline{\mathbf{M}}_{DP}.
\end{aligned}$$

When $\mathbf{M}_{SP}$ is treated as a general or elliptical retarder, the solutions 5.10 permit a wide range of possible retardance vectors $\mathbf{R}$. For example, figure 5.1 shows every possible $\mathbf{R}$ corresponding to the randomly generated double pass retarder MM

$$\overline{\mathbf{M}}_{DP} = \begin{bmatrix} 1 & 0 & 0 & 0 \\ 0 & 0.9489 & 0.1405 & 0.2825 \\ 0 & 0.1405 & 0.6136 & -0.7770 \\ 0 & -0.2825 & 0.7770 & 0.5625 \end{bmatrix}. \tag{5.11}$$

The red line in figure 5.1 is the set of solutions following equation 5.5, while the blue line is the set following equation 5.6. Equation 5.5 with $R'_C = 0$ gives the minimum retardance possible in order to explain $\overline{\mathbf{M}}_{DP}$, while the maximum retardance is always π.

5.2.2 Non-depolarizing Mueller Matrices in Double Pass

Next, allow $\mathbf{M}_{SP}$ and $\overline{\mathbf{M}}_{DP}$ to have some diattenuation as well as retardance, but no depolarization. As in subsection 5.2.1, there will be multiple possible solutions for the single pass MM. The Lu-Chipman decomposition of any non-depolarizing MM is

$$\mathbf{M} = c\mathbf{M}_R\mathbf{M}_D$$

where c is a scalar constant with $0 \leq c \leq 1$ [83]. Starting with equation 5.2 and decomposing both $\overline{\mathbf{M}}_{DP}$ and $\mathbf{M}_{SP}$ in this way,[5]

$$c_{DP}\mathbf{M}_{R,DP}\,\mathbf{M}, D_{DP} = c^2\mathbf{Q}\,\mathbf{M}_D^T\,\mathbf{M}_R^T\,\mathbf{Q}\,\mathbf{M}_R\,\mathbf{M}_D. \tag{5.12}$$

[5]It is possible for a depolarizing single pass matrix $\mathbf{M}_{SP}$ to lead to a non-depolarizing $\overline{\mathbf{M}}_{DP}$. Such cases are ignored for simplicity.

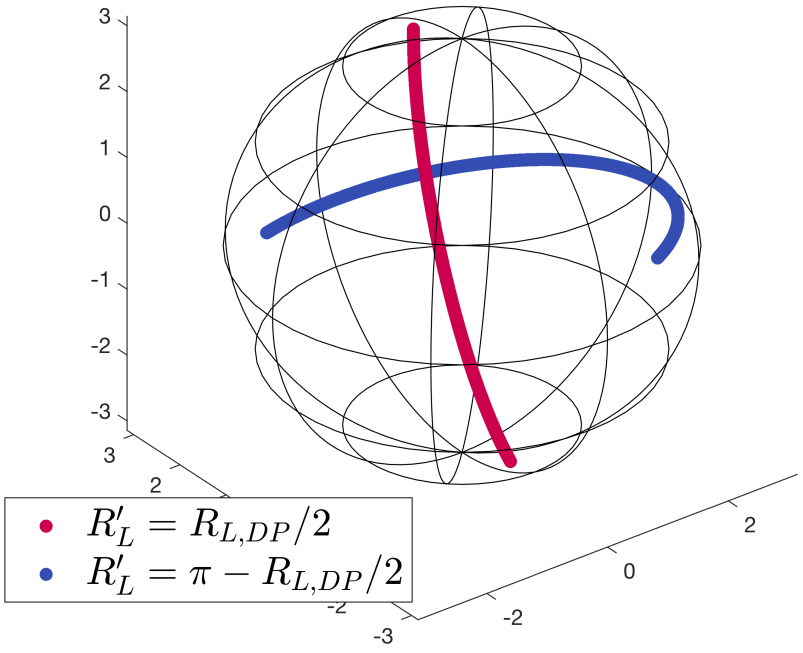

Figure 5.1: Possible locations of the single pass retardance vector $\mathbf{R}$ for the randomly generated double pass retarder MM 5.11, with a reference sphere of radius π.

Using equations 2.37 and 2.29,

$$\overline{\mathbf{M}}_{DP} = \frac{c_{DP}}{1+D_{DP}} \begin{bmatrix} 1 & \mathbf{D}_{DP}^T \\ \mathbf{m}_{R,DP}\,\mathbf{D}_{DP} & \mathbf{m}_{R,DP}\,\mathbf{m}_{D,DP} \end{bmatrix} \tag{5.13}$$

$$= \frac{c^2}{(1+D)^2} \begin{bmatrix} 1+\mathbf{D}^T\,\mathbf{m}_q\,\mathbf{D} & \mathbf{D}^T+\mathbf{D}^T\,\mathbf{m}_q\,\mathbf{m}_D \\ \mathbf{q}\,\mathbf{D}+\mathbf{q}\,\mathbf{m}_D^T\,\mathbf{m}_q\,\mathbf{D} & \mathbf{q}\,\mathbf{D}\,\mathbf{D}^T+\mathbf{q}\,\mathbf{m}_D^T\,\mathbf{m}_q\,\mathbf{m}_D \end{bmatrix} \tag{5.14}$$

$$\mathbf{m}_q \equiv \mathbf{m}_R^T\,\mathbf{q}\,\mathbf{m}_R. \tag{5.15}$$

Because $\mathbf{q}$ is a diagonal matrix and $\mathbf{m}_R^T = \mathbf{m}_R^{-1}$, equation 5.15 provides an eigen decomposition of $\mathbf{m}_q$ [60]. Therefore, $\mathbf{m}_q$ has two distinct eigenvalues, ± 1. The -1 eigenvalue has a multiplicity of one, and the associated eigenvector $\hat{\mathbf{v}}$ is given by the last row of $\mathbf{m}_R$: $\hat{\mathbf{v}} \equiv \mathbf{m}_R^T\,[0,\,0,\,1]^T$. The $+1$ eigenvalue has a multiplicity of two, and so is associated with a two dimensional eigenspace. Because $\mathbf{m}_R$ is orthogonal, this eigenspace is the plane orthogonal to $\hat{\mathbf{v}}$. Consider first the case in which $\mathbf{D}$ is parallel to $\hat{\mathbf{v}}$. Then, $\mathbf{m}_q\,\mathbf{D} = -\mathbf{D}$. Applying this to equation 5.14, it follows that

$$\overline{\mathbf{M}}_{DP} = \frac{c^2(1-D)}{(1+D)} \begin{bmatrix} 1 & \mathbf{0}^T \\ \mathbf{0} & \mathbf{q}\,\mathbf{m}_R^T\,\mathbf{q}\mathbf{m}_R \end{bmatrix} \tag{5.16}$$

that is, the diattenuation only affects the overall transmission of the double pass matrix, which is otherwise the same as a retarder in double pass. Generally, c is not known and may be influenced by the illumination and gain settings of the polarimeter (see section 2.3), so it is not feasible to use the overall transmission to calculate D. Equation 5.16 also shows that the assumption that $\mathbf{D}$ is parallel to $\hat{\mathbf{v}}$ is inconsistent unless $D_{DP} = 0$.

If the single pass $\mathbf{M}_{SP}$ has zero retardance, then $\mathbf{D}$ is parallel to $\hat{\mathbf{v}}$ if and only if $\mathbf{M}_{SP}$ is a circular diattenuator. Therefore, equation 5.16 shows that a circular diattenuator, multiplied by a scalar, will cancel itself out in double pass:

$$\mathbb{I} = \mathbf{Q}\,(\sqrt{\frac{1+|D_C|}{1-|D_C|}}\mathbf{M}_{CD}^T)\,\mathbf{Q}\,(\sqrt{\frac{1+|D_C|}{1-|D_C|}}\mathbf{M}_{CD}) \tag{5.17}$$

$$\mathbf{M}_{CD}(D_C) \equiv \frac{1}{1+|D_C|} \begin{bmatrix} 1 & 0 & 0 & D_C \\ 0 & \sqrt{1-D_C^2} & 0 & 0 \\ 0 & 0 & \sqrt{1-D_C^2} & 0 \\ D_C & 0 & 0 & 1 \end{bmatrix}.$$

If instead $\mathbf{D}$ is perpendicular to $\hat{\mathbf{v}}$, then $\mathbf{m}_q\mathbf{D} = +\mathbf{D}$. It will be shown that this assumption uniquely determines the diattenuation vector, which will be called the *principal*

diattenuation vector and labelled $\mathbf{D}_p$. Later it will be proved that $\mathbf{D}_p$ is related in a simple way to the double pass diattenuation vector, and D_p is the minimum possible single pass diattenuation, hence the name principal. Likewise $c = c_p$ is uniquely determined, but the retardance can take a range of possible values. Inserting $\mathbf{m}_q\mathbf{D}_p = +\mathbf{D}_p$ into equation 5.14,

$$\overline{\mathbf{M}}_{DP} = \frac{c_p^2}{(1+D_p)^2}\begin{bmatrix} 1+D_p^2 & 2\mathbf{D}_p^T \\ 2\mathbf{q}\,\mathbf{D}_p & \mathbf{q}\,\mathbf{m}_q\left((1-D_p^2)\mathbb{I} + 2\mathbf{D}_p\,\mathbf{D}_p^T\right) \end{bmatrix} \tag{5.18}$$

Comparing the $(1,1)$ element of 5.18 with equation 5.13,

$$\frac{c_{DP}}{1+D_{DP}} = \frac{c_p^2(1+D_p^2)}{(1+D_p)^2}. \tag{5.19}$$

Comparing $(1, 2:4)$ elements of equations 5.18 and 5.13 and applying equation 5.19,

$$\begin{aligned} \frac{c_{DP}}{1+D_{DP}}\mathbf{D}_{DP} = \frac{2c_p^2}{(1+D_p)^2}\mathbf{D}_p \quad &\Longrightarrow \\ \mathbf{D}_{DP} = \frac{2}{1+D_p^2}\mathbf{D}_p. \end{aligned} \tag{5.20}$$

Equation 5.20 shows how single and double pass diattenuation, as calculated using the Lu-Chipman decomposition, may be related to each other. For a weak single pass diattenuator ($D_p^2 \approx 0$), the diattenuation magnitude is approximately doubled in double pass. For a strong single pass diattenuator ($D_p^2 \approx 1$), the diattenuation magnitudes are approximately the same. However, this is only strictly true under the assumption that $\mathbf{D}_p$ is perpendicular to $\hat{\mathbf{v}}$.

Equation 5.20 shows that $\mathbf{D}_{DP}$ and $\mathbf{D}_p$ are parallel, and are related by a positive scalar. In order to obtain $\mathbf{D}_p$ as a function of $\mathbf{D}_{DP}$, write $\mathbf{D}_p = a\mathbf{D}_{DP}$ for a yet unknown positive scalar a. Squaring both sides of equation 5.20 and plugging this in,

$$\begin{aligned} D_{DP}^2 = \frac{4a^2D_{DP}^2}{(1+a^2D_{DP}^2)^2} \quad &\Longrightarrow \\ 0 = D_{DP}^4a^4 + (2D_{DP}^2 - 4)a^2 + 1 \quad &\Longrightarrow \\ a^2 = \frac{2 - D_{DP}^2 \pm 2\sqrt{1-D_{DP}^2}}{D_{DP}^4} \end{aligned} \tag{5.21}$$

where the quadratic equation has been used to solve for a^2. The magnitude of the diattenuation vector must always be between zero and one, so $1 \geq D_p^2 = a^2D_{DP}^2$ and $1 \geq D_{DP}^2$.

Therefore,

$$\begin{aligned} 1 \geq a^2 D_{DP}^2 \quad &\Longrightarrow \\ 1 \geq \frac{2 - D_{DP}^2 \pm 2\sqrt{1 - D_{DP}^2}}{D_{DP}^2} \quad &\Longrightarrow \\ D_{DP}^2 \geq 1 \pm \sqrt{1 - D_{DP}^2} \quad &\Longrightarrow \\ 1 \geq D_{DP}^2 \geq 1 \pm \sqrt{1 - D_{DP}^2} \end{aligned}$$

This inequality can only be satisfied by taking the negative-signed solution for a. Finally, it follows that

$$\begin{aligned} a^2 &= \frac{2 - D_{DP}^2 - 2\sqrt{1 - D_{DP}^2}}{D_{DP}^4} \\ &= \frac{(1 - \sqrt{1 - D_{DP}^2})^2}{D_{DP}^4} \quad \Longrightarrow \\ a &= \frac{1 - \sqrt{1 - D_{DP}^2}}{D_{DP}^2} \qquad (5.22) \\ \mathbf{D}_p &= \frac{1 - \sqrt{1 - D_{DP}^2}}{D_{DP}^2} \mathbf{D}_{DP} \qquad (5.23) \end{aligned}$$

The positive square root was taken because equation 5.20 implies that a is positive. a is uniquely determined by 5.22 and so $\mathbf{D}_p$ is uniquely determined. a is exactly the factor that appears in the definition of the diattenuation matrix (equation 2.29): $\mathbf{m}_{DP} = \sqrt{1 - D_{DP}^2}\mathbb{I} + a\mathbf{D}_{DP}\mathbf{D}_{DP}^T$.

Considering equation 5.19 and using $D_p = aD_{DP}$, it can be shown that $c_p = \sqrt{c_{DP}}$. Next, using the principal diattenuation vector and comparing equations 5.13 and 5.18, the lower right 3×3 submatrix of $\overline{\mathbf{M}}_{DP}$ is given by

$$\begin{aligned} \frac{c_{DP}}{1 + D_{DP}} \mathbf{m}_{R,DP}\, \mathbf{m}_{D,DP} &= \frac{c_p^2}{(1 + D_p)^2} \mathbf{q}\, \mathbf{m}_q \left((1 - D_p^2)\mathbb{I} + 2\mathbf{D}_p\, \mathbf{D}_p^T\right) \quad &\Longrightarrow \\ (1 + D_p^2)\mathbf{m}_{R,DP}\, \mathbf{m}_{D,DP} &= \mathbf{q}\, \mathbf{m}_q \left((1 - D_p^2)\mathbb{I} + 2\mathbf{D}_p\, \mathbf{D}_p^T\right) \quad &\Longrightarrow \\ (1 + a^2 D_{DP}^2)\mathbf{m}_{R,DP}\, \mathbf{m}_{D,DP} &= \mathbf{q}\, \mathbf{m}_q \left((1 - a^2 D_{DP}^2)\mathbb{I} + 2a^2 \mathbf{D}_{DP}\, \mathbf{D}_{DP}^T\right) \quad &\Longrightarrow \\ (2a)\mathbf{m}_{R,DP}\, \mathbf{m}_{D,DP} &= \mathbf{q}\, \mathbf{m}_q \left(2a\sqrt{1 - D_{DP}^2}\mathbb{I} + 2a^2 \mathbf{D}_{DP}\, \mathbf{D}_{DP}^T\right) \quad &\Longrightarrow \\ \mathbf{m}_{R,DP}\, \mathbf{m}_{D,DP} &= \mathbf{q}\, \mathbf{m}_q\, \mathbf{m}_{D_{DP}} \qquad (5.24) \end{aligned}$$

where the identities $1 + a^2 D_{DP}^2 = 2a$ and $1 - a^2 D_{DP}^2 = 2a\sqrt{1 - D_{DP}^2}$ can be proved using equation 5.22. Assuming $D_{DP} \neq 1$, $\mathbf{m}_{D,DP}$ is invertible, and

$$\begin{aligned}\mathbf{m}_{R,DP} &= \mathbf{q}\,\mathbf{m}_q \\ &= \mathbf{q}\,\mathbf{m}_R^T\,\mathbf{q}\,\mathbf{m}_R.\end{aligned}$$

This is the 3×3 submatrix of a retarder in double pass, which was analyzed in subsection 5.2.1. This permits a range of different $\mathbf{m}_R$. Let the principle retardance matrix $\mathbf{m}_{R_p}$ be the version with the minimum possible retardance, which is obtained by simply halving the retardance of $\mathbf{m}_{R,DP}$. It also follows from subsection 5.2.1 that $\mathbf{m}_{R,DP}$ has zero circular retardance. This is a conclusion about $\overline{\mathbf{M}}_{DP}$ itself that is independent of the assumption that $\mathbf{D}$ is perpendicular to $\hat{\mathbf{v}}$: all nondepolarizing, double pass MMs have zero circular retardance.

If $D_{DP} = 1$, then it follows from 5.23 that $\mathbf{D}_p = \mathbf{D}_{DP}$. Equation 5.24 reduces to

$$\mathbf{q}\,\mathbf{D}_{DP} = \mathbf{q}\,\mathbf{m}_q\,\mathbf{D}_{DP}. \tag{5.25}$$

This does not uniquely define $\mathbf{m}_q$. The Lu-Chipman decomposition of $\overline{\mathbf{M}}_{DP}$ also relies on $\mathbf{m}_{D,DP}$ being invertible [53, 83]. If $D_{DP} = 1$, then any $\mathbf{m}_{R,DP}$ such that $\mathbf{m}_{R,DP}\,\mathbf{D}_{DP} = \mathbf{q}\,\mathbf{D}_{DP}$ is valid[6]. This equation is identical in form to equation 5.25, with $\mathbf{q}\,\mathbf{m}_q$ replaced by $\mathbf{m}_{R,DP}$, and both matrices must be orthogonal with a determinant of $+1$. Therefore, $\mathbf{m}_{R,DP}$ and $\mathbf{q}\,\mathbf{m}_q$ are both constrained to the same range of possible values. One can optionally choose them to be equal, in continuity with the $D_{DP} \neq 1$ case described above. When $D_{DP} = 1$, Lu and Chipman have shown how to find $\mathbf{m}_{R,DP}$ having the minimum possible retardance [83]. This retardance, which must be linear, can then be halved to obtain the minimum possible single pass retardance $\mathbf{R}_p$.

Given any non-depolarizing $\overline{\mathbf{M}}_{DP}$, these results can be used to calculate a possible single pass matrix $\mathbf{M}_p$. First, perform the Lu-Chipman decomposition of $\overline{\mathbf{M}}_{DP}$ to obtain c_{DP}, $\mathbf{D}_{DP}$, and $\mathbf{R}_{DP}$. Then, let the single pass vectors be given by $\mathbf{D}_p = a\mathbf{D}_{DP}$ (or $\mathbf{D}_p = 0$ if $\mathbf{D}_{DP} = 0$) and $\mathbf{R}_p = \mathbf{R}_{DP}/2$, and take $c_p = \sqrt{c_{DP}}$. Then $\mathbf{M}_p = c_p \mathbf{M}_{R_p}\,\mathbf{M}_{D_p}$ is a valid single pass matrix obeying $\overline{\mathbf{M}}_{DP} = \mathbf{Q}\,\mathbf{M}_p^T\,\mathbf{Q}\,\mathbf{M}_p$. $\mathbf{M}_p$ has the unique property that its diattenuation and retardance vectors are both parallel to the corresponding double pass diattenuation and retardance vectors.

Now that one possible single pass MM can be determined, others may be found by left multiplying it by a MM that cancels out in double pass. It has been shown that the

[6] Assuming, as always in this subsection, that $\overline{\mathbf{M}}_{DP}$ is non-depolarizing.

matrices $\mathbf{M}_{CR/HLR}$ and $(1+|D'_C|)/(1-|D'_C|)\mathbf{M}_{CD}(D'_C)$ all have this property. Therefore, the MM

$$\mathbf{M}_{SP} = c_p \frac{1+|D'_C|}{1-|D'_C|} \mathbf{M}_{CR/HLR}\, \mathbf{M}_{CD}(D'_C)\, \mathbf{M}_{R_p}\, \mathbf{M}_{D_p} \tag{5.26}$$

for $-1 < D'_C < 1$ also obeys $\overline{\mathbf{M}}_{DP} = \mathbf{Q}\, \mathbf{M}_{SP}^T\, \mathbf{Q}\, \mathbf{M}_{SP}$. Equation 5.26 can be rewritten as

$$\begin{aligned}
\mathbf{M}_{SP} &= c_p \frac{1+|D'_C|}{1-|D'_C|} \mathbf{M}_{CR/HLR}\, \mathbf{M}_{R_p}\, (\mathbf{M}_{R_p}^T\, \mathbf{M}_{CD}(D'_C)\, \mathbf{M}_{R_p})\, \mathbf{M}_{D_p} \\
&= c_p \frac{1+|D'_C|}{1-|D'_C|} \mathbf{M}_{CR/HLR}\, \mathbf{M}_{R_p}\, (c_B\, \mathbf{M}_{R_B}\, \mathbf{M} D_B) \\
&= c\, \mathbf{M}_R\, \mathbf{M}_D \\
c &= c_B\, c_p \frac{1+|D'_C|}{1-|D'_C|} \qquad (5.27) \\
\mathbf{M}_R &= \mathbf{M}_{CR/HLR}\, \mathbf{M}_{R_p}\, \mathbf{M}_{R_B} \qquad (5.28) \\
\mathbf{M}_D &= \mathbf{M}_{D_B}
\end{aligned}$$

where the Lu-Chipman decomposition has been used to rewrite

$$\begin{aligned}
\mathbf{M}_B &\equiv (\mathbf{M}_{R_p}^T\, \mathbf{M}_{CD}(D'_C)\, \mathbf{M}_{R_p})\, \mathbf{M}_{D_p} \qquad (5.29) \\
&= c_B\, \mathbf{M}_{R_B}\, \mathbf{M}_{D_B}.
\end{aligned}$$

$\mathbf{M}_R$ and $\mathbf{M}_D$ give the retardance and diattenuation of the new single pass MM. $\mathbf{M}_R$ differs from $\mathbf{M}_{R_p}$ both by the usual left multiplication by $\mathbf{M}_{CR/HLR}$ and by right multiplication by $\mathbf{M}_{R_B}$. It is possible to obtain an expression for $\mathbf{M}_{R_B}$ in terms of D'_C, $\mathbf{R_p}$, and $\mathbf{D}_p$, but this is not necessary or particularly illuminating. On the other hand, it is simple to show that the new diattenuation is

$$\mathbf{D} = D'_C \sqrt{1-D_p^2}\, \hat{\mathbf{v}}_p + \mathbf{D}_p \tag{5.30}$$

where $\hat{\mathbf{v}}_p \equiv \mathbf{m}_{R_p}^T [0,0,1]^T$. Because $\mathbf{M}_R \neq \mathbf{M}_{R_p}$, it can be the case that $\hat{\mathbf{v}}_p \neq \hat{\mathbf{v}}$ so the subscript is necessary. Note that $\mathbf{D}_p$ is perpendicular to $\hat{\mathbf{v}}_p$ by definition. Rewriting this in terms of a new parameter $d \equiv D'_C \sqrt{1-D_p^2}$,

$$\begin{aligned}
\mathbf{D} &= d\hat{\mathbf{v}}_p + \mathbf{D}_p \qquad (5.31) \\
-\sqrt{1-D_p^2} &< d < \sqrt{1-D_p^2}.
\end{aligned}$$

This derivation assumes that $\mathbf{M}_{SP}$ has the particular form of 5.26. In Appendix D it is shown that every possible $\mathbf{M}_{SP}$ can be written in this way. Therefore equation 5.31 gives all possible single pass diattenuation vectors such that $\overline{\mathbf{M}}_{DP} = \mathbf{Q}\,\mathbf{M}_{SP}^T\,\mathbf{Q}\,\mathbf{M}_{SP}$. The parameter d can be freely chosen as long as it obeys the inequality, so there is one degree of freedom in selecting $\mathbf{D}$. This result expresses $\mathbf{D}$ as the sum of two perpendicular components: one of which ($\mathbf{D}_p$) is parallel to the double pass diattenuation $\mathbf{D}_{DP}$, and the other of which ($d\hat{\mathbf{v}}_p$) cancels out and has no impact on $\overline{\mathbf{M}}_{DP}$. Equation 5.31 is the equation of a straight line, in the direction $\hat{\mathbf{v}}_p$ and passing through the point $\mathbf{D}_p$. Also, $D^2 = d^2 + D_p^2 \geq D_p^2$, proving that the principal diattenuation vector gives the minimum possible value of diattenuation.

The work of this subsection can be applied as a simple algorithm capable of finding every possible non-depolarizing single pass MM corresponding to a given non-depolarizing double pass MM. Then use the Lu-Chipman decomposition of $\overline{\mathbf{M}}_{DP}$ to calculate $\mathbf{D}_{DP}$ as well as $\mathbf{M}_{R,DP}$. Calculate the principal single pass retardance matrix $\mathbf{M}_{R_p}$ by halving the retardance of $\mathbf{M}_{R,DP}$. Use this to find $\hat{\mathbf{v}}_p = \mathbf{m}_{R_p}^T[0,0,1]^T$. Calculate the principal single pass diattenuation vector $\mathbf{D}_p = a\mathbf{D}_{DP}$, and then calculate $\mathbf{D}$ using 5.31, selecting any value of d that obeys the inequality. Calculate

$$\mathbf{M}_a \equiv \mathbf{Q}\,\mathbf{M}_D^{-1}\,\mathbf{Q}\,\overline{\mathbf{M}}_{DP}\,\mathbf{M}_D^{-1}.$$

It can be shown using 5.13 that $\mathbf{M}_a = c^2\mathbf{Q}\,\mathbf{M}_R^T\,\mathbf{Q}\,\mathbf{M}_R$ and $c = \sqrt{M_a(1,1)}$. Therefore the matrix $\mathbf{M}_a/c^2$ is a double pass retarder, so the linear retardance R_{La} and fast axis θ_a can be calculated using 2.38. Finally, the single pass retarder MM can be calculated as either $\mathbf{M}_R = \mathbf{M}_{CR}(R'_C)\,\mathbf{M}_{LR}(R_{La}/2, \theta_a)$ or as $\mathbf{M}_R = \mathbf{M}_{CR}(R'_C)\,\mathbf{M}_{LR}(\pi - R_{La}/2, \theta_a + \pi/2)$, for any $0 \leq R'_C \leq 2\pi$. Then $\mathbf{M}_{SP} = c\mathbf{M}_R\,\mathbf{M}_D$ is a valid single pass MM corresponding to $\overline{\mathbf{M}}_{DP}$.

As an example, 20 000 possible non-depolarizing $\mathbf{M}_{SP}$ were found for the randomly generated non-depolarizing double pass MM

$$\overline{\mathbf{M}}_{DP} = \begin{bmatrix} 0.4813 & 0.3025 & -0.1233 & -0.3383 \\ 0.3025 & 0.1898 & -0.1564 & -0.2036 \\ -0.1233 & -0.1564 & 0.0046 & 0.0338 \\ 0.3383 & 0.2036 & -0.0338 & -0.2868 \end{bmatrix}. \tag{5.32}$$

This was done by randomly selecting 10 000 d and R'_C, and calculating two possible $\mathbf{M}_{SP}$ for each using $\mathbf{M}_R = \mathbf{M}_{CR}(R'_C)\,\mathbf{M}_{LR}(\pi - R_{La}/2, \theta_a + \pi/2)$ and $\mathbf{M}_R = \mathbf{M}_{CR}(R'_C)\,\mathbf{M}_{LR}(\pi - R_{La}/2, \theta_a + \pi/2)$. It was confirmed that all of the resulting $\mathbf{M}_{SP}$ gave the same double pass MM 5.32 when inserted into equation 5.2. Figure 5.2 shows the resulting single pass

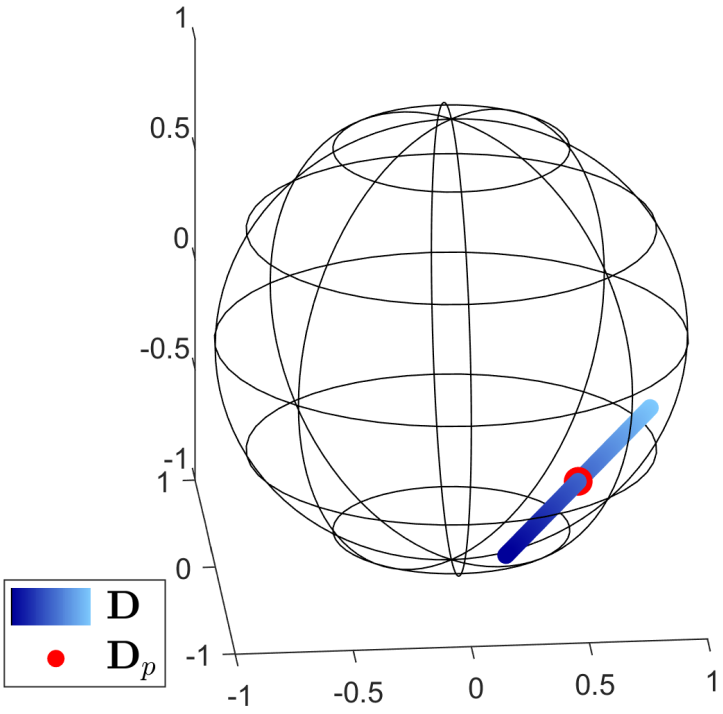

Figure 5.2: Possible $\mathbf{D}$ and the principal diattenuation vector $\mathbf{D}_p$ for the randomly generated nondepolarizing double pass MM 5.32 shown with a reference unit sphere.

diattenuation vectors $\mathbf{D}$ represented as points in 3D space, alongside a unit sphere. These points are represented by a blue color gradient, where the darkest part of the gradient corresponds to $d \to -\sqrt{1-D_p^2}$ while the lightest part corresponds to $d \to +\sqrt{1-D_p^2}$. At either of these extremes, $|D_C| \to 1$ and so according to equation 5.27, $c \to \infty$. Therefore while these values provide valid $\mathbf{M}_{SP}$, for real experimental data it values of $\mathbf{D}$ closer to the center are more likely. Shown in red is the principal diattenuation vector $\mathbf{D}_p$, which corresponds to $d = 0$ and lies exactly in the middle of the line.

Figure 5.3a shows the set of possible single pass retardance vectors $\mathbf{R}$ in a reference sphere of radius π. Two branches are shown depending on if it was chosen that $(R'_L, \theta') = (R_{La}/2, \theta_a)$ or $(R'_L, \theta') = (\pi - R_{La}/2, \theta_a + \pi/2)$. Once again, each is represented by a color gradient where the darkest part of the gradient corresponds to $d \to -\sqrt{1-D_p^2}$ while the lightest part corresponds to $d \to +\sqrt{1-D_p^2}$. The principal retardance vector $\mathbf{R}_p$ is also shown in red. Right multiplication by $\mathbf{M}_{R_B}$ (equation 5.28) leads to a wider range of

possible $\mathbf{R}$ than were present in figure 5.1 for the case of a retarder $\overline{\mathbf{M}}_{DP}$.

Figure 5.3b shows the linear retardance parameters (R_L, 2θ) of each single pass MM in a polar plot, where the conventions are the same as in 5.3a. Geometrically, this is the projection of the points in figure 5.3a onto the equatorial plane. It can be seen that a large range of values of R_L and θ are possible, some of which are very different from the principal retardance $\mathbf{R}_p$ (in red) which was calculated by halving the double pass linear retardance. Figure 5.3c shows instead the compound linear retardance parameters (R'_L, $2\theta'$) of each single pass MM, calculated using equations 5.3. This is the same as the set of $\mathbf{R}$ such that $R'_C = R_C = 0$. Geometrically, this is the intersection of the shape in figure 5.3a with the equatorial plane. The range of possible values is reduced compared to the ordinary retardance parameters R_L and θ, but there is still a variety of possibilities. It can also be seen clearly on this plot that $\mathbf{R}_p$ does not necessarily give the minimum possible retardance magnitude, because there are other points that come nearer to the origin.

This same procedure was run for several other randomly generated non-depolarizing RI MMs. The possible diattenuation vectors were observed to be qualitatively very similar to those shown in figure 5.2. The retardance vectors however showed a variety of different qualitative behaviours. Figures 5.4a, 5.4b and 5.4c show an example for which the magnitude of the double pass retardance was small, while the double pass diattenuation was significant. The corresponding single pass retardance values have an especially large range of possibilities.

Figures 5.5a, 5.5b, and 5.5c show the result if the magnitude of the double pass diattenuation is small. R'_L and θ' are confined to a narrow range of values, which are similar to the case of a double pass retarder as discussed in subsection 5.2.1.

These results give insight into how single and double pass MMs are related when zero depolarization is present. The double pass MM is insufficient to fully determine the single pass polarimetry properties of the sample. Uncertainty in the single pass MM arises due to three sources: firstly, circular retardance R'_C that cancels out in double pass; secondly, a diattenuation component $b\hat{\mathbf{v}}_p$ that cancels out in double pass (equation 5.31); and thirdly, the two options (R'_L, θ') and $(\pi - R'_L, \theta' + \pi/2)$ depending on if the physical double pass retardance exceeds π. These ambiguities are summarized by the statement that given one possible non-depolarizing $\mathbf{M}_{SP}$, all other non-depolarizing $\mathbf{M}'_{SP}$ are given by

$$\mathbf{M}'_{SP} = \frac{1 + |D'_C|}{1 - |D'_C|} \mathbf{M}_{CR/HLR}\, \mathbf{M}_{CD}\, \mathbf{M}_{SP} \tag{5.33}$$

where $\mathbf{M}_{CR/HLR}$ is a circular retarder or half wave linear retarder, while $\mathbf{M}_{CD}$ is a circular diattenuator with diattenuation D'_C. While a given non-depolarizing double pass MM

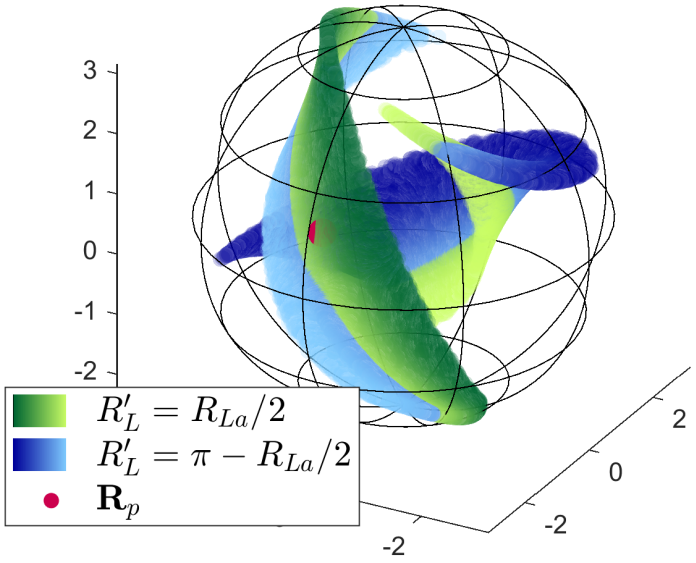

(a) Possible $\mathbf{R}$ shown in 3D space.

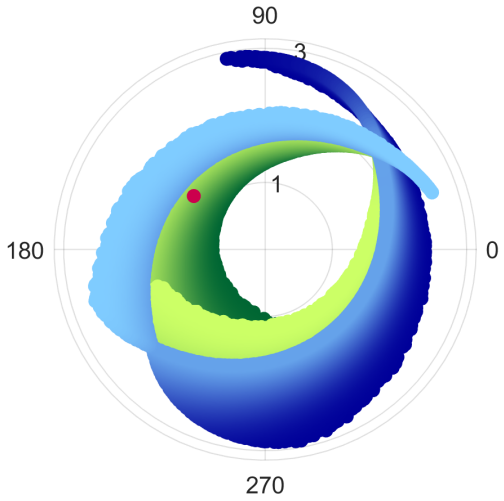

(b) Polar plot of possible $(R_L, 2\theta)$ pairs.

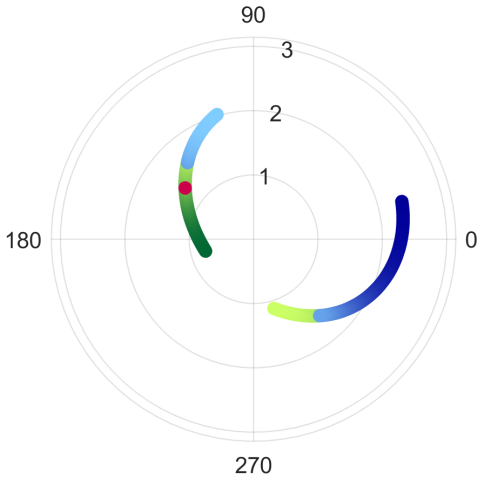

(c) Polar plot of possible $(R'_L, 2\theta')$ pairs.

Figure 5.3: Range of single pass retardance values $\mathbf{R}$, R_L, θ, R'_L, and θ' that are possible for the randomly generated nondepolarizing double pass MM 5.32. The legend applies to all three figures.

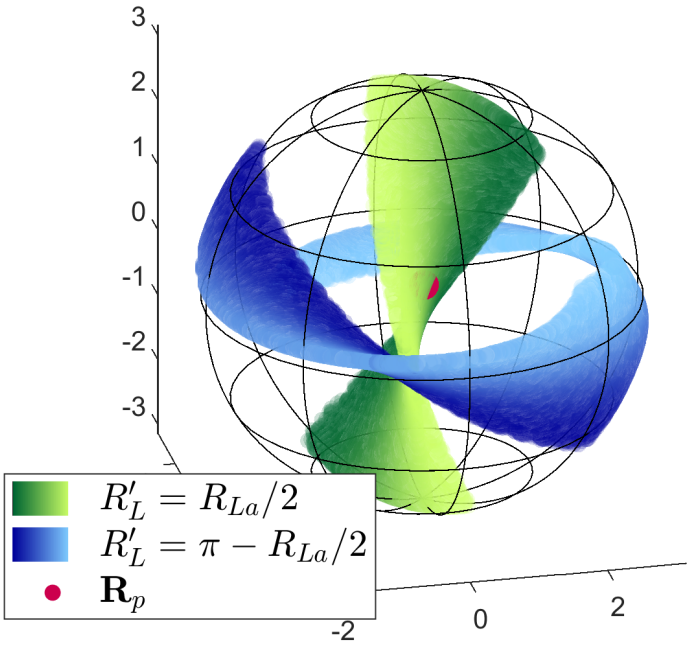

(a) Possible $\mathbf{R}$ shown in 3D space.

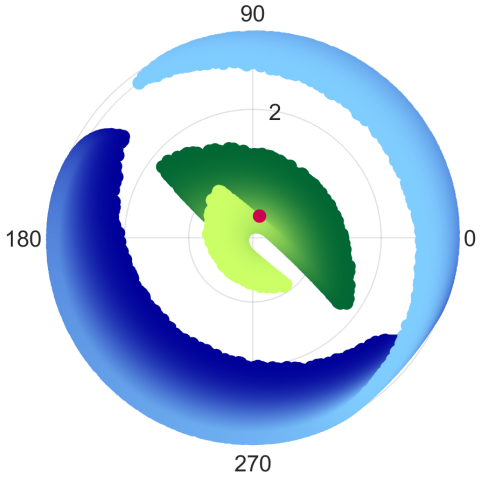

(b) Polar plot of possible $(R_L, 2\theta)$ pairs.

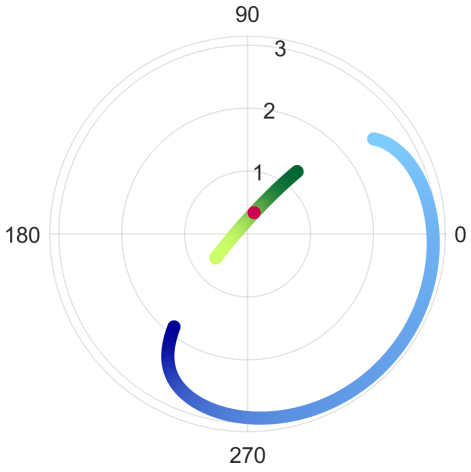

(c) Polar plot of possible $(R'_L, 2\theta')$ pairs.

Figure 5.4: Range of single pass retardance values $\mathbf{R}$, R_L, θ, R'_L, and θ' that are possible for a randomly generated nondepolarizing double pass matrix with small double pass retardance and significant double pass diattenuation.

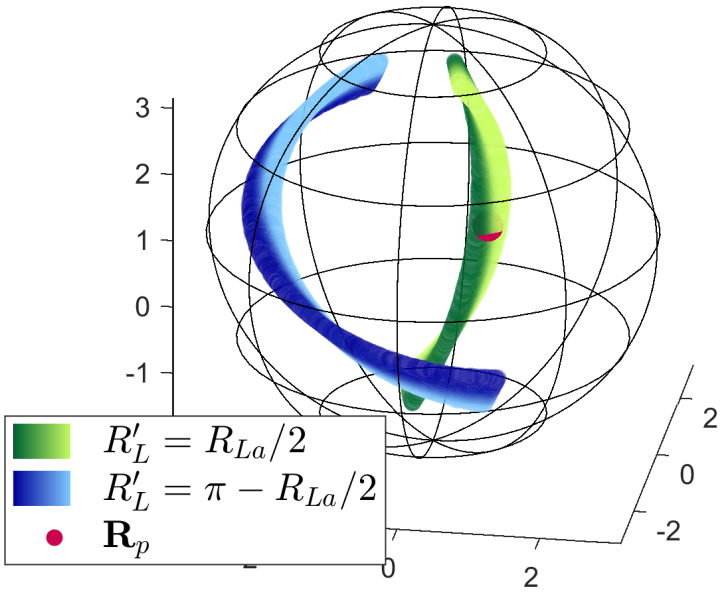

(a) Possible **R** shown in 3D space.

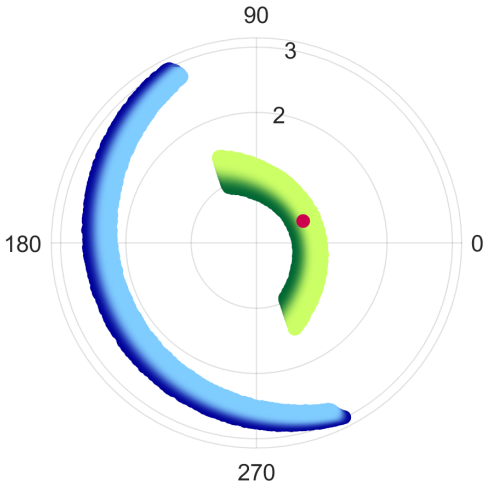

(b) Polar plot of possible $(R_L, 2\theta)$ pairs.

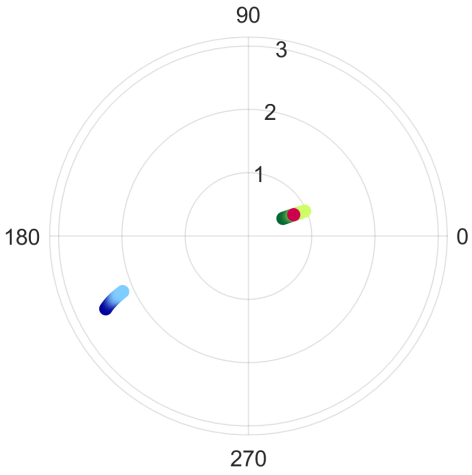

(c) Polar plot of possible $(R'_L, 2\theta')$ pairs.

Figure 5.5: Range of single pass retardance values **R**, R_L, θ, R'_L, and θ' that are possible for a randomly generated nondepolarizing double pass matrix with small double pass diattenuation.

could have a large variety of possible single pass properties, many of these options may be unlikely for the physical sample. For example, if the sample is known to contain only small amounts of diattenuation and circular retardance, then the true single pass $\mathbf{D}$ and $\mathbf{R}$ will be close to the principal values $\mathbf{D}_p$ and $\mathbf{R}_p$. The same result can be shown if there are significant amounts of diattenuation but $\mathbf{D}$ and $\mathbf{R}$ are linear and parallel, as is the case for a linear anisotropic material governed by the constitutive relation 2.22. For these types of samples, the Lu-Chipman decomposition of the double pass MM gives results that are consistent with the single pass polarization properties of the sample. This is because of the close relationship between the principal vectors $\mathbf{D}_p$ and $\mathbf{R}_p$ and the double pass vectors $\mathbf{D}_{DP}$ and $\mathbf{R}_{DP}$ calculated from $\overline{\mathbf{M}}_{DP}$.

Sheppard *et al.* have presented equations relating the double pass and single pass c-vector elements [117]. These elements contain information corresponding to diattenuation and retardance, while treating the sample as a uniform medium. They discuss assumptions about the single pass c-vectors that allow these equations to be solved. They find that if one c-vector element is assumed to be zero, the other three can be determined. As well, they show that if the medium is known to have low retardance and low diattenuation, then the linear components of both properties can be calculated, while the circular components are indeterminate. These assumptions are different than the ones discussed in the previous paragraph. Writing the single and double pass MMs using the Lu-Chipman decomposition has led to a simple interpretation of which polarimetric properties cancel out in double pass, and allowed for the visualization of possible single pass properties in the figures presented in this subsection. As well, it allows for the results to be partially extended to depolarizing double pass MMs, which will be discussed in the following subsection.

5.2.3 General Mueller Matrices in Double Pass

Finally, consider the case in which the single pass MM is allowed to have any combination of properties, including depolarization. Using the Lu-Chipman decomposition, any MM can be written

$$\mathbf{M}_{SP} = c\,\mathbf{M}_{\Delta P}\,\mathbf{M}_R\,\mathbf{M}_D \tag{2.58}$$

as discussed in section 2.3.2 [83]. $\mathbf{M}_{SP}$ can be left multiplied by a circular retarder, half wave linear retarder, or circular diattenuator without altering $\overline{\mathbf{M}}_{DP}$. Considering the

retarders,

$$\begin{aligned}\mathbf{M}'_{SP} = \mathbf{M}_{CR/HLR}\,\mathbf{M}_{SP} &= c\,\mathbf{M}_{CR/HLR}\,\mathbf{M}_{\Delta P}\,\mathbf{M}_R\,\mathbf{M}_D \\ &= c\,(\mathbf{M}_{CR/HLR}\,\mathbf{M}_{\Delta P}\,\mathbf{M}^T_{CR/HLR})\,\mathbf{M}_{CR/HLR}\,\mathbf{M}_R\,\mathbf{M}_D \\ &= c\,\mathbf{M}'_{\Delta P}\,(\mathbf{M}_{CR/HLR}\,\mathbf{M}_R)\,\mathbf{M}_D. \end{aligned} \tag{5.34}$$

$\mathbf{M}'_{\Delta P} \equiv \mathbf{M}_{CR/HLR}\,\mathbf{M}_{\Delta P}\,\mathbf{M}^T_{CR/HLR}$ is a depolarization matrix with the same depolarization power as $\mathbf{M}_{\Delta P}$, so equation 5.34 is the Lu-Chipman decomposition of $\mathbf{M}'_{SP}$. The new retardance matrix $\mathbf{M}_{CR/HLR}\,\mathbf{M}_R$ can have a range of retardance vectors, such as those visualized previously in figure 5.1. This shows that the results of subsection 5.2.1 are relevant to general MMs in double pass as well. In particular, it means that the compound circular retardance R'_C of $\mathbf{M}_R$ cannot be determined from $\overline{\mathbf{M}}_{DP}$ regardless of the amount of diattenuation and depolarization present in $\mathbf{M}_{SP}$, and the compound linear retardance $(R'_L,\, \theta')$ is always indistinguishable from $(\pi - R'_L,\, \theta' + \pi/2)$. However, there are two important ways in which the findings of subsection 5.2.1 do not generalize. Firstly, the relationship between $\mathbf{M}_R$ and $\mathbf{M}_{R,DP}$ may differ from what it was in subsection 5.2.1- that is, linear retardance may not be exactly doubled in double pass. Secondly, there are other possible single pass retardance matrices besides $\mathbf{M}_{CR/HLR}\,\mathbf{M}_R$, because of left multiplication by $\mathbf{M}_{CD}$ and other unknown ambiguities.

The effects of left multiplication by $\mathbf{M}_{CD}$ can be understood most easily by considering the "reverse decomposition" of $\mathbf{M}_{SP}$, which was developed by Ossikovski [97]:

$$\mathbf{M}_{SP} = c\,\mathbf{M}_P\,\mathbf{M}_{R_{rev}}\,\mathbf{M}_{\Delta D} \quad [53,\ 97] \tag{5.35}$$

$$\mathbf{M}_{\Delta D} = \begin{bmatrix} 1 & \mathbf{D}^T_{\Delta D} \\ \mathbf{0} & \mathbf{m}_{\Delta D} \end{bmatrix} \quad [53,\ 97] \tag{5.36}$$

$$\mathbf{M}_P = \frac{1}{1+P}\begin{bmatrix} 1 & \mathbf{P}^T \\ \mathbf{P} & \sqrt{1-P^2}\,\mathbb{I} + \frac{1-\sqrt{1-P^2}}{P^2}\mathbf{P}\mathbf{P}^T \end{bmatrix} \quad [53,\ 97]. \tag{5.37}$$

$\mathbf{M}_P$ is a diattenuator matrix, but using the polarizance vector of $\mathbf{M}_{SP}$, $\mathbf{P} = M_{SP}(2:4, 1)$ rather than the diattenuation vector $\mathbf{D}^T = M_{SP}(1, 2:4)$ (equation 2.61). $\mathbf{M}_{\Delta D}$ has zero retardance and zero polarizance, but may include nonzero diattenuation $\mathbf{D}_{\Delta D}$ [53]. Its submatrix $\mathbf{m}_{\Delta D}$ is symmetric [53]. The retardance matrix $\mathbf{M}_{R_{rev}}$ is not exactly equal to the Lu-Chipman retardance $\mathbf{M}_R$ [R. Ossikovski, personal communication, September 7 2020]. The difference between the two matrices approaches zero in the limit of zero depolarization in $\mathbf{M}_{SP}$.

The product

$$c\,\frac{1+|D'_C|}{1-|D'_C|}\,\mathbf{M}_{CD}(D'_C)\,\mathbf{M}_P\,\mathbf{M}_{R_{rev}}$$

is a non-depolarizing MM that can be "reverse decomposed" as $c'\,\mathbf{M}'_P\,\mathbf{M}'_{R_{rev}}$. Therefore the effect of left multiplication by a circular diattenuator is

$$\begin{aligned}\mathbf{M}'_{SP} &= c\,\frac{1+|D'_C|}{1-|D'_C|}\,\mathbf{M}_P\,\mathbf{M}_{R_{rev}}\,\mathbf{M}_{\Delta D}\\ &= c'\,\mathbf{M}'_P\,\mathbf{M}'_{R_{rev}}\,\mathbf{M}_{\Delta D}.\end{aligned}$$

It can be shown that writing $\mathbf{P} = [P_H,\ P_{45},\ P_C]^T$,

$$\mathbf{P}' = \frac{1}{1+D'_C P_C}[\sqrt{1-D'^2_C}P_H,\ \sqrt{1-D'^2_C}P_{45},\ (D'_C+P_C)]^T. \tag{5.38}$$

$\mathbf{P}' = M'_{SP}(2:4,1)$ is the polarizance vector of $\mathbf{M}'_{SP}$, so equation 5.38 shows how polarizance can be altered without changing the double pass MM. This requires also replacing the reverse retardance $\mathbf{M}_{R_{rev}}$ with a new retarder $\mathbf{M}'_{R_{rev}}$, which has an impact on the Lu-Chipman retardance matrix $\mathbf{M}_R$.

In this section, it has been shown how to find multiple single pass MMs that correspond to the same double pass MM. For non-depolarizing MMs, it was possible to find all corresponding single pass MMs. This has highlighted how some single pass polarimetric properties, particularly circular retardance and polarizance, can be altered significantly without changing the double pass MM. This implies that these properties cannot be inferred reliably from the double pass MM.

5.3 Double Pass Decomposition

The problem of finding every possible $\mathbf{M}_{SP}$ corresponding to a general $\overline{\mathbf{M}}_{DP}$ is complex, and is left as an avenue for future work. Instead, a novel method is developed for finding a subset of all $\mathbf{M}_{SP}$. The starting point of this analysis is the symmetric decomposition developed by Ossikovski [95, 53]. Using their algorithm, any MM (whether it is RI or not) can be written as the product

$$\mathbf{M} = \mathbf{M}_{D2}\,\mathbf{M}_{R2}\,\mathbf{M}_{\Delta I/II}\,\mathbf{M}_{R1}\,\mathbf{M}_{D1} \tag{5.39}$$

where $\mathbf{M}_{\Delta I/II}$ has one of two different forms, depending on if $\mathbf{M}$ is a so-called "type I" MM or "type II" MM [53]. Equation 5.39 resembles the double pass model, with the depolarizer $\mathbf{M}_{\Delta I/II}$ taking the place of the reflection matrix. A simpler algorithm developed by Otsuki [98] assumes that $\mathbf{M}_{R1} = \mathbf{M}_{R2}$ is a horizontal linear retarder, while $\mathbf{M}_{D1} = \mathbf{M}_{D2}$ is a

horizontal linear diattenuator. However, not all double pass MMs can be decomposed using Otsuki's method, while Ossikovski's algorithm can be applied to any MM.

In Appendix E it is shown that if $\mathbf{M}$ is RI and type I, the algorithm of Ossikovski can be modified to give

$$\begin{aligned} \mathbf{M} &= (\mathbf{X}\,\mathbf{M}_{SP}^{T}\,\mathbf{X})\,(\mathbf{X}\,\mathbf{Z})\,\mathbf{M}_{SP} \\ \mathbf{M}_{SP} &= \mathbf{M}_{\Delta}\,\mathbf{M}_{R}\,\mathbf{M}_{D} \end{aligned} \tag{5.40}$$

where $\mathbf{M}_{\Delta}$ is diagonal and where $\mathbf{Z}$ has the form $\mathbf{Z} = \mathrm{diag}(1, \pm 1, \pm 1, \pm 1)$. This decomposition replaces the mirror matrix $\mathbf{Y}$ with $\mathbf{X}\,\mathbf{Z}$. The details of the algorithm are provided in Appendix E, and there are found to be twenty-four different pairs $(\mathbf{M}_{SP}, \mathbf{Z})$ that can satisfy equation 5.40. It has been assumed that $\mathbf{M}$ is type I, according to the definitions in [53]. Type II MMs are rare and only occur when the length of an auxiliary vector is exactly equal to one (see Appendix E).

There are several features of 5.40 that need to be discussed. Firstly, the algorithm described in Appendix E has been designed to start with $\mathbf{M}$, and not $\overline{\mathbf{M}}$. This is an arbitrary choice; it could be modified to allow starting with $\overline{\mathbf{M}}$ instead, and the single pass matrix $\mathbf{M}_{SP}$ would be the same in either case. Secondly, this method fails if $\mathbf{M}$ is non-depolarizing. In that case, the single pass matrix can be determined as described in section 5.2.2. Thirdly, this approach finds single pass matrices under the assumption that $\mathbf{M}_{\Delta}$ is diagonal. There could be other possible single pass matrices with non-diagonal $\mathbf{M}_{\Delta P}$ of the form 2.59, so only a subset of possible $\mathbf{M}_{SP}$ is found using this method. Ossikovski *et al.* have stated that "a number of important depolarizing media seem to be expressible in terms of diagonal depolarization matrices" [97], so this subset may be especially likely to match the true physical single pass MM.

Finally, the decomposition 5.40 only matches the regular double pass model 3.16 if $\mathbf{X}\,\mathbf{Z} = \mathbf{Y}$. This requires that $\mathbf{Z} = \mathrm{diag}(1, +1, +1, -1)$. In Appendix E, it is shown that for any $\mathbf{M}$, in all twenty-four different pairs $(\mathbf{M}_{SP}, \mathbf{Z})$ that satisfy equation 5.40, $\mathbf{Z}$ must have the same number of negative entries on the diagonal. Therefore, there are four distinct cases depending on if $\mathbf{Z}$ contains zero, one, two, or three negative entries.

If $\mathbf{Z}$ has one negative entry, it can be shown that eight out of the twenty-four possible decompositions will have the correct form such that $\mathbf{X}\,\mathbf{Z} = \mathbf{Y}$. This means that there are eight possible single pass MMs $\mathbf{M}_{SP}$ that obey the double pass model $\mathbf{M} = \mathbf{X}\,\mathbf{M}_{SP}^{T}\,\mathbf{X}\,\mathbf{Y}\,\mathbf{M}_{SP}$. Using the results of Appendix E, it can be shown that all eight possible diattenuation matrices $\mathbf{M}_{D}$ are the same. All eight depolarization matrices $\mathbf{M}_{\Delta}$ have the same diagonal entries, but permuted in different ways. Depolarization power Δ is invariant to the order

of the diagonal elements of $\mathbf{M}_\Delta$:

$$\Delta = 1 - \frac{\text{trace}(\mathbf{M}_\Delta) - 1}{3} \quad [83]. \tag{2.45}$$

Therefore all eight $\mathbf{M}_{SP}$ have the same Δ. The eight retardance matrices $\mathbf{M}_R$ differ by permuting their middle two rows, or by inverting the sign of any of the last three rows, while maintaining $\det(\mathbf{M}_R) = +1$ (see Appendix E). They will have very different retardance vectors. However, it can be shown that they are all related to one another through left multiplication by a circular retarder or by a half wave linear retarder. These are the same single pass retarder ambiguities that were discussed in subsection 5.2.1. Based on the results of that section, if equations 5.3 are used to calculate the compound linear retardance (R'_L, θ') for one of the possible $\mathbf{M}_R$, then all of the other possibilities must either have compound linear retardance of (R'_L, θ') or $(\pi - R'_L, \theta' + \pi/2)$. Therefore, if $\mathbf{Z}$ has exactly one negative entry, then this algorithm can be used to calculate uniquely defined values of single pass diattenuation, depolarization power, and two complementary values of compound linear retardance.

If however $\mathbf{M}$ is type II, or if it is found that $\mathbf{Z}$ contains zero, two, or three negative entries, then this algorithm fails to find any single pass MMs that fit the double pass model $\mathbf{M} = \mathbf{X}\,\mathbf{M}_{SP}^T\,\mathbf{X}\,\mathbf{Y}\,\mathbf{M}_{SP}$. There are two potential explanations for this. The first is that every possible single pass MM $\mathbf{M}_{SP}$ satisfying this equation has a non-diagonal $\mathbf{M}_{\Delta P}$. In simulations that will be described in the following section, 60 000 double pass MMs were calculated using randomly generated single pass MMs with non-diagonal $\mathbf{M}_{\Delta P}$. For all 60 000 double pass MMs, the double pass decomposition was successful in finding $\mathbf{M}_{SP}$ with diagonal depolarization matrices. In other words, every double pass MM in the simulation proved to be type I and had $\mathbf{Z}$ with exactly one negative entry. This suggests that in most if not all cases, $\mathbf{M}_{DP}$ can be written using a single pass MM $\mathbf{M}_{SP}$ with a diagonal depolarization matrix. An algebraic proof is necessary to determine if this is true of all double pass MMs, which is left to future work.

The second potential explanation is that there are no matrices $\mathbf{M}_{SP}$ satisfying $\mathbf{M} = \mathbf{X}\,\mathbf{M}_{SP}^T\,\mathbf{X}\,\mathbf{Y}\,\mathbf{M}_{SP}$; that is, $\mathbf{M}$ is not a double pass MM. It is easy to show that there are RI MMs that cannot be written as double pass MMs; for example the double pass model 3.16 implies that $\det(\mathbf{M}_{DP}) > 0$, but it is possible to find examples of RI MMs that have negative determinant. Additionally, there are some positive determinant RI MMs that are also not mathematically consistent with the double pass model. This latter type may be difficult to identify. The double pass decomposition could be therefore used as a test of the validity of the double pass model for describing $\mathbf{M}$. If a large number of pixel-by-pixel MMs measured by *in vivo* retinal polarimetry prove to have $\mathbf{Z}$ with zero, two, or three negative

entries, it would suggest that the double pass model is inaccurate for that measurement. In principle this deviation from the double pass model could be caused by experimental errors such as detector noise. However, there is reason to think that experimental errors should be unlikely to change the number of negative entries of $\mathbf{Z}$. As part of the algorithm described in Appendix E, three scalar values $-1 \leq a_1, a_2, a_3 \leq 1$ are calculated from $\mathbf{M}$. These are used to calculate $\mathbf{Z}$ and $\mathbf{M}_\Delta$ using

$$\mathbf{M}_\Delta \equiv \begin{bmatrix} 1 & 0 & 0 & 0 \\ 0 & \sqrt{|a_1|} & 0 & 0 \\ 0 & 0 & \sqrt{|a_2|} & 0 \\ 0 & 0 & 0 & \sqrt{|a_3|} \end{bmatrix} \tag{E.5}$$

$$\mathbf{Z} \equiv \begin{bmatrix} 1 & 0 & 0 & 0 \\ 0 & \text{sign}(a_1) & 0 & 0 \\ 0 & 0 & \text{sign}(a_2) & 0 \\ 0 & 0 & 0 & \text{sign}(a_3) \end{bmatrix}. \tag{E.6}$$

Unless the single pass depolarization is very high, a_1, a_2, and a_3 must also be far from zero (whether positive or negative). So, assuming that a small experimental error in $\mathbf{M}$ leads also to small errors in a_1, a_2, and a_3, it is unlikely that one of them will change sign. Therefore the number of negative entries of $\mathbf{Z}$ is a strong indicator whether a RI MM is consistent with the double pass model.

Finally, if the experimental MM is inconsistent with the double pass model, it might be explainable using a modified double pass model. For example, Qi *et al* suggest that if a sample is made up of scatterers with sizes on the order of the wavelength of the incident light or larger, the reflection matrix will take a form similar to $\mathbf{X}$ instead of $\mathbf{Y}$ [105]. If this is the case for the reflection that occurs deep in the retina in *in vivo* retinal polarimetry, then $\mathbf{Z}$ would have zero diagonal entries. The double pass decomposition could then be used to calculate single pass MMs within a modified double pass model with $\mathbf{X}$ replacing $\mathbf{Y}$. Therefore the double pass decomposition described in this section and in Appendix E may be able to probe the nature of the reflection that occurs in the retina.

5.4 Simulations

In subsection 5.2.2, the relationship between single and double pass polarimetric properties of non-depolarizing MMs was fully explored algebraically. Subsection 5.2.3 showed several ways in which depolarizing single pass MMs can be altered without affecting the double

pass MM, but did not explicitly show the connection between single and double pass values. To supplement this, this section uses simulations to compare single and double pass properties calculated by the Lu-Chipman decomposition in the presence of depolarization. Then, the same simulations will be used to assess different strategies of inferring single pass Lu-Chipman properties from the double pass MM. In particular, the "double pass decomposition" will be compared to methods that start instead with the Lu-Chipman decomposition of the double pass MM.

A set of 30 000 single pass MMs $\mathbf{M}_{SP}$ were randomly generated, as described in Appendix B.1. This was done in such a way that the diattenuation and retardance vectors $\mathbf{D}$ and $\mathbf{R}$ had nearly uniformly distributed magnitudes (in the ranges $(0, 1)$ and $(0, \pi)$ respectively), and uniformly distributed orientations in $3D$ space. Depolarization power Δ of this set was approximately normally distributed with mean 0.42 and standard deviation 0.15 (see figure B.1). The depolarization matrices of the single pass MMs were non-diagonal, having the form of $\mathbf{M}_{\Delta P}$ (equation 2.59). Then, the double pass matrices $\overline{\mathbf{M}}_{DP}$ were calculated using equation 5.2. The Lu-Chipman decomposition was applied to both $\mathbf{M}_{SP}$ and $\overline{\mathbf{M}}_{DP}$.

Figure 5.6 shows six scatter plots depicting the diattenuation vector $\mathbf{D}$ and polarizance vector $\mathbf{P}$ (equation 2.61). In each plot, the horizontal axis is the single pass value, while the vertical axis is the double pass value. The left column contains a plot each for the linear diattenuation, circular diattenuation, and linear diattenuation orientation (see equations 2.33, 2.34 and 2.35), which together completely determine $\mathbf{D}$. In each case there is an approximately linear relationship between the single and double pass values, with a slope close to one. The right column shows analogous plots for the polarizance $\mathbf{P}$, *i.e.*

$$\mathbf{P} = \begin{bmatrix} P_H \\ P_{45} \\ P_C \end{bmatrix}$$
$$P_L = \sqrt{P_H^2 + P_{45}^2}$$
$$P_\theta = (1/2)\arctan2(P_{45}, P_H).$$

The single and double pass polarizance are evidently much less similar to one another than the diattenuation. In particular, circular polarizance is nearly uncorrelated between the two MMs. This is in agreement with the equation 5.38 found in section 5.2.3, which shows how the single pass polarizance can be altered without changing the double pass MM.

Figure 5.7 shows scatter plots relating the single and double pass retardance and depolarization power. Figure 5.7a shows the ordinary linear retardance R_L, as well as the

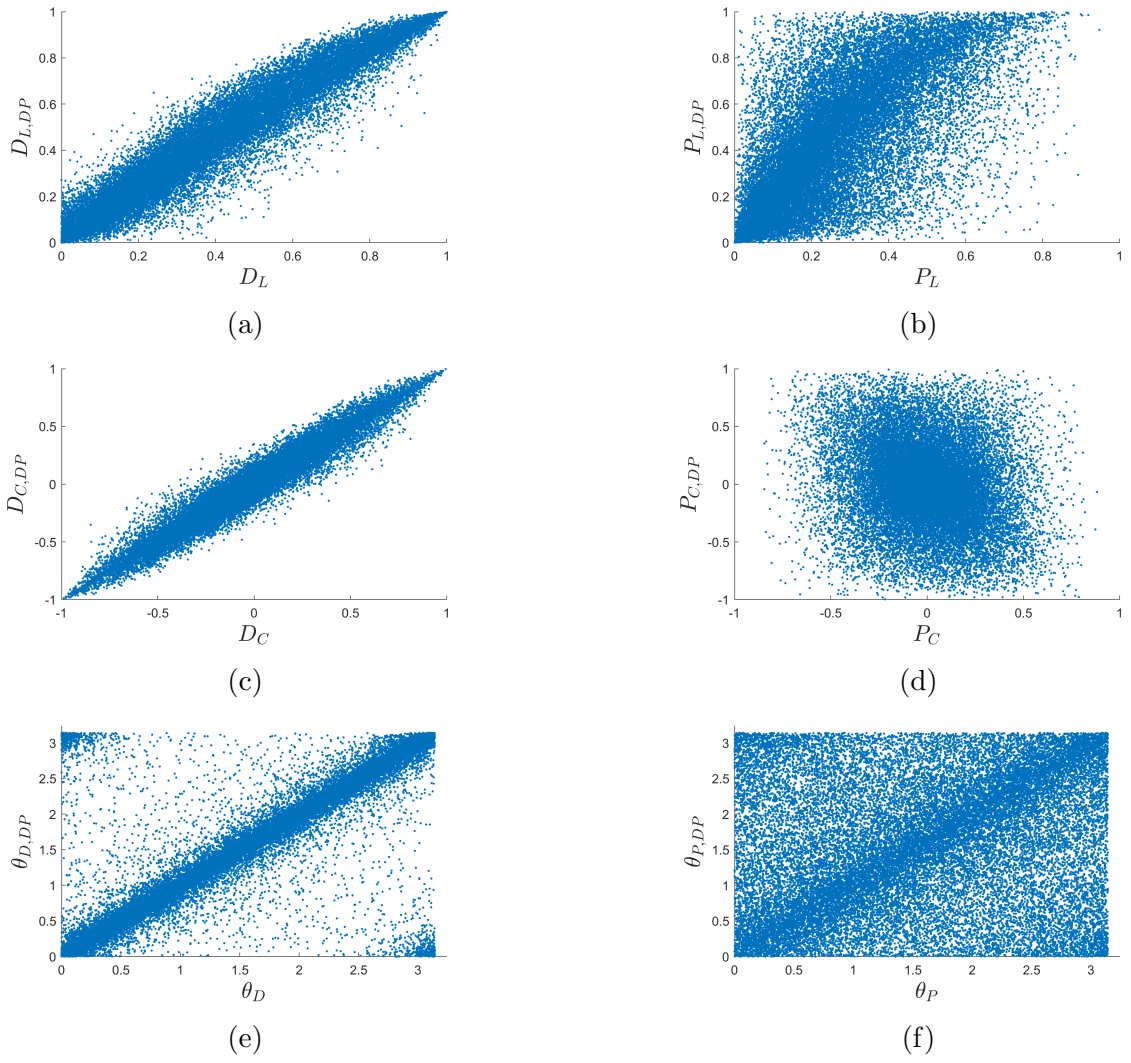

Figure 5.6: Relationship between and single and double pass diattenuation and polarizance as calculated using Lu-Chipman direction.

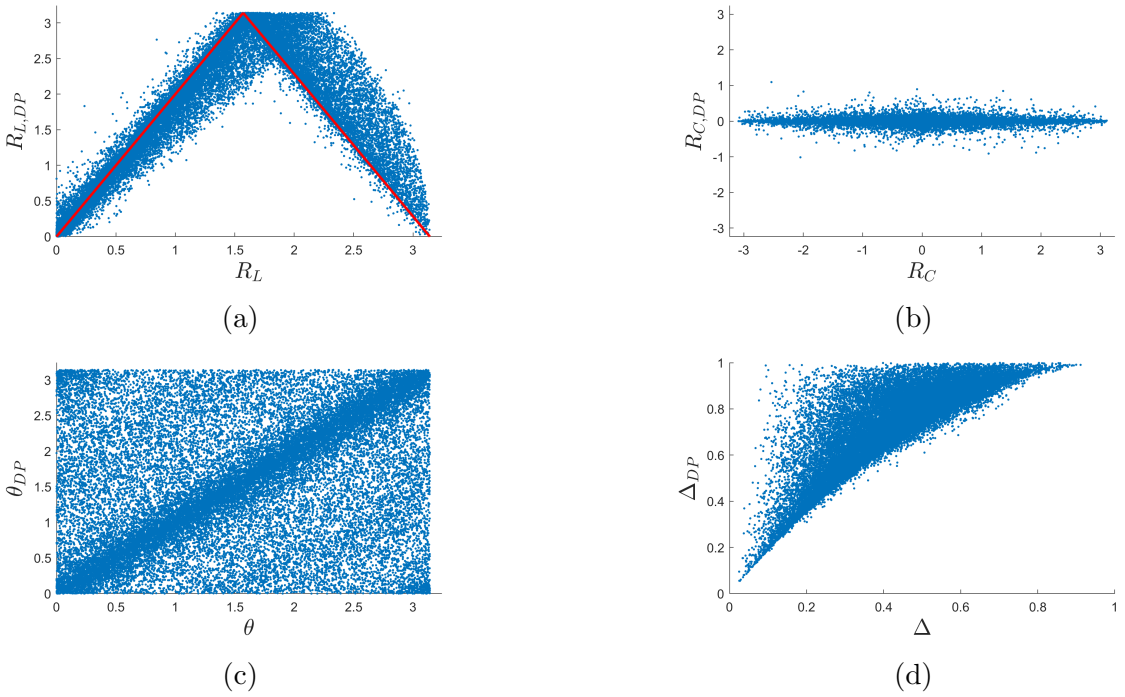

Figure 5.7: Relationship between and single and double pass retardance and depolarization power as calculated using Lu-Chipman direction.

line

$$\begin{aligned} y &= 2x, \quad 0 \leq x \leq \pi/2 \\ y &= 2\pi - 2x, \quad \pi/2 < x \leq \pi. \end{aligned} \tag{5.41}$$

Equation 5.41 is the relationship between single and double pass R_L if $\mathbf{M}_{SP}$ is a linear retarder (subsection 5.2.1). In these simulations, which include the effects of circular retardance, diattenuation, and depolarization in addition to linear retardance, a general behaviour similar to 5.41 is still discernible. In contrast to the non-depolarizing case, a depolarizing $\overline{\mathbf{M}}_{DP}$ can have a small amount of circular retardance, as shown by figure 5.7b. However, this circular retardance appears to be unrelated to the single pass value. This is in agreement with section 5.2.3, which showed that R'_C cannot be inferred from $\overline{\mathbf{M}}_{DP}$. Lastly, figure 5.7d shows that the double pass depolarization power is frequently much larger than the single pass value.

Next, these simulations can describe a situation (such as *in vivo* retinal polarimetry) in which one wishes to predict single pass Lu-Chipman properties from the measured

double pass MM. One approach is to start with the double pass Lu-Chipman properties. Based on figures 5.6a, 5.6c, and 5.6e, $D_{L,DP}$, $D_{C,DP}$, and $\theta_{D,DP}$ each approximate their corresponding single pass values[7]. Polarizance and circular retardance are excluded from this discussion, because of the lack of a clear relationship between single and double pass values in figures 5.6b, 5.6d, 5.6f, and 5.7b. In many studies, single pass linear retardance R_L is estimated by dividing the double pass linear retardance by two [49, 74, 78, 138]. Figure 5.7a shows that for some samples this may be inaccurate, particularly if $R_L > \pi/2$. As discussed in section 5.2.3, the single pass retardance matrix can be left multiplied by any circular retarder or halfwave linear retarder without altering $\overline{\mathbf{M}}_{DP}$, making R_L and θ difficult to predict. However, a different measure of single pass linear retardance can be defined as follows:

$$(R'_{L<},\, \theta'_{<}) \equiv \begin{cases} (R'_L,\, \theta') & \text{if } R'_L < \pi/2 \\ (\pi - R'_L,\, \theta' + \pi/2) & \text{if } R'_L > \pi/2 \end{cases} \tag{5.42}$$

where R'_L and θ' are the compound linear retardance and linear retardance fast axis defined in equations 5.3. It follows from section 5.2.1 that $R'_{L<}$ and $\theta'_{<}$ are unaffected by left multiplication by any circular retarder or halfwave linear retarder. Therefore, $(R'_{L<},\, \theta'_{<})$ can be predicted much more reliably from the double pass model than $(R_L,\, \theta)$, and will be used instead for the remaining comparisons. It will be found that $(R_{DP}/2, \theta_{DP})$ is a better predictor of this modified single pass linear retardance definition than it is of $(R_L,\, \theta)$.

Lastly, figure 5.7d shows that single and double pass depolarization power are dissimilar. Typically, the double pass depolarization power Δ_{DP} is calculated using the three eigenvalues (e_1, e_2, e_3) of the depolarizing submatrix $\mathbf{m}_{\Delta_{DP}P}$:

$$\Delta_{DP} = 1 - \frac{e_1 + e_2 + e_3}{3}. \tag{5.43}$$

It was observed that for a diagonal depolarizer $\mathbf{M}_{SP} = \mathbf{M}_\Delta$,

$$\overline{\mathbf{M}}_{DP} = \mathbf{M}_{\Delta,DP} = \mathbf{Q}\,\mathbf{M}_\Delta^T\,\mathbf{Q}\,\mathbf{M}_\Delta = \mathbf{M}_\Delta^2. \tag{5.44}$$

Based on this squared relationship, it was postulated that the modified depolarization power

$$\Delta'_{DP} \equiv 1 - \frac{\sqrt{e_1} + \sqrt{e_2} + \sqrt{e_3}}{3} \tag{5.45}$$

[7]One could generate linear (or higher order) fits for each of figures 5.6a, 5.6c, and 5.6e, using the resulting parameters in order to optimally predict $\mathbf{D}$ from $\mathbf{D}_{DP}$. However this would risk overfitting, and the results may depend on the properties of the MMs used in the simulation. The line $y = x$ is used instead for simplicity, because it evidently provides a reasonable fit for each of figures 5.6a, 5.6c, and 5.6e.

should show a more linear correspondence to the single pass depolarization power than Δ_{DP}.

In addition, the double pass decomposition algorithm described in Appendix E was applied to $\mathbf{M}_{DP}$ to extract a new set of predicted single pass polarimetric properties, labelled with the subscript SYM (in reference to the double pass decomposition algorithm being based on the symmetric decomposition of Ossikovski [95]). This returns a possible $\mathbf{M}_{SP,SYM}$ under the condition that $\mathbf{M}_{\Delta,SYM}$ is diagonal, which may differ from the "true" single pass $\mathbf{M}_{SP}$. $\mathbf{D}_{SYM}$ and Δ_{SYM} were calculated as normal from the $\mathbf{M}_{D,SYM}$ and $\mathbf{M}_{\Delta,SYM}$ provided by the decomposition. Linear retardance and linear fast axis were calculated from $\mathbf{M}_{R,SYM}$ in the same way as for the true single pass values, in order to make them invariant to left multiplication by a circular retarder or linear half wave retarder. The resulting values are labelled $(R'_{L<,SYM}, \theta'_{<,SYM})$.

The same set of 30 000 single pass and corresponding double pass MMs was used to compare the true single pass polarimetric properties with values calculated from $\overline{\mathbf{M}}_{DP}$. The right column of figure 5.8 shows scatter plots relating $\mathbf{D}_{SYM}$ to the true single pass values $\mathbf{D}$. The left column shows for comparison the same plots with the Lu-Chipman calculated vector $\mathbf{D}_{DP}$ instead of $\mathbf{D}_{SYM}$ (identical to figures 5.6a, 5.6c, and 5.6e). A more quantitative analysis of these results will be presented later in this section, but from figure 5.8, it is clear that $\mathbf{D}_{SYM}$ tends to correspond more closely with the "true" single pass values $\mathbf{D}$ than $\mathbf{D}_{DP}$. This is especially the case for larger diattenuation magnitudes.

Figure 5.9 shows the same type of comparison for linear retardance, linear retardance fast axis, and depolarization power. Figures 5.9a and 5.9c show that $(R_{L,DP}/2,\, \theta_{DP})$ are more similar to the modified linear retardance values $(R'_{L<},\, \theta'_{<})$ than they are to (R_L, θ) (compare to figures 5.7a and 5.7c). Figures 5.9b and 5.9d show that the values extracted using the double pass decomposition, $(R'_{L<,SYM},\, \theta'_{<,SYM})$, are slightly better predictors of the true single pass value than $(R_{L,DP}/2,\, \theta_{DP})$. This will be confirmed quantitatively in the following paragraph. Finally, figure 5.9e compares the modified depolarization power Δ'_{DP} with the single pass value Δ. Compared to figure 5.7d which used the ordinary double pass depolarization power Δ_{DP}, this modification has brought points closer to the $y = x$ line. However, Δ'_{DP} still tends to overestimate the true single pass Δ. Figure 5.9f on the other hand shows that using the double pass decomposition allows for a more accurate prediction of Δ, with the majority of points lying close to the line $y = x$.

The twelve plots in figures 5.8 and 5.9 were assessed quantitatively based on their similarity to the line $y = x$. For each point $(x_i,\, y_i)$, the vertical distance from the line $y = x$ was calculated as $\delta_i = y_i - x_i$. This is the difference between the true single pass value (x_i) of that polarimetric property and the value calculated from $\overline{\mathbf{M}}_{DP}$ (y_i). For each

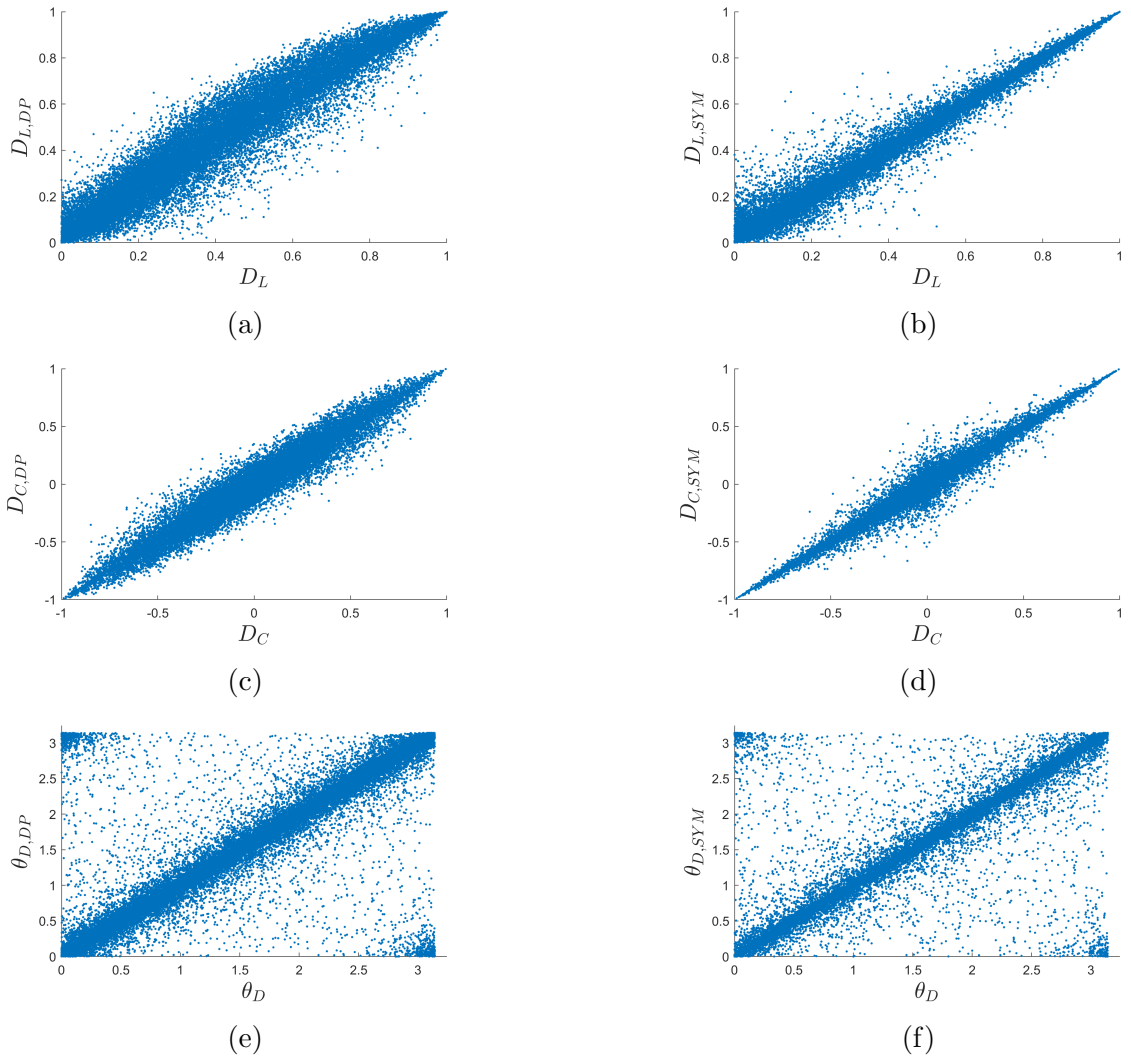

Figure 5.8: Comparison of the true single pass diattenuation with that calculated from $\overline{\mathbf{M}}_{DP}$ using the Lu-Chipman decomposition and double pass decomposition.

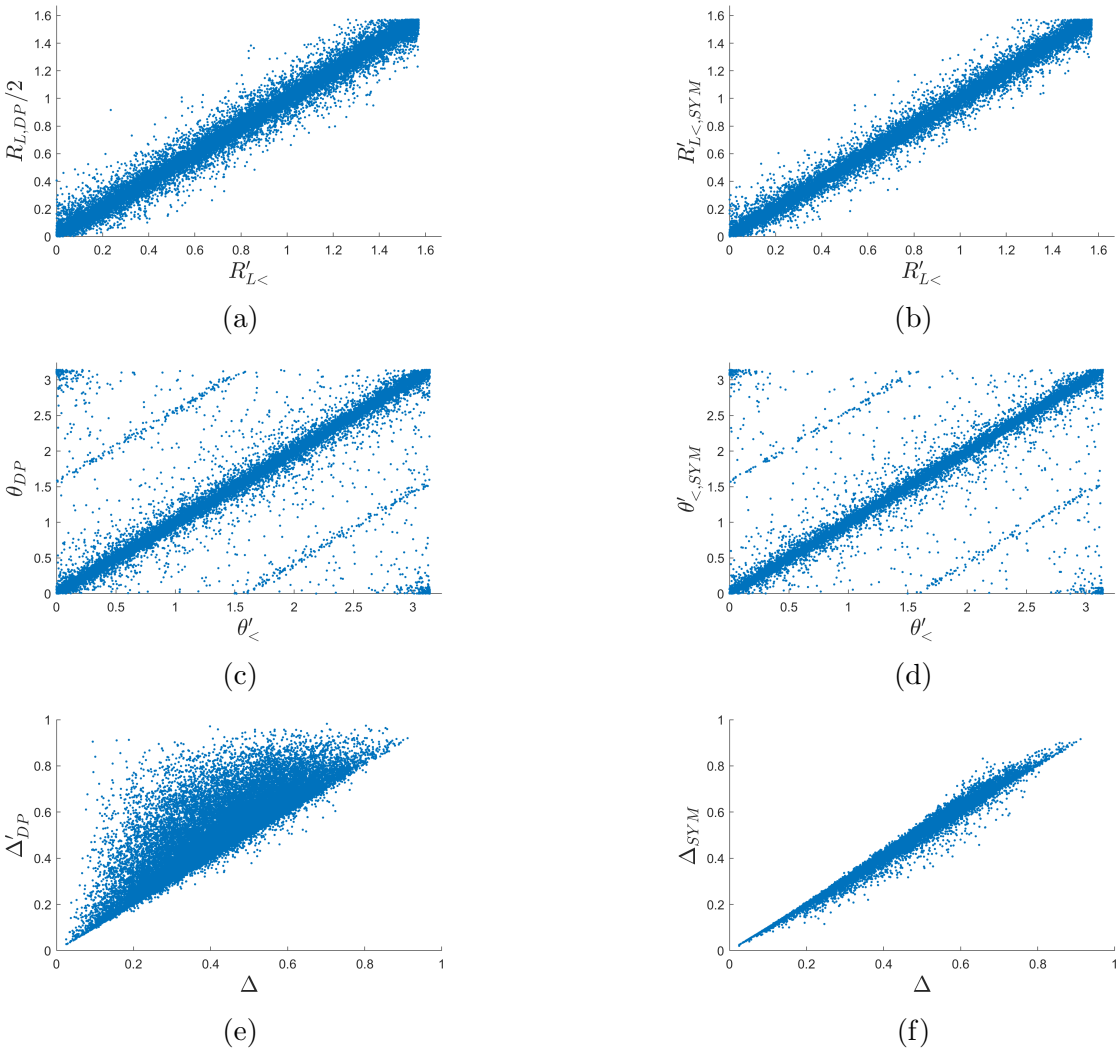

Figure 5.9: Comparison of the true single pass linear retardance, linear retardance fast axis, and depolarization power with that predicted from $\overline{\mathbf{M}}_{DP}$ using the Lu-Chipman decomposition and double pass decomposition.

Polarimetric Properties			$\overline{\delta}$		$\hat{\delta}$	
Single Pass	DP	SYM	DP	SYM	DP	SYM
D_L	$D_{L,DP}$	$D_{L,SYM}$	0.0431	0.0062	0.0870	0.0405
D_C	$D_{C,DP}$	$D_{C,SYM}$	0.0004	0.0002	0.0861	0.0514
θ_D	$\theta_{D,DP}$	$\theta_{D,SYM}$	-0.0006	-0.0012	0.2396	0.2138
$R'_{L<}$	$R_{L,DP}/2$	$R'_{L<,SYM}$	0.0018	0.0015	0.0544	0.0407
$\theta'_<$	θ_{DP}	$\theta'_{<,SYM}$	0.0010	0.0008	0.2131	0.1763
Δ	Δ'_{DP}	Δ_{SYM}	0.0856	0.0058	0.1285	0.0170

Table 5.1: Table showing the similarities between polarimetric properties calculated from general single pass and corresponding double pass MMs.

plot, two metrics were calculated:

$$\overline{\delta} = \sum_i \frac{\delta_i}{N} \tag{5.46}$$

$$\hat{\delta} = \sqrt{\sum_i \frac{\delta_i^2}{N}}. \tag{5.47}$$

$\overline{\delta}$ is the mean of δ; while $\hat{\delta}$ is the square root of the variance about 0 [56]. $\overline{\delta}$ indicates how much y_i tends to over or underestimate x_i, while $\tilde{\delta}$ is characteristic of the size of the error. Table 5.1 shows the results for all twelve of the plots in figures 5.8 and 5.9. Columns labelled DP are for polarimetric properties calculated from $\overline{\mathbf{M}}_{DP}$ using Lu-Chipman decomposition, with the modifications described earlier in this section. Columns labelled SYM are for polarimetric properties calculated using the double pass decomposition. Note that θ_D, $R'_{L<}$, $\theta'_<$, and the properties they are compared to are all recorded in radians. θ_D and $\theta'_<$ are both π periodic, which was taken into account by calculating δ_i using

$$\delta_i = \text{mod}(y_i - x_i + \pi/2,\, \pi) - \pi/2$$

in order to give values of δ_i in the range $(-\pi/2,\, \pi/2)$.

Generally, table 5.1 confirms that for this set of single pass MMs, polarimetric properties calculated using the double pass decomposition are better predictors of the true single pass values than those calculated using the Lu-Chipman decomposition of $\overline{\mathbf{M}}_{DP}$. The difference between the two is most dramatic for depolarization power Δ, which tends to be overestimated by Δ'_{DP}.

However, this result is dependent on the statistical properties of the set of single pass MMs. The set used in these simulations so far was designed to have a wide range of

Polarimetric Properties			$\overline{\delta}$		$\hat{\delta}$	
Single Pass	DP	SYM	DP	SYM	DP	SYM
D_L	$D_{L,DP}$	$D_{L,SYM}$	0.0286	0.0191	0.0502	0.0510
D_C	$D_{C,DP}$	$D_{C,SYM}$	-0.0001	-0.0004	0.0456	0.0588
θ_D	$\theta_{D,DP}$	$\theta_{D,SYM}$	-0.0028	0.0001	0.4337	0.4496
$R'_{L<}$	$R_{L,DP}/2$	$R'_{L<,SYM}$	0.0010	0.0010	0.0332	0.0333
$\theta'_<$	θ_{DP}	$\theta'_{<,SYM}$	0.0010	0.0010	0.1479	0.1490
Δ	Δ'_{DP}	Δ_{SYM}	0.0085	0.0053	0.0139	0.0129

Table 5.2: Table showing the similarities between polarimetric properties calculated from weakly diattenuating and polarizing single pass and corresponding double pass MMs.

polarimetric properties (see Appendix B), and not necessarily to be realistic to single pass MMs of the retina and amyloid deposits. It can be observed from figure 5.8 that the double pass decomposition performs best for large values of diattenuation. However, retinal amyloid deposits measured *ex vivo* are typically weakly diattenuating [68] and previous *in vivo* ocular measurements have shown low (but non-negligible) amounts of diattenuation [28, 126]. Therefore, as described in Appendix B, a second set of 30 000 single pass MMs was randomly generated, this time restricting the magnitudes of the single pass diattenuation D and depolarizer-polarizance $P_{\Delta P}$ to be in the range $[0, 0.2]$ (while in the original set they were in the range $[0, 1]$). The results of this simulation are shown in table 5.2. Under these conditions, the Lu-Chipman decomposition of $\overline{\mathbf{M}}_{DP}$ and the double pass decomposition have very similar results for linear retardance, linear retardance fast axis, and depolarization power. As a corollary, this indicates that the tendency of Δ'_{DP} to overestimate Δ in the first simulation (see figure 5.9e and table 5.1) was due to the presence of high amounts of diattenuation. Neither approach provides a good estimate of the single pass diattenuation, but the Lu-Chipman decomposition of $\overline{\mathbf{M}}_{DP}$ performs slightly better.

These simulations compare the interpretive power of the Lu-Chipman decomposition of $\overline{\mathbf{M}}_{DP}$ and the double pass decomposition developed in section 5.3, as assessed by how closely the polarimetric properties they extract resemble the true single pass values. The double pass decomposition has large advantages when the sample may be strongly diattenuating, but these disappear under conditions that are more realistic for *in vivo* retinal polarimetry. Still, the double pass decomposition is appealing for its ability to explicitly extract a possible single pass MM from $\mathbf{M}_{DP}$, and as discussed in section 5.3 it can test whether an experimental MM is consistent with the double pass model. As well, it may be useful for other non-retinal samples that fit a double pass model (*e.g.* [13, 41, 138]). A next step would be to compare the results of the two decompositions when applied to

experimental results from *in vivo* retinal polarimetry.

5.5 Conclusion

This chapter has explored the relationship between single and double pass polarimetric properties. In section 5.2, it was demonstrated that a single pass MM can be left multiplied by the MM of a circular retarder, half wave linear retarder, or a scaled circular diattenuator without altering the double pass MM. When no depolarization is present, it was shown how to calculate the "principal" single pass MM from the Lu-Chipman decomposition of the double pass MM, which has the property that single pass retardance and diattenuation are parallel to double pass retardance and diattenuation. All other possible single pass non-depolarizing MMs can be determined through transformations of the principal MM. Sets of single pass retardance and diattenuation vectors that corresponded to the same double pass MM were visualized in 3D space, showing the plurality of possible single pass properties. The effects of these transformations on depolarizing MMs were also considered, leading to results which show the ambiguity of the single pass circular polarizance and circular retardance.

The "double pass decomposition" was developed in section 5.3, which allows a single pass MM to be inferred from the double pass MM even when depolarization is present. Applied to experimental RI MMs measured in *in vivo* retinal polarimetry, this method could also be a test of the validity of the double pass model, and probe the nature of the reflection occurring in the retina. Section 5.4 used simulations to test the similarity of single and double pass polarimetric properties. These confirmed the lack of a correlation between single and double pass values of circular polarizance and circular retardance. Simulations were also used to compare the relative merits of the double pass decomposition and the Lu-Chipman decomposition as methods of interpreting the double pass MM. The double pass decomposition was found to have major advantages when it was possible for the sample to have large amounts of diattenuation. These results are useful both for the current *ex vivo* work of Campbell Labs, in order to identify polarimetric properties that are accessible in double pass, and for future *in vivo* work, in order to interpret double pass MMs.

Chapter 6

Discussion

This thesis has proposed a partial polarimetry approach to *in vivo* measurements of the human retina, which could be used for AD diagnosis. This approach is based on the double pass model without additional assumptions about the polarimetric properties of the retina or of retinal amyloid deposits. It has been shown how to use the mathematical structure implied by the double pass model advantageously for measuring and interpreting double pass MMs.

Chapter 3, following the work of previous authors, described the reciprocity theorem and used it to express the double pass model in terms of MMs. This provided two results: firstly, it indicated that double pass MMs are RI, meaning they obey a set of linear restrictions between MM elements. Secondly, it explicitly relates single pass MMs and double pass MMs. Additionally, a polarization ray tracing model was introduced in order to provide additional support for the notion that the MM measured in *in vivo* retinal polarimetry should be RI. It was noted that past MMs measured by full *in vivo* retinal polarimeters were partially non-RI. This was postulated to be due to a lack of symmetry between the input and output branches of those instruments, meaning that the strict applicability of the double pass model might vary between instruments.

Chapter 4 made use of the fact that RI MMs have fewer degrees of freedom than ordinary MMs. This reduces the minimum number of measurements necessary to determine the MM from sixteen to nine or ten, depending on the type of reciprocal invariance. It was shown how to incorporate the restrictions on RI MMs into the polarimetric measurement equation. This approach can be used to reconstruct a RI MM from a set of only nine or ten irradiance measurements. Additionally, a novel technique was developed for optimizing the error performance of a partial polarimeter for measuring RI MMs. The technique was

demonstrated by finding several designs for a PSG and PSA that each consisted of a linear polarizer and rotating QWP, using as few as nine or ten measurements. Using a simulation, these designs were shown to have comparable error performance to a standard sixteen measurement full polarimeter design. The reduction in the number of necessary measurements can allow for faster determination of the MM, which is particularly important for the application of finding retinal amyloid *in vivo*. These designs were also able to account for practical considerations like the time required to rotate the QWPs, and the possibility of dropped measurements due to blinks or eye movement. In total, six new PSG and PSA designs were listed, which used different numbers of measurements or prioritized different objectives. These designs could be used for faster measurement of double pass MMs in the retina *in vivo*. The methodology demonstrated in chapter 4 could also be applied for optimizing PSGs and PSAs made up of different optical components than a linear polarizer and rotating QWP. As well, it could be used to optimize partial polarimeters for measuring MMs with other symmetries besides reciprocal invariance, which could be useful outside the field of *in vivo* retinal polarimetry.

Chapter 5 has considered the relationship between single and double pass polarimetric properties. It was shown that for a given double pass MM, there is a large set of possible corresponding single pass MMs. In the case where no depolarization is present, an algorithm was developed that can find every possible single pass MM. Several transformations were found that can be performed on the single pass MM without altering the double pass MM: left multiplication by a circular retarder, linear half-wave retarder, or scaled circular diattenuator. By applying these transformations to depolarizing single pass MMs, it was shown that single pass circular retardance and circular polarizance can take a wide range of values for any individual double pass MM. Next, the double pass decomposition algorithm was developed, which is a novel adaptation of the existing symmetric decomposition of Ossikovski [95]. This algorithm returns possible single pass polarimetric properties for double pass MMs that contain depolarization. Using a simulation, the double pass decomposition was compared to the Lu-Chipman decomposition in terms of their ability to predict the true single pass polarimetric properties from a double pass MM. For MMs with significant amounts of diattenuation, it was found that the double pass decomposition returned values of linear retardance, diattenuation, and depolarization that were more similar to the true single pass values than those based on the Lu-Chipman decomposition. The double pass decomposition provides a new way of interpreting double pass MMs which may give additional insight into the microstructural features of the sample.

These ideas could be applied in a future *in vivo* retinal polarimeter imaging retinal amyloid deposits for the purpose of AD diagnosis.

References

[1] Sanaz Alali and Alex Vitkin. Polarized light imaging in biomedicine: emerging Mueller matrix methodologies for bulk tissue assessment. *Journal of Biomedical Optics*, 20(6):1–9, mar 2015. 1, 14

[2] Andrey S Alenin and J. Scott Tyo. Structured decomposition design of partial Mueller matrix polarimeters. *Journal of the Optical Society of America A*, 32(7):1302, jul 2015. 39

[3] Andrey S Alenin and J. Scott Tyo. Design of channeled partial Mueller matrix polarimeters. *Journal of the Optical Society of America A*, 33(6):1060, jun 2016. 39

[4] Amrit Ambirajan. Optimum angles for a polarimeter: part I. *Optical Engineering*, 34(6):1651, 1995. 19, 22, 38, 43, 55

[5] Guillaume Anna, François Goudail, and Daniel Dolfi. Optimal discrimination of multiple regions with an active polarimetric imager. *Optics Express*, 19(25):25367–25378, 2011. 39

[6] N P Armitage. Constraints on Jones transmission matrices from time-reversal invariance and discrete spatial symmetries. *Phys. Rev. B*, 90(3):35135, jul 2014. 26

[7] Pablo Artal, Ignacio Iglesias, Norberto López-Gil, and Daniel G Green. Double-pass measurements of the retinal-image quality with unequal entrance and exit pupil sizes and the reversibility of the eye's optical system. *Journal of the Optical Society of America A*, 12(10):2358–2366, 1995. 3

[8] Oriol Arteaga and Adolf Canillas. Analytic inversion of the Mueller-Jones polarization matrices for homogeneous media. *Opt. Lett.*, 35(4):559–561, feb 2010. 13

[9] Oriol Arteaga and Razvigor Ossikovski. Complete Mueller matrix from a partial polarimetry experiment: the 12-element case. *Journal of the Optical Society of America A*, 36(3):416, mar 2019. 39

[10] James Arvo. Fast random rotation matrices. In *Graphics Gems III (IBM Version)*, pages 117–120. Elsevier Science, Burlington :, 1992. 119

[11] Alzheimer's Association. 2019 Alzheimer's disease facts and figures. *Alzheimer's & Dementia*, 15(3):321–387, 2019. 1, 2

[12] Arthur J Atkinson, Wayne A Colburn, Victor G DeGruttola, David L DeMets, Gregory J Downing, Daniel F Hoth, John A Oates, Carl C Peck, Robert T Schooley, Bert A Spilker, Janet Woodcock, and Scott L Zeger. Biomarkers and surrogate endpoints: Preferred definitions and conceptual framework. *Clinical pharmacology and therapeutics*, 69(3):89–95, 2001. 2

[13] R M A Azzam. Return-path ellipsometry and a novel normal-incidence null ellipsometer (NINE). *Optica Acta: International Journal of Optics*, 24(10):1039–1049, 1977. 19, 63, 96

[14] Neil A Beaudry, Yanming Zhao, and Russell Chipman. Dielectric tensor measurement from a single Mueller matrix image. *J. Opt. Soc. Am. A*, 24(3):814–824, mar 2007. 19

[15] Rajendra Bhandari. Reciprocity constraints on the matrix of reflection from optically anisotropic surfaces. *J. Opt. Soc. Am. A*, 26(11):2368–2372, nov 2009. 29

[16] Valérie Biousse, Beau B Bruce, and Nancy J Newman. Ophthalmoscopy in the 21st century: the 2017 H. Houston Merritt Lecture. *Neurology*, 90(4):167–175, 2018. 1

[17] C Bohley and T Scharf. Polarization of light reflected by cholesteric blue phases. *Journal of Optics A: Pure and Applied Optics*, 6(3):S77–S80, 2004. 65

[18] Anmole S Bolla and Ronny Priefer. Blood glucose monitoring- an overview of current and future non-invasive devices. *Diabetes & Metabolic Syndrome: Clinical Research & Reviews*, 14(5):739–751, 2020. 13

[19] M. Born and E. Wolf. *Principles of Optics 7th edition*. Cambridge University Press, 1999. 1, 6, 7, 8, 10, 11, 12

[20] Anatoli Borovoi, Alexander Konoshonkin, and Natalia Kustova. Backscattering reciprocity for large particles. *Opt. Lett.*, 38(9):1485–1487, may 2013. 29, 32

[21] Juan M Bueno. Measurement of parameters of polarization in the living human eye using imaging polarimetry. *Vision Research*, 40(28):3791–3799, 2000. 3, 36

[22] Juan M Bueno. Depolarization effects in the human eye. *Vision Research*, 41(21):2687–2696, 2001. 3, 36

[23] Juan M Bueno. Indices of linear polarization for an optical system. *Journal of Optics A: Pure and Applied Optics*, 3(6):470–476, oct 2001. 36

[24] Juan M Bueno. Reversibilidad óptica en polarización: aplicación al ojo humano. *Revista Digital Puntex*, (152), 2001. 2, 24, 25, 29, 31, 32, 63, 65, 66, 123

[25] Juan M Bueno. Polarimetry in the human eye using an imaging linear polariscope. *Journal of Optics A: Pure and Applied Optics*, 4(5):553–561, 2002. 3, 36, 38

[26] Juan M Bueno. The influence of depolarization and corneal birefringence on ocular polarization. *Journal of Optics A: Pure and Applied Optics*, 6(3):S91–S99, feb 2004. 3, 24, 31, 36

[27] Juan M Bueno and Pablo Artal. Double-pass imaging polarimetry in the human eye. *Opt. Lett.*, 24(1):64–66, jan 1999. 3, 36

[28] Juan M Bueno and Pablo Artal. Average double-pass ocular diattenuation using foveal fixation. *Journal of Modern Optics*, 55(4-5):849–859, feb 2008. 3, 36, 96

[29] Juan M Bueno and Melanie C W Campbell. Confocal scanning laser ophthalmoscopy improvement by use of Mueller-matrix polarimetry. *Opt. Lett.*, 27(10):830–832, may 2002. 3, 19, 31, 51, 115

[30] Juan M Bueno and Melanie C W Campbell. Polarization properties of the in vitro old human crystalline lens. *Ophthalmic and Physiological Optics*, 23(2):109–118, 2003. 2, 3

[31] Juan M Bueno, Jennifer J Hunter, Christopher J Cookson, Marsha L Kisilak, and Melanie C W Campbell. Improved scanning laser fundus imaging using polarimetry. *Journal of the Optical Society of America A*, 24(5):1337–1348, 2007. 36

[32] Juan M Bueno and Jaroslaw Jaronski. Spatially resolved polarization properties for in vitro corneas. *Ophthalmic and Physiological Optics*, 21(5):384–392, sep 2001. 2

[33] Juan M Bueno and Brian Vohnsen. Polarimetric high-resolution confocal scanning laser ophthalmoscope. *Vision Research*, 45(28):3526 – 3534, 2005. 36, 49, 124

[34] Stephen A Burns, Ann E Elsner, Mariane B Mellem-Kairala, and Ruthanne B Simmons. Improved contrast of subretinal structures using polarization analysis. *Investigative Ophthalmology & Visual Science*, 44(9):4061–4068, sep 2003. 36

[35] M C W Campbell, L J F Gowing, Y Choi, and Z Leonenko. Imaging of amyloid-beta deposits in the postmortem retina in Alzheimer's disease. *Investigative Ophthalmology & Visual Science*, 51(13):5778, apr 2010. 2

[36] Subrahmanyan Chandrasekhar. *Radiative transfer*. Dover Publications, New York, 1960. 29

[37] Russell A Chipman. Polarization analysis of optical systems. *Optical Engineering*, 28(2):90 – 99, 1989. 32

[38] Russell A Chipman. Mechanics of polarization ray tracing. *Optical Engineering*, 34(6):1636 – 1645, 1995. 32

[39] Russell A Chipman. Mueller matrices. In Michael Bass and Virendra N. Mahajan, editors, *Handbook of Optics Volume I*, chapter 14. McGraw Hill, New York, 3 edition, 2010. 12, 14, 16, 17, 31, 68, 119, 120, 124

[40] Russell A Chipman. Polarimetry. In Michael Bass and Virendra N. Mahajan, editors, *Handbook of Optics Volume I*, chapter 15. McGraw Hill, New York, 3 edition, 2010. 1, 7, 17, 19, 20, 21, 22, 38, 40, 41, 54

[41] Shane Cloude. *Polarisation: Applications in Remote Sensing*. Oxford University Press, feb 2010. 7, 11, 12, 13, 19, 27, 30, 66, 96

[42] Shane R Cloude. Conditions for the physical realisability of matrix operators in polarimetry. In Russell A Chipman, editor, *Polarization Considerations for Optical Systems II*, volume 1166, pages 177 – 187. SPIE, 1990. 18, 54, 118, 120

[43] Frank Corapi, Melanie C W Campbell, Laura Emptage, Rachel Redekop, Monika Kitor, Veronica Hirsch-Reinshagen, Robin Hsiung, and Ian Mackenzie. Correlation between amyloid beta deposits in ex vivo retinas and severity of Alzheimer's brain pathology. *Investigative Ophthalmology & Visual Science*, 59(9):1582, jul 2018. 2, 23

[44] A T de Hoop. A reciprocity theorem for the electromagnetic field scattered by an obstacle. *Applied Scientific Research, Section B*, 8(1):135–140, 1960. 26, 27

[45] David DeVries, Melanie C W Campbell, Laura Emptage, Chris Cookson, Marsha Kisilak, Francisco J Avila, Juan M Bueno, Rachel Redekop, and Matthew Wilson. Polarization properties of amyloid beta deposits in ex vivo human retinas from those with Alzheimer's disease differ from surrounding retina. *Investigative Ophthalmology & Visual Science*, 56(7):2385, jun 2015. 2, 14

[46] Adrian Doicu, Thomas Wriedt, and Yuri A Eremin. *Light scattering by systems of particles: null-field method with discrete sources: theory and programs*, volume 124. Springer, 2006. 12, 26

[47] William J Donnelly and Austin Roorda. Optimal pupil size in the human eye for axial resolution. *J. Opt. Soc. Am. A*, 20(11):2010–2015, nov 2003. 32, 35

[48] Andreas W Dreher and Klaus Reiter. Scanning laser polarimetry of the retinal nerve fiber layer. In Dennis H Goldstein and Russell A Chipman, editors, *Polarization Analysis and Measurement*, volume 1746, pages 34 – 41. SPIE, 1992. 36

[49] Andreas W Dreher, Klaus Reiter, and Robert N Weinreb. Spatially resolved birefringence of the retinal nerve fiber layer assessed with a retinal laser ellipsometer. *Appl. Opt.*, 31(19):3730–3735, jul 1992. 3, 13, 36, 66, 91

[50] Matthieu Dubreuil, Philippe Babilotte, Loïc Martin, David Sevrain, Sylvain Rivet, Yann Le Grand, Guy Le Brun, Bruno Turlin, and Bernard Le Jeune. Mueller matrix polarimetry for improved liver fibrosis diagnosis. *Opt. Lett.*, 37(6):1061–1063, mar 2012. 1, 13, 23

[51] Ann E Elsner, Anke Weber, Michael C Cheney, Dean A VanNasdale, and Masahiro Miura. Imaging polarimetry in patients with neovascular age-related macular degeneration. *J. Opt. Soc. Am. A*, 24(5):1468–1480, may 2007. 2

[52] William Ford. Chapter 7 - Vector and Matrix Norms, 2014. 45

[53] José J. Gil Pérez and Razvigor Ossikovski. *Polarized Light and the Mueller Matrix Approach*. CRC Press, jul 2017. 6, 7, 8, 9, 10, 12, 13, 14, 15, 16, 17, 18, 21, 23, 27, 28, 29, 31, 35, 54, 65, 74, 83, 84, 85, 118, 120, 121, 122, 127, 131, 132, 133, 134, 135

[54] Jean-Jacques Greffet and Manuel Nieto-Vesperinas. Field theory for generalized bidirectional reflectivity: derivation of Helmholtz's reciprocity principle and Kirchhoff's law. *Journal of the Optical Society of America A*, 15(10):2735–2744, 1998. 26, 29

[55] Matthew Hayman, Scott Spuler, Bruce Morley, and Joseph VanAndel. Polarization lidar operation for measuring backscatter phase matrices of oriented scatterers. *Opt. Express*, 20(28):29553–29567, dec 2012. 39

[56] William Lee Hays. *Statistics*. Holt, Rinehart, and Winston, New York, 1988. 95

[57] Honghui He, Ran Liao, Nan Zeng, Pengcheng Li, Zhenhua Chen, Xi Liu, and Hui Ma. Mueller matrix polarimetry-An emerging new tool for characterizing the microstructural feature of complex biological specimen, 2019. 1, 13, 14, 19

[58] Eugene Hecht. *Optics; 5th ed.* Pearson, Boston, MA, jul 2015. 1, 6, 7, 8, 9, 10, 12, 13

[59] Christian Heinrich, Jean Rehbinder, and Jihad Zallat. Revisiting the generalized polar decomposition of Mueller matrices. *J. Opt. Soc. Am. A*, 37(8):1327–1339, aug 2020. 120

[60] Roger A. Horn and Charles R. Johnson. *Topics in Matrix Analysis*. Cambridge University Press, apr 1991. 8, 71, 115, 116, 133

[61] Roger A Horn and Charles R Johnson. *Matrix analysis*. Cambridge university press, 2012. 42, 44, 45, 48, 116, 119

[62] Jinxin Huang and Jannick P Rolland. *Imaging Techniques for the Visualization and Evaluation of Tear Film Dynamics*, pages 373–385. Springer International Publishing, Cham, 2019. 3, 38

[63] Xiang-Run Huang and Robert W Knighton. Theoretical model of the polarization properties of the retinal nerve fiber layer in reflection. *Appl. Opt.*, 42(28):5726–5736, oct 2003. 32

[64] David G Hunter, Julie C Sandruck, Soma Sau, Saurabh N Patel, and David L Guyton. Mathematical modeling of retinal birefringence scanning. *Journal of the Optical Society of America A*, 16(9):2103–2111, 1999. 2, 24, 31, 63

[65] Henry Hurwitz and R Clark Jones. A new calculus for the treatment of optical systems II. proof of three general equivalence theorems. *J. Opt. Soc. Am.*, 31(7):493–499, jul 1941. 13, 29, 66

[66] John David Jackson. *Jackson - Classical Electrodynamics*. Wiley, 1962. 6, 7, 10, 13, 26

[67] Tao Jin, Laura Emptage, David DeVries, and Melanie C W Campbell. Mapping the birefringence of amyloid deposits found in retinas in association with Alzheimer's disease. In *Frontiers in Optics 2016*, page FTh5D.4. Optical Society of America, 2016. 2

[68] Jin, Tao. Polarimetric and birefringence analysis of presumed amyloid-beta deposits in the retina in association with Alzheimer's disease, 2018. 2, 3, 23, 24, 96

[69] R Clark Jones. A new calculus for the treatment of optical systems I. description and discussion of the calculus. *Journal of the Optical Society of America*, 31(7):488–493, 1941. 29

[70] Nate J Kemp, Haitham N Zaatari, Jesung Park, H Grady Rylander III, and Thomas E Milner. Form-biattenuance in fibrous tissues measured with polarization-sensitive optical coherence tomography (PS-OCT). *Opt. Express*, 13(12):4611–4628, jun 2005. 13

[71] Hélène Kergoat, Marie-Jeanne Kergoat, Lisette Justino, Howard Chertkow, Alain Robillard, and Howard Bergman. An evaluation of the retinal nerve fiber layer thickness by scanning laser polarimetry in individuals with dementia of the Alzheimer type. *Acta Ophthalmologica Scandinavica*, 79(2):187–191, 2001. 2

[72] H B klein Brink and G J van Blokland. Birefringence of the human foveal area assessed in vivo with Mueller-matrix ellipsometry. *J. Opt. Soc. Am. A*, 5(1):49–57, jan 1988. 3, 36

[73] Robert W Knighton and Xiang-Run Huang. Analytical methods for scanning laser polarimetry. *Opt. Express*, 10(21):1179–1189, oct 2002. 2, 3, 38

[74] Robert W Knighton, Xiang-Run Huang, and David S Greenfield. Analytical model of scanning laser polarimetry for retinal nerve fiber layer assessment. *Investigative Ophthalmology & Visual Science*, 43(2):383–392, jan 2002. 2, 3, 24, 31, 62, 63, 66, 91

[75] Yosef Koronyo, David Biggs, Ernesto Barron, David S Boyer, Joel A Pearlman, William J Au, Shawn J Kile, Austin Blanco, Dieu-Trang Fuchs, Adeel Ashfaq, Sally Frautschy, Gregory M Cole, Carol A Miller, David R Hinton, Steven R Verdooner, Keith L Black, and Maya Koronyo-Hamaoui. Retinal amyloid pathology and proof-of-concept imaging trial in Alzheimer's disease. *JCI insight*, 2(16):e93621, aug 2017. 2

[76] Gerhard Kristensson. *Scattering of electromagnetic waves by obstacles*. Electromagnetics and radar. The Institution of Engineering and Technology, Stevenage, 2016. 26, 27, 30

[77] Akhlesh Lakhtakia, Vijay K Varadan, and Vasundara V Varadan. *Time-harmonic electromagnetic fields in chiral media*, volume 335. Springer, 1989. 12

[78] David Lara and Chris Dainty. Double-pass axially resolved confocal Mueller matrix imaging polarimetry. *Opt. Lett.*, 30(21):2879–2881, nov 2005. 65, 66, 91, 123

[79] David Lara and Carl Paterson. High-resolution confocal full polarimeter for the living human retina. *Investigative Ophthalmology & Visual Science*, 53(14):3090, 2012. 3

[80] David Lara Saucedo. *Three-dimensional complete polarisation sensitive imaging using a confocal Mueller matrix polarimeter*. PhD thesis, Imperial College London, 2005. 63, 66

[81] D Layden, M F G Wood, and I A Vitkin. Optimum selection of input polarization states in determining the sample Mueller matrix: a dual photoelastic polarimeter approach. *Opt. Express*, 20(18):20466–20481, aug 2012. 22, 38, 39, 43, 51, 115, 116

[82] Xiaobo Li, Haofeng Hu, Lan Wu, and Tiegen Liu. Optimization of instrument matrix for Mueller matrix ellipsometry based on partial elements analysis of the Mueller matrix. *Opt. Express*, 25(16):18872–18884, aug 2017. 38

[83] Shih-Yau Lu and Russell A Chipman. Interpretation of Mueller matrices based on polar decomposition. *Journal of the Optical Society of America A*, 13(5):1106, may 1996. 14, 15, 16, 17, 18, 23, 63, 69, 74, 82, 86, 119, 120, 131

[84] Ian J C MacCormick, Gabriela Czanner, and Brian Faragher. Developing retinal biomarkers of neurological disease: an analytical perspective. *Biomarkers in Medicine*, 9(7):691–701, 2015. 1

[85] C Macias-Romero and P Török. Eigenvalue calibration methods for polarimetry. *Journal of the European Optical Society - Rapid publications*, 7(0), 2012. 116

[86] S Manhas, M K Swami, P Buddhiwant, N Ghosh, P K Gupta, and K Singh. Mueller matrix approach for determination of optical rotation in chiral turbid media in backscattering geometry. *Opt. Express*, 14(1):190–202, jan 2006. 66, 67

[87] Mario Martinelli and Paolo Martelli. Polarization, mirrors, and reciprocity: birefringence and its compensation in optical retracing circuits. *Adv. Opt. Photon.*, 9(1):129–168, mar 2017. 66

[88] Susana Martinez-Conde, Stephen L Macknik, and David H Hubel. The role of fixational eye movements in visual perception. *Nature reviews neuroscience*, 5(3):229–240, 2004. 3, 38, 52

[89] MATLAB. *9.8.0.1323502 (R2020a)*. The MathWorks Inc., Natick, Massachusetts, 2020. 15, 42, 53

[90] James P McGuire and Russell A Chipman. Diffraction image formation in optical systems with polarization aberrations. I: Formulation and example. *J. Opt. Soc. Am. A*, 7(9):1614–1626, sep 1990. 32

[91] Michael I Mishchenko, Joop W Hovenier, and Larry D Travis. Light scattering by nonspherical particles: theory, measurements, and applications. *Atoms, Molecules, Lasers*, 2000. 30

[92] Christine T O Nguyen, Flora Hui, Jason Charng, Shajan Velaedan, Anna K van Koeverden, Jeremiah K H Lim, Zheng He, Vickie H Y Wong, Algis J Vingrys, Bang V Bui, and Magnus Ivarsson. Retinal biomarkers provide "insight" into cortical pharmacology and disease. *Pharmacology & Therapeutics*, 175:151 – 177, 2017. 1, 2

[93] H D Noble and R A Chipman. Mueller matrix roots algorithm and computational considerations. *Opt. Express*, 20(1):17–31, jan 2012. 118

[94] R Oldenbourg and T Ruiz. Birefringence of macromolecules. Wiener's theory revisited, with applications to DNA and tobacco mosaic virus. *Biophysical Journal*, 56(1):195 – 205, 1989. 13

[95] Razvigor Ossikovski. Analysis of depolarizing Mueller matrices through a symmetric decomposition. *Journal of the Optical Society of America A*, 26(5):1109, may 2009. 64, 84, 92, 99, 121, 131

[96] Razvigor Ossikovski and Oriol Arteaga. Complete Mueller matrix from a partial polarimetry experiment: the nine-element case. *Journal of the Optical Society of America A*, 36(3):403, mar 2019. 39

[97] Razvigor Ossikovski, Antonello De Martino, and Steve Guyot. Forward and reverse product decompositions of depolarizing Mueller matrices. *Opt. Lett.*, 32(6):689–691, mar 2007. 64, 83, 85

[98] Soichi Otsuki. Symmetry relationships for multiple scattering of polarized light in turbid spherical samples: theory and a Monte Carlo simulation. *J. Opt. Soc. Am. A*, 33(2):258–269, feb 2016. 84

[99] Joel A Papay and Ann E Elsner. Near-infrared polarimetric imaging and changes associated with normative aging. *J. Opt. Soc. Am. A*, 35(9):1487–1495, sep 2018. 2

[100] Bernhard C E Pelz, Christian Weschenmoser, Stefan Goelz, Joerg P Fischer, Reinhard O W Burk, and Josef F Bille. In-vivo measurement of the retinal birefringence with regard to corneal effects using an electro-optical ellipsometer. In *Proc.SPIE*, volume 2930, dec 1996. 3, 24, 31, 36, 62

[101] Angelo Pierangelo, Sandeep Manhas, Abdelali Benali, Clément Fallet, Jean-Laurent Totobenazara, Maria Rosaria Antonelli, Tatiana Novikova, Brice Gayet, Antonello De Martino, and Pierre Validire. Multispectral Mueller polarimetric imaging detecting residual cancer and cancer regression after neoadjuvant treatment for colorectal carcinomas. *Journal of Biomedical Optics*, 18(4):1–10, 2013. 1, 23

[102] M Planitz. Inconsistent systems of linear equations. *The Mathematical Gazette*, 63(425):181, 1979. 22, 41

[103] Jason Porter, Antonio Guirao, Ian G Cox, and David R Williams. Monochromatic aberrations of the human eye in a large population. *J. Opt. Soc. Am. A*, 18(8):1793–1803, aug 2001. 32

[104] R J Potton. Reciprocity in optics. *Reports on Progress in Physics*, 67(5):717–754, 2004. 26, 29

[105] Ji Qi, Honghui He, Hui Ma, and Daniel S Elson. Extended polar decomposition method of Mueller matrices for turbid media in reflection geometry. *Opt. Lett.*, 42(20):4048–4051, oct 2017. 65, 87, 123

[106] Yunyi Qiu, Tao Jin, Erik Mason, and Melanie C W Campbell. Predicting thioflavin fluorescence of retinal amyloid deposits associated with Alzheimer's disease from their polarimetric properties. *Translational Vision Science & Technology*, 9(2):47, aug 2020. 3, 14, 24, 65

[107] R Rawer, W Stork, and K-D Müller-Glaser. Polarimetric methods for measurement of intra ocular glucose concentration. *Biomedizinische Technik/Biomedical Engineering*, 47(s1a):186–188, 2002. 13

[108] Austin John Roorda. *Double pass reflections in the human eye*. PhD thesis, University of Waterloo, 1996. 3

[109] D S Sabatke, M R Descour, E L Dereniak, W C Sweatt, S A Kemme, and G S Phipps. Optimization of retardance for a complete Stokes polarimeter. *Optics Letters*, 25(11):802, jun 2000. 45, 55

[110] Derek S Sabatke, Ann M Locke, Michael R Descour, William C Sweatt, John Phillips Garcia, Eustace L Dereniak, Shanalyn A Kemme, and Gary S Phipps. Figures of merit for complete Stokes polarimeter optimization. In *Proc.SPIE*, volume 4133, nov 2000. 44, 46

[111] Dusan Sarenac, Connor Kapahi, Andrew E Silva, David G Cory, Ivar Taminiau, Benjamin Thompson, and Dmitry A Pushin. Direct discrimination of structured light by humans. *Proceedings of the National Academy of Sciences*, 117(26):14682–14687, 2020. 1

[112] Sergey N Savenkov. Optimization and structuring of the instrument matrix for polarimetric measurements. *Optical Engineering*, 41(5):965, 2002. 38, 39

[113] Sergey N Savenkov. Analysis of generalized polarimetric measurement equation. In Joseph A Shaw and J Scott Tyo, editors, *Polarization Science and Remote Sensing III*, volume 6682, pages 347 – 358. SPIE, 2007. 38, 39

[114] David S Saxon. Tensor scattering matrix for the electromagnetic field. *Physical Review*, 100(6):1771–1775, dec 1955. 26, 27

[115] Alfred Schönhofer and Hans Georg Kuball. Symmetry properties of the Mueller matrix. *Chemical Physics*, 115(2):159–167, 1987. 28, 29, 63

[116] Zdeněk Sekera. Scattering matrices and reciprocity relationships for various representations of the state of polarization. *Journal of the Optical Society of America*, 56(12):1732, dec 1966. 27, 28

[117] Colin J R Sheppard, Artemi Bendandi, Aymeric Le Gratiet, and Alberto Diaspro. Polarization in reflectance imaging. *J. Opt. Soc. Am. A*, 37(3):491–500, mar 2020. 63, 64, 82

[118] Colin J R Sheppard, Artemi Bendandi, Aymeric Le Gratiet, and Alberto Diaspro. Eigenvalues of the coherency matrix for exact backscattering. *Journal of the Optical Society of America A*, 36(9):1540, sep 2019. 30

[119] Prashant Shukla and Asima Pradhan. Mueller decomposition images for cervical tissue: Potential for discriminating normal and dysplastic states. *Opt. Express*, 17(3):1600–1609, feb 2009. 1, 23

[120] Matthew H Smith. Optimization of a dual-rotating-retarder Mueller matrix polarimeter. *Appl. Opt.*, 41(13):2488–2493, may 2002. 38

[121] A Stanworth and E J Naylor. Polarized light studies of the cornea. *Journal of Experimental Biology*, 30(2):160, jun 1953. 2

[122] Homayoun Tabandeh and Morton F Goldberg. *The Retina in Systemic Disease: A Color Manual of Ophthalmoscopy*. Thieme, 2009. 1

[123] Hirokazu Takahashi, Tomomi Goto, Takuhei Shoji, Masaki Tanito, Masami Park, and Etsuo Chihara. Diabetes-associated retinal nerve fiber damage evaluated with scanning laser polarimetry. *American Journal of Ophthalmology*, 142(1):88 – 94, 2006. 2

[124] Shelby E Temple, Juliette E McGregor, Camilla Miles, Laura Graham, Josie Miller, Jordan Buck, Nicholas E Scott-Samuel, and Nicholas W Roberts. Perceiving polarization with the naked eye: characterization of human polarization sensitivity. *Proceedings of the Royal Society B: Biological Sciences*, 282(1811):20150338, 2015. 1

[125] K M Twietmeyer and R A Chipman. Optimization of Mueller matrix polarimeters in the presence of error sources. *Optics Express*, 16(15):11589, jul 2008. 4, 21, 22, 38, 39, 43, 44, 45, 51, 115, 116

[126] K M Twietmeyer, R A Chipman, A E Elsner, Y Zhao, and D VanNasdale. Mueller matrix retinal imager with optimized polarization conditions. *Opt. Express*, 16(26):21339–21354, dec 2008. 3, 36, 49, 52, 96, 124

[127] Karen Marie Twietmeyer. *GDx-MM: An Imaging Mueller Matrix Retinal Polarimeter*. PhD thesis, University of Arizona, 2007. 15, 16, 36

[128] J Scott Tyo. Considerations in polarimeter design. In David B Chenault, Michael J Duggin, Walter G Egan, Dennis H Goldstein, Walter G Egan, and Michael J Duggin, editors, *Polarization Analysis, Measurement, and Remote Sensing III*, volume 4133, pages 65–74. International Society for Optics and Photonics, SPIE, 2000. 19, 22, 51, 55, 115

[129] J Scott Tyo. Extending optimization to active Mueller polarimeters. In *Proc.SPIE*, volume 4819, sep 2002. 38, 43, 51, 115

[130] J. Scott Tyo, Zhipeng Wang, Sergio J. Johnson, and Brian G. Hoover. Design and optimization of partial Mueller matrix polarimeters. *Applied Optics*, 49(12):2326–2333, apr 2010. 4, 38, 39, 41, 46

[131] H C van de Hulst. *Light scattering by small particles*. Dover books on physics. Dover, New York, NY, 1981. 9, 27, 28, 30, 49

[132] N Vansteenkiste, P Vignolo, and A Aspect. Optical reversibility theorems for polarization: application to remote control of polarization. *Journal of the Optical Society of America A*, 10(10):2240–2245, 1993. 29, 63, 66

[133] Israel J Vaughn and Brian G Hoover. Noise reduction in a laser polarimeter based on discrete waveplate rotations. *Opt. Express*, 16(3):2091–2108, feb 2008. 38, 55

[134] Hermann von Helmholtz. Helmholtz's treatise on physiological optics, 1927. 26

[135] Talbot H Waterman and Kenneth W Horch. Mechanism of polarized light perception. *Science*, 154(3748):467–475, 1966. 1

[136] Robert H Webb, George W Hughes, and Francois C Delori. Confocal scanning laser ophthalmoscope. *Appl. Opt.*, 26(8):1492–1499, apr 1987. 31, 49, 124

[137] Robert N Weinreb, Andreas W Dreher, Anne Coleman, Harry Quigley, Blake Shaw, and Klaus Reiter. Histopathologic validation of Fourier-ellipsometry measurements of retinal nerve fiber layer thickness. *Archives of Ophthalmology*, 108(4):557–560, apr 1990. 19

[138] Justin E Wolfe and Russell A Chipman. Polarimetric characterization of liquid-crystal-on-silicon panels. *Appl. Opt.*, 45(8):1688–1703, mar 2006. 19, 63, 66, 91, 96, 123

[139] J Zallat, Aïnouz S, and M Ph Stoll. Optimal configurations for imaging polarimeters: impact of image noise and systematic errors. *Journal of Optics A: Pure and Applied Optics*, 8(9):807–814, jul 2006. 4, 22, 38, 39, 43, 44, 45, 46, 51, 55, 115

[140] Linda M Zangwiil, Christopher Bowd, and Robert N Weinreb. Evaluating the optic disc and retinal nerve fiber layer in glaucoma II: optical image analysis. *Seminars in Ophthalmology*, 15(4):206–220, jan 2000. 2

[141] Q Zhou. Retinal scanning laser polarimetry and methods to compensate for corneal birefringence. *Bulletin de la Societe belge d'ophtalmologie*, (302):89–106, 2006. 62

[142] Qienyuan Zhou, Jerry Reed, Ryan W Betts, Peter Karl Trost, Pak-Wai Lo, Charles Wallace, Richard H Bienias, Guoqiang Li, Ross Winnick, William A Papworth, and Michael Sinai. Detection of glaucomatous retinal nerve fiber layer damage by scanning laser polarimetry with variable corneal compensation. In Fabrice Manns, Per G Söderberg, and Arthur Ho, editors, *Ophthalmic Technologies XIII*, volume 4951, pages 32 – 41. SPIE, 2003. 2, 3, 13, 36, 62

[143] Qienyuan Zhou and Robert N Weinreb. Individualized compensation of anterior segment birefringence during scanning laser polarimetry. *Investigative Ophthalmology & Visual Science*, 43(7):2221–2228, jul 2002. 2

APPENDICES

Appendix A

Kronecker Factorization of the Measurement Matrix

Section 4.3 described how in order to optimize the PSG and PSA, it is necessary first to write the measurement matrix $\mathbf{W} = \mathbf{W}(\boldsymbol{\psi})$ as a function of parameters $\boldsymbol{\psi}$ that describe how the PSG and PSA can be modified. Subsection 4.4.1 defined a "p by q" polarimeter design as one for which the PSG has q unique states while the PSA has p different states, and the irradiance is measured for all pq combinations of states [29, 81, 128, 129, 139]. This greatly reduces the number of parameters that need to be optimized in $\mathbf{W}$. Under these conditions, the measurement matrix itself can be written as the Kronecker product

$$\mathbf{W} = \mathbf{G}^T \otimes \mathbf{A} \tag{A.1}$$

where $\mathbf{G}$ and $\mathbf{A}$ are $4 \times q$ and $p \times 4$ matrices respectively [125]. $\mathbf{G}$ depends only on the PSG states, while $\mathbf{A}$ depends only on the PSA states [125]. Due to the properties of the Kronecker product, the measurement equation 4.1 can be simplified into the form

$$\mathbf{I} = \mathbf{AMG}, \tag{A.2}$$

where $\mathbf{I}$ is the irradiance vector $\vec{\mathbf{I}}$ reshaped into a matrix of dimension $p \times q$ [60]. This expression is widely used and has several popular advantages over the more general equation 4.1 [29, 81, 128, 129, 139]. It can be shown that

$$\kappa_2(\mathbf{W}) = \kappa_2(\mathbf{G})\,\kappa_2(\mathbf{A}) \quad [125] \tag{A.3}$$

where $\kappa_2(\mathbf{G})$ and $\kappa_2(\mathbf{A})$ are obtained by using the singular values of $\mathbf{G}$ or $\mathbf{A}$ instead of those of $\mathbf{W}$ in equation 4.15, and using $df = 4$. Similarly, using the properties of the

Kronecker product and singular value decomposition [60]

$$\xi(\mathbf{W}) = \xi(\mathbf{G})\,\xi(\mathbf{A}). \tag{A.4}$$

Therefore, minimizing the optimization metrics of $\mathbf{G}$ and $\mathbf{A}$ separately will give the same results as minimizing the optimization metrics of $\mathbf{W}$. This simplifies the optimization process. Equation A.2 is fundamental to the eigenvalue calibration method [85] as well as a geometrical interpretation of optimization results [81, 125]. Despite how frequently this form is used, it is still an assumption: for n measurements, the PSG and PSA could each have n unique states, and then $\mathbf{W}$ may not be Kronecker factorizable. However, in the case of the full polarimeter rotating QWP design with $n = 16$, the author has found that optimizing all $2n = 32$ angles separately using ξ gives the same result as optimizing while assuming a four by four design.

Next, it was considered if similar simplifications could be found for the modified measurement equation 4.7. To the best of the author's knowledge, this analysis is novel. In general, even if $\mathbf{W}$ is Kronecker factorizable (equation A.1), $\mathbf{W}_{RI}$ may not be. The Kronecker factorizability of $\mathbf{W}_{RI}$ would be guaranteed if the matrix $\mathbf{z}$ can be written in the form $\mathbf{z} = \mathbf{E} \otimes \mathbf{F}$ where $\mathbf{E}$ and $\mathbf{F}$ are matrices of appropriate dimensions:

$$\begin{aligned} \mathbf{W}_{RI} &= \mathbf{W}\mathbf{z} \\ &= (\mathbf{G}^T \otimes \mathbf{A})(\mathbf{E} \otimes \mathbf{F}) && \text{(A.5)} \\ &= (\mathbf{G}^T\mathbf{E}) \otimes (\mathbf{A}\mathbf{F}) \quad [60]. && \text{(A.6)} \end{aligned}$$

This last equation would allow for the PSG and PSA to be optimized separately, and potentially for the eigenvalue calibration method to be extended to RI MMs. However, it was found that no such decomposition exists for any of the possible versions of $\mathbf{z}$ (even without the requirement that $\mathbf{z}^T\mathbf{z} = \mathbf{I}$). Equation A.6 requires that $\mathbf{E}$ and $\mathbf{F}$ are multiplication compatible with $\mathbf{G}^T$ and $\mathbf{A}$, which implies that they are of dimension $4 \times r$ and $4 \times s$ respectively for whole numbers r and s. As well, recall that $\mathbf{z}$ is $16 \times a$ and $\text{rank}(\mathbf{z}) = a$ where $a = 9, 10$ for nine and ten parameter RI MMs. The equation $\mathbf{z} = \mathbf{E} \otimes \mathbf{F}$ requires that $rs = a$ and $\text{rank}(\mathbf{E})\text{rank}(\mathbf{F}) = a$ [60]. The rank of a matrix cannot be larger than its smallest dimension [61], so additionally $\text{rank}(\mathbf{E}) \leq \min\{4, r\}$ and $\text{rank}(\mathbf{F}) \leq \min\{4, s\}$.

For ten parameter RI MMs, it can be shown by exhaustion that there are no whole numbers r and s that can simultaneously satisfy all of these restrictions. This means that $\mathbf{z}$ is not Kronecker factorizable and $\mathbf{W}_{RI}$ cannot be written as in equation A.6. For nine parameter RI MMs, the restrictions can be satisfied if $\mathbf{E}$ and $\mathbf{F}$ are both 4×3. However, a proof by contradiction was found that shows that $\mathbf{z}$ is still not Kronecker factorizable: take

a known $\mathbf{z}$ with $\mathbf{z}^T\mathbf{z} = \mathbf{I}$. Every other possible version of $\mathbf{z}$ can be written as $\mathbf{z}' = \mathbf{z}\mathbf{C}$ with $\det(\mathbf{C}) \neq 0$. Suppose there exist 4×3 matrices $\mathbf{E}$, $\mathbf{F}$ and $\mathbf{C}$ such that $\mathbf{E} \otimes \mathbf{F} = \mathbf{z}' = \mathbf{z}\mathbf{C}$. Then $\mathbf{z}^T(\mathbf{E} \otimes \mathbf{F}) = \mathbf{C}$. This matrix was analyzed algebraically using MATLAB, using twenty-four independent variables to represent the entries of $\mathbf{E}$ and $\mathbf{F}$. It was found that $\det(\mathbf{z}^T(\mathbf{E} \otimes \mathbf{F})) = 0$ for all 4×3 matrices $\mathbf{E}$ and $\mathbf{F}$. Therefore $\mathbf{C}$ is singular, which is a contradiction. This implies that no version of $\mathbf{z}$ is Kronecker factorizable[1]. As a result, there is no analog to equation A.2 for RI MMs, and the PSG and PSA must be optimized simultaneously.

The same arguments lead to the conclusion that no "p by q" polarimeter can possibly measure RI MMs using the minimum number of measurements. For ten parameter RI MMs, it can be shown that five by two and ten by one designs lead to an $\mathbf{W}_{RI}$ of insufficient rank, so it will not have an inverse. For nine parameter RI MMs, the only option is a three by three design. In the previous paragraph, it was shown that $\det(\mathbf{z}^T(\mathbf{E} \otimes \mathbf{F})) = 0$ for all 4×3 matrices $\mathbf{E}$ and $\mathbf{F}$. This implies that

$$\begin{aligned} \det(\mathbf{W}_{RI}) &= \det((\mathbf{G}^T \otimes \mathbf{A})\mathbf{z}) && \text{(A.7)} \\ &= \det(\mathbf{z}^T\,(\mathbf{A}^T \otimes \mathbf{G})) && \text{(A.8)} \\ &= 0 && \text{(A.9)} \end{aligned}$$

because for a three by three design, $\mathbf{A}^T$ and $\mathbf{G}$ are both 4×3 matrices. Therefore, for any three by three design $\mathbf{W}_{RI}$ has no inverse and cannot be used to determine $\vec{\mathbf{M}}$.

While "p by q" designs are convenient options for full polarimeters because of the fact that they allow the PSG and PSA to be optimized separately, it has been shown that this feature does not extend to $\mathbf{W}_{RI}$. As well, it has been shown that "p by q" designs cannot determine RI MMs in the minimum number of measurements. Therefore, the designs found in chapter 4 use different parameterizations of $\mathbf{W}(\boldsymbol{\psi})$.

[1]Thanks to Dr. Ignacio Ojeda for an interesting correspondence that contributed to the development of this proof by contradiction.

Appendix B

Random Generation of Mueller Matrices

At several points in this thesis, simulations have been performed using example MMs. The results of these tests naturally depend on the properties of the example set. It was decided to use randomly generated MMs in order to be able to easily adjust the distributions of polarimetric properties of the set.

One method that has been used by Noble and Chipman [93] is to simply randomly generate real 4×4 matrices and throw out those that are not valid MMs (the criterion for a matrix to be a valid MM (also called a *physical* or *physically realizable* MM) can be found in [42, 53]). The odds can be improved somewhat by setting $M(1,1) = 1$ and forcing the other fifteen elements to be in the range $[-1, 1]$. This method is computationally costly: Noble and Chipman found that of a set of 10^9 matrices generated in this way, only 76,336 were physical MMs [93]. The methods used in this thesis are based instead on the idea of inverting one of the decompositions described in section 2.3.2. This can be far less computationally expensive, and also allows one to control the distributions of some polarimetric properties of the generated MMs. After these methods were developed, Heinrich *et al.* published a paper that used randomly generated MMs produced by inverting the Lu-Chipman decomposition, similar to what is done in Appendix B.1.

B.1 Methodology for Section 5.4

In section 5.4, MMs were generated using a method based on the Lu-Chipman decomposition

$$\mathbf{M} = c\,\mathbf{M}_{\Delta P}\,\mathbf{M}_R\,\mathbf{M}_D. \tag{2.58}$$

Unit vectors with arbitrary orientation can be generated using

$$\hat{\mathbf{D}} = [2\cos(2\pi x_1)\sqrt{x_2(1-x_2)},\ 2\sin(2\pi x_1)\sqrt{x_2(1-x_2)},\ 2x_2 - 1]^T \tag{B.1}$$

where x_1 and x_2 are random variables each taken from a uniform distribution over the interval $[0, 1]$ [10]. A set of $\hat{\mathbf{D}}$ generated in this way will be uniformly distributed over the surface of the unit sphere [10]. The diattenuation magnitude D was also taken from a uniform distribution over the interval $[0, 1]$. The resulting diattenuation vector $\mathbf{D} = D\hat{\mathbf{D}}$ was not uniformly distributed by volume, which would have required higher values of D to be produced more often. It was considered to be preferable to have a uniformly distributed diattenuation magnitude D. $\mathbf{M}_D$ can be calculated from $\mathbf{D}$ using equation 2.29.

The retardance fast axis $\hat{\mathbf{R}}$ was generated the exact same way as $\hat{\mathbf{D}}$. The retardance magnitude R was taken from a uniform distribution over $[0, \pi]$, after which $\mathbf{M}_R$ could be calculated from $\mathbf{R} = R\hat{\mathbf{R}}$ using expressions found in [39].

In the depolarizer matrix

$$\mathbf{M}_{\Delta P} = \begin{bmatrix} 1 & \mathbf{0}^T \\ \mathbf{P}_{\Delta P} & \mathbf{m}_{\Delta P} \end{bmatrix}, \tag{2.59}$$

$\mathbf{P}_{\Delta P}$ is a polarizance vector and so must have $P_{\Delta P} \leq 1$, while $\mathbf{m}_{\Delta P}$ must be symmetric [83]. These constraints are not enough to guarantee that $\mathbf{M}_{\Delta P}$ is physically realizable. Therefore it will be necessary to throw out some of the MMs that are generated using this method, keeping only those that are physical.

Because $\mathbf{m}_{\Delta P}$ is symmetric, it has an eigendecomposition of the form

$$\mathbf{m}_{\Delta P} = \mathbf{m}_{R_\Delta}^T\,\mathrm{diag}(e_1,\, e_2,\, e_3)\,\mathbf{m}_{R_\Delta}$$

where $\mathbf{m}_{R_\Delta}$ is a real-valued matrix with $\mathbf{m}_{R_\Delta}\,\mathbf{m}_{R_\Delta}^T = \mathbf{I}_3$ and $\det(\mathbf{m}_{R_\Delta}) = +1$ [61]. $\mathbf{m}_{R_\Delta}$ is nothing other than a retarder matrix, so $\mathbf{R}_\Delta$ and $\mathbf{m}_{R_\Delta}$ can be generated in exactly the same way as $\mathbf{R}$ and $\mathbf{m}_R$.

There is a subtlety related to the signs of the three eigenvalues (e_1, e_2, e_3). If $\mathbf{M}$ has positive determinant, the polar decomposition always returns $\mathbf{m}_{\Delta P}$ having all positive

eigenvalues [83]. However, there is a very small proportion of depolarizing MMs that have negative determinant [39], which implies that one (or all three) of the eigenvalues of $\mathbf{m}_{\Delta P}$ must be negative. Different authors suggest different procedures in this case [53, 83], and it has been suggested that the Lu-Chipman decomposition should not be used at all for negative determinant MMs [39]. While it would have been possible to generate these MMs, it was unknown in what proportion to include them relative to positive determinant MMs. Because of their rarity it was expected that they would have very little impact on the averages that were reported in section 5.4. Therefore, only positive determinant MMs were generated. The recent paper by Heinrich *et al.* [59] uses a similar approach to generating MMs but includes those with negative determinant.

The orientation of the depolarizer-polarizance vector, $\hat{\mathbf{P}}_{\Delta P}$, was generated in the same way as the diattenuation and retardance orientations. The only remaining parameters necessary to determine the MM are e_1, e_2, e_3, and $P_{\Delta P}$. These were generated using

$$e_i = y_i^{\lambda}, \quad i = 1, 2, 3 \tag{B.2}$$

$$P_{\Delta P} = y_4^{1/\lambda} \tag{B.3}$$

where y_1, y_2, y_3, and y_4 are random variables each taken from a uniform distribution over the interval $[0, 1]$. The extra parameter $\lambda > 0$ was introduced as a convenient way to adjust the average amount of depolarization in the generated matrices. Initially with $\lambda = 1$, it was found that depolarization power Δ (equation 2.45) tended to be very high for physical MMs that were generated. Figure B.1 shows the histograms for Δ when two different values of λ were used. Based on these observations, $\lambda = 0.5$ was used for the matrices generated in section 5.4.

The resulting $\mathbf{M}_{\Delta P}$, $\mathbf{M}_R$, and $\mathbf{M}_D$ were multiplied together to obtain the single pass $\mathbf{M}_{SP}$. The scalar constant c would have had no impact on any of the results in section 5.4, so it was set equal to one. A set of 2×10^5 $\mathbf{M}_{SP}$ were generated this way. Then, these were checked using Cloude's criterion [42, 53] and all unphysical matrices were discared. This resulted in a set of $\approx 35\,000$ physical MMs, of which $30\,000$ were selected at random. These MMs had nearly uniformly distributed D and R, uniformly oriented $\hat{\mathbf{D}}$ and $\hat{\mathbf{R}}$, and Δ distributed as in the red curve in figure B.1.

Later in section 5.4, a second set was generated with the goal of showing behaviour for a weakly diattenuating sample. The same procedure was used as above, except for that the variables D and P_Δ were uniformly distributed on the interval $[0, 0.2]$.

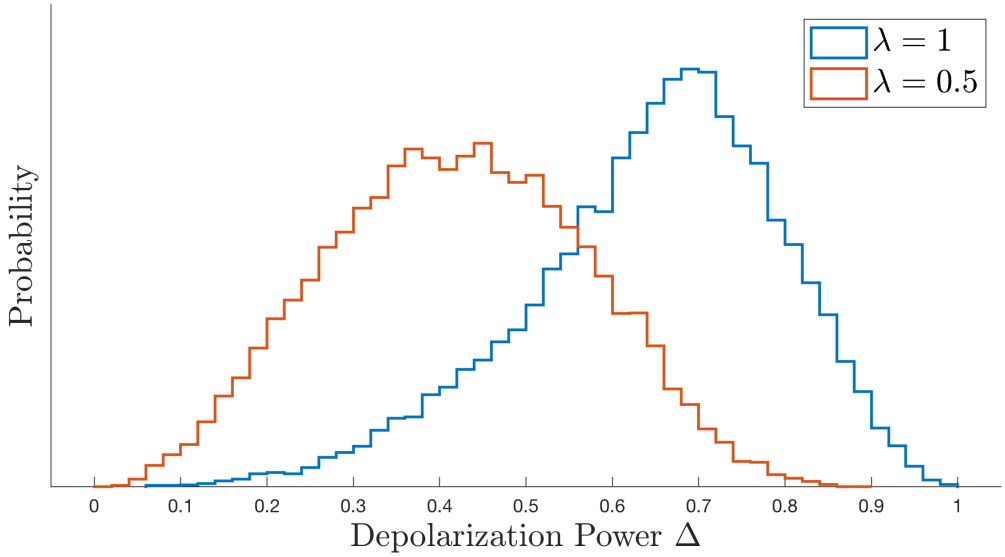

Figure B.1: Histograms of Δ for randomly generated MMs using two different values of the parameter λ.

B.2 Methodology for Section 4.4

The simulations described in section 4.4 required the random generation of both nine and ten parameter RI MMs. Similar to how general MMs can be generated by inverting the Lu-Chipman decomposition, this can be done by inverting the "double pass decomposition" developed in section 5.3 and Appendix E. Using the results of those sections, it can be shown that most RI MMs can be written in the form

$$\mathbf{M} = \mathbf{X}\,(\mathbf{M}_R\,\mathbf{M}_D)^T\,\mathbf{B}\,\mathbf{M}_R\,\mathbf{M}_D$$

where

$$\mathbf{B} = \begin{bmatrix} 1 & 0 & 0 & 0 \\ 0 & b_1 & 0 & 0 \\ 0 & 0 & b_2 & 0 \\ 0 & 0 & 0 & b_3 \end{bmatrix},$$

with $-1 \leq b_i \leq 1$ and $\mathbf{X} = \mathrm{diag}(1, 1, -1, 1)$ as defined in section 3.2. A class of MMs known as "type II" MMs [53, 95] cannot be decomposed this way, even if they are RI.

However, these matrices are expected to be rare and therefore their omission should not significantly effect the simulation results (see Appendix E).

The retarder and diattenuator MMs $\mathbf{M}_R$ and $\mathbf{M}_D$ were generated in the same way as in Appendix B.1. For ten parameter RI MMs, the three eigenvalues b_1, b_2, and b_3 were each selected independently from a uniform distribution on the interval $[-1, 1]$. The resulting matrix was not guaranteed to be a physical MM. Similar to in Appendix B.1, the coherency matrix was calculated for every $\mathbf{M}$ and only physical MMs were kept. Out of the randomly generated set of 10^5 matrices, 33 434 were physical MMs. To keep a consistent number of MMs between the nine parameter and ten parameter sets, 30 000 of these were chosen at random. Finally, each MM was multiplied by the scalar factor

$$\frac{1}{M(1,1)\left(1+\sqrt{M(1,2)^2+M(1,3)^2+M(1,4)^2}\right)}. \tag{B.4}$$

This re-scaling guarantees that for an input Stokes vector having $s_{IN,0} = 1/2$, the output irradiance $s_{OUT,0} \leq 1/2$ [53].

Nine parameter RI MMs must also obey the trace condition 3.14. Using the matrix $\mathbf{G} = \mathrm{diag}(1, -1, -1, -1)$, the trace condition is equivalent to

$$\begin{aligned} 0 &= M_{1,1} - M_{2,2} + M_{3,3} - M_{4,4} \qquad \text{(B.5)} \\ &= \mathrm{trace}(\mathbf{G}\,\mathbf{X}\,\mathbf{M}) \\ &= \mathrm{trace}(\mathbf{G}\,\mathbf{X}\,\mathbf{X}\,(\mathbf{M}_R\,\mathbf{M}_D)^T\,\mathbf{B}\,\mathbf{M}_R\,\mathbf{M}_D) \\ &= \mathrm{trace}(\mathbf{M}_R\,\mathbf{B}\,\mathbf{M}_R\,\mathbf{M}_D\,\mathbf{G}\,\mathbf{M}_D^T) \\ &= (1-D^2)\mathrm{trace}(\mathbf{B}\,\mathbf{M}_R\,\mathbf{G}\,\mathbf{M}_R^T) \\ &= (1-D^2)\mathrm{trace}(\mathbf{B}\,\mathbf{G}) \implies \\ 0 &= 1 - b_1 - b_2 - b_3 \qquad \text{(B.6)} \end{aligned}$$

where the identities $\mathbf{M}_D\,\mathbf{G}\,\mathbf{M}_D^T = (1-D^2)\mathbf{G}$ and $\mathbf{M}_R\,\mathbf{G}\,\mathbf{M}_R^T = \mathbf{G}$ follow from the definitions of $\mathbf{M}_D$ (equation 2.29) and $\mathbf{M}_R$ (equation 2.37), and the cyclical property of the trace has been used several times. To guarantee that expression B.6 was fulfilled, first three random variables b_1', b_2', and b_3' were each selected independently from a uniform distribution on the interval $[-1, 1]$. Then the true eigenvalues were given by

$$b_i = b_i' + \frac{1 - b_1' - b_2' - b_3'}{3} \tag{B.7}$$

for $i = 1, 2, 3$ which guarantees that they satisfy $1 - b_1 - b_2 - b_3 = 0$. Unphysical resultant matrices were dropped, and the matrices were re-scaled, in the same way as for ten parameter RI MMs. Out of 10^5 generated matrices, 74 950 were physical, but 30 000 were randomly selected for use in the simulations of section 4.5.

Appendix C

Reflections and Coordinate Systems

In sections 5.2 and 5.4, the Lu-Chipman decomposition was applied to the double pass matrix $\overline{\mathbf{M}}_{DP}$ after a change of coordinates. This appendix explains and justifies the coordinate system convention used.

In general, a MM depends on the coordinate systems that are used for both the input and output waves. Suppose a wave enters the eye while travelling in the direction $\hat{\mathbf{n}}$ while the (detected) wave exits in the opposite direction $-\hat{\mathbf{n}}$. In order to maintain right-handed coordinate systems for both, if the input Jones and Stokes vectors are defined with respect to the coordinates ($\hat{\mathbf{t_1}}$, $\hat{\mathbf{t_2}}$), the output vectors can be defined relative to ($\hat{\mathbf{t_1}}$, -$\hat{\mathbf{t_2}}$). This was the choice made during chapter 3, and it underlies both the definition of reciprocal invariance (equation 3.14 and 3.13) and the double pass model (equation 3.16). Let the MM with respect to these coordinates be written $\mathbf{M}$.

While this convention was convenient during chapter 3, several authors suggest using the same coordinate system ($\hat{\mathbf{t_1}}$, $\hat{\mathbf{t_2}}$) for both the input and output waves [24, 78, 105]. It can be shown that changing the coordinates of the output beam from ($\hat{\mathbf{t_1}}$, -$\hat{\mathbf{t_2}}$) to ($\hat{\mathbf{t_1}}$, $\hat{\mathbf{t_2}}$) is equivalent to left multiplying the MM by the mirror matrix $\mathbf{Y} = \text{diag}(1, 1, -1, -1)$ [78, 105, 138].

Therefore, the new MM[1] in these coordinates is

$$\overline{\mathbf{M}} \equiv \mathbf{Y}\,\mathbf{M}. \tag{5.1}$$

$\overline{\mathbf{M}}$ can be calculated in one of two ways. If the PSA is defined relative to the ($\hat{\mathbf{t_1}}$, -$\hat{\mathbf{t_2}}$) coordinates, then $\mathbf{M}$ will be measured directly (this is the assumption in chapter 4).

[1] The results of this section are applicable to any reflection MM, not just double pass matrices. Therefore, the subscript DP is dropped.

Note however that the beam path might include several mirrors or beamsplitters before reaching the PSA (*e.g.* [33, 126, 136]), so the effects of each of these must be accounted for to ensure the correct coordinate system is used. Then $\overline{\mathbf{M}}$ can be calculated using equation 5.1. Alternatively, expression 2.46 for an individual irradiance measurement can be written as

$$\begin{aligned} I_i &= c_A\, c_G [1\,0\,0\,0]\, \mathbf{M}_{PSA,i}\, \mathbf{M}\, \mathbf{M}_{PSG,i}\, [1\,0\,0\,0]^T \\ &= c_A\, c_G [1\,0\,0\,0]\, \mathbf{M}_{PSA,i}\, (\mathbf{Y}\mathbf{Y})\, \mathbf{M}\, \mathbf{M}_{PSG,i}\, [1\,0\,0\,0]^T \\ &= c_A\, c_G [1\,0\,0\,0]\, (\mathbf{Y}\mathbf{M}_{PSA,i}\mathbf{Y})\, \overline{\mathbf{M}}\, \mathbf{M}_{PSG,i}\, [1\,0\,0\,0]^T, \end{aligned}$$

because $\mathbf{Y}\mathbf{Y} = \mathbf{I}$ and $[1\,0\,0\,0] = [1\,0\,0\,0]\,\mathbf{Y}$. $\mathbf{Y}\mathbf{M}_{PSA,i}\mathbf{Y}$ is the PSA expressed in the ($\hat{\mathbf{t_1}}$, $\hat{\mathbf{t_2}}$) coordinates. By examining the product $\mathbf{Y}\mathbf{M}_{PSA,i}\mathbf{Y}$, it can be shown that if a PSA component is represented by an azimuthal angle θ measured relative to ($\hat{\mathbf{t_1}}$, $-\hat{\mathbf{t_2}}$)), it must be replaced by $-\theta$. Additionally, if the PSA contains any components with circular retardance or diattenuation, the sign of these must be inverted due to ($\hat{\mathbf{t_1}}$, $\hat{\mathbf{t_2}}$, $-\hat{\mathbf{n}}$) being left handed. If the PSA is represented in this way, then $\overline{\mathbf{M}}$ is measured directly instead of $\mathbf{M}$.

When analyzed using the Lu-Chipman decomposition, $\mathbf{M}$ and $\overline{\mathbf{M}}$ have different polarimetric properties. This begs the question of which set of properties to use. It will be shown that the polarimetric properties of $\mathbf{M}$ behave in an inconsistent way under rotations of the coordinates ($\hat{\mathbf{t_1}}$, $\hat{\mathbf{t_2}}$). For an ordinary transmission measurement (both input and output waves defined relative to the same coordinates ($\hat{\mathbf{t_1}}$, $\hat{\mathbf{t_2}}$)), a rotation of ($\hat{\mathbf{t_1}}$, $\hat{\mathbf{t_2}}$) by angle θ about $\hat{\mathbf{n}}$ transforms the MM $\mathbf{M}_{Tra}$ according to

$$\mathbf{M}_{Tra,Rot} \equiv \mathbf{R}(\theta)^T\, \mathbf{M}_{Tra}\, \mathbf{R}(\theta) \quad [39] \tag{C.1}$$

where

$$\mathbf{R}(\theta) \equiv \begin{bmatrix} 1 & 0 & 0 & 0 \\ 0 & \cos 2\theta & -\sin 2\theta & 0 \\ 0 & \sin 2\theta & cos2\theta & 0 \\ 0 & 0 & 0 & 1 \end{bmatrix} \quad [39].$$

It can be shown that $\mathbf{M}_{Tra,Rot}$ and $\mathbf{M}_{Tra}$ have identical linear and circular diattenuation (equation 2.29), linear and circular retardance (equation 2.38), and depolarization power (equation 2.45). However, for the reflection matrix $\mathbf{M}$, the input and output coordinates are not the same and so C.1 is not the correct transformation. Instead, a rotation of ($\hat{\mathbf{t_1}}$, $\hat{\mathbf{t_2}}$) has the effect

$$\mathbf{M}_{rot} = \mathbf{R}(\theta)\, \mathbf{M}\, \mathbf{R}(\theta) \quad [39]. \tag{C.2}$$

The polarimetric properties mentioned above are *not* invariant upon transformation C.2. If the Lu-Chipman decomposition is used to interpret $\mathbf{M}$, quantities such as linear retardance will change with a rotation of the coordinate axes ($\hat{\mathbf{t_1}}$, $\hat{\mathbf{t_2}}$). This problem is alleviated by analyzing $\overline{\mathbf{M}}$ instead of $\mathbf{M}$:

$$\begin{aligned} \mathbf{M}_{rot} &\equiv \mathbf{R}(\theta)\,\mathbf{M}\,\mathbf{R}(\theta) \implies \\ (\mathbf{Y}\,\mathbf{M}_{rot}) &= (\mathbf{Y}\,\mathbf{R}(\theta)\,\mathbf{Y})\,(\mathbf{Y}\,\mathbf{M})\,\mathbf{R}(\theta) \implies \\ \overline{\mathbf{M}}_{rot} &= \mathbf{R}(\theta)^T\,\overline{\mathbf{M}}\,\mathbf{R}(\theta) \end{aligned}$$

which is the same transformation as equation C.1. Therefore, the aforementioned polarimetric properties of $\overline{\mathbf{M}}$ are invariant with a coordinate system rotation. This justifies why the Lu-Chipman decomposition was applied to $\overline{\mathbf{M}}_{DP}$ instead of $\mathbf{M}_{DP}$ throughout chapter 5.

Appendix D

Derivation of All Possible Single Pass Mueller Matrices For Non-depolarizing Double Pass Mueller Matrices

In subsection 5.2.2, the relationship between the single and double pass properties of non-depolarizing MMs was considered. Applying the Lu-Chipman decomposition to both,

$$c_{DP}\mathbf{M}_{R,DP}\,\mathbf{M}_{D,DP} = c^2\mathbf{Q}\,\mathbf{M}_D^T\,\mathbf{M}_R^T\,\mathbf{Q}\,\mathbf{M}_R\,\mathbf{M}_D. \tag{5.12}$$

Assuming that c_{DP}, $\mathbf{M}_{R,DP}$, and $\mathbf{M}_{D,DP}$ are known, this Appendix will derive all possible $\mathbf{M}_{SP}$. Using equations for the MMs of retarders and diattenuators (2.37 and 2.29), the left and right side of equation 5.12 are expanded as

$$\overline{\mathbf{M}}_{DP} = \frac{c_{DP}}{1+D_{DP}}\begin{bmatrix} 1 & \mathbf{D}_{DP}^T \\ \mathbf{m}_{R,DP}\,\mathbf{D}_{DP} & \mathbf{m}_{R,DP}\,\mathbf{m}_{D,DP} \end{bmatrix} \tag{5.13}$$

$$= \frac{c^2}{(1+D)^2}\begin{bmatrix} 1+\mathbf{D}^T\,\mathbf{m}_q\,\mathbf{D} & \mathbf{D}^T+\mathbf{D}^T\,\mathbf{m}_q\,\mathbf{m}_D \\ \mathbf{q}\,\mathbf{D}+\mathbf{q}\,\mathbf{m}_D^T\,\mathbf{m}_q\,\mathbf{D} & \mathbf{q}\,\mathbf{D}\,\mathbf{D}^T+\mathbf{q}\,\mathbf{m}_D^T\,\mathbf{m}_q\,\mathbf{m}_D \end{bmatrix} \tag{5.14}$$

$$\mathbf{m}_q \equiv \mathbf{m}_R^T\,\mathbf{q}\,\mathbf{m}_R. \tag{5.15}$$

In subsection 5.2.2, the eigenvector of $\mathbf{m}_q$ given by $\hat{\mathbf{v}} \equiv \mathbf{m}_R^T\,[0,\,0,\,1]^T$ was defined. Two cases were considered: first if $\mathbf{D}$ is parallel (or antiparallel) to $\hat{\mathbf{v}}$, and second if $\mathbf{D}$ is

perpendicular to $\hat{\mathbf{v}}$. Assuming $\mathbf{D}$ is perpendicular to $\hat{\mathbf{v}}$, it was shown that it must have the uniquely determined value

$$\mathbf{D}_p = \frac{1 - \sqrt{1 - D_{DP}^2}}{D_{DP}^2} \mathbf{D}_{DP}. \tag{5.23}$$

Continuing with this assumption, it was shown how to calculate the principal single pass MM

$$\mathbf{M}_p = c_p \, \mathbf{M}_{R_p} \, \mathbf{M}_{D_p}$$

which obeys $\overline{\mathbf{M}}_{DP} = \mathbf{Q} \, \mathbf{M}_p^T \, \mathbf{Q} \, \mathbf{M}_p$ and has the property that $\mathbf{D}_p \perp \hat{\mathbf{v}}_p$ where $\hat{\mathbf{v}}_p \equiv \mathbf{m}_{R_p}^T \, [0, \, 0, \, 1]^T$.

Suppose there is a second single pass matrix $\mathbf{M}_{SP}$ which gives the same double pass MM as $\mathbf{M}_p$. Then,

$$\begin{aligned}
\mathbf{Q} \, \mathbf{M}_p^T \, \mathbf{Q} \, \mathbf{M}_p &= \mathbf{Q} \, \mathbf{M}_{SP}^T \, \mathbf{Q} \, \mathbf{M}_{SP} \quad \Longrightarrow \\
\mathbf{M}_p^T \, \mathbf{Q} \, \mathbf{M}_p &= \mathbf{M}_{SP}^T \, \mathbf{Q} \, \mathbf{M}_{SP} \quad \Longrightarrow \\
\mathbf{Q} &= (\mathbf{M}_p^T)^{-1} \, \mathbf{M}_{SP}^T \, \mathbf{Q} \, \mathbf{M}_{SP} \, \mathbf{M}_p^{-1} \quad \Longrightarrow \\
\mathbb{I} &= \mathbf{Q} \, \mathbf{M}_A^T \, \mathbf{Q} \, \mathbf{M}_A \qquad \text{(D.1)} \\
\mathbf{M}_A &\equiv \mathbf{M}_{SP} \, \mathbf{M}_p^{-1}. \qquad \text{(D.2)}
\end{aligned}$$

It has been assumed that $\mathbf{M}_p$ is invertible, which is the true as long as $D_p^2 \neq 1$. The $D_p^2 = 1$ case will be treated later. Products and inverses of non-depolarizing MMs are always non-depolarizing MMs [53], therefore $\mathbf{M}_A$ is a non-depolarizing MM. Equation D.1 shows that $\mathbf{M}_A$ must "cancel out" in double pass. Therefore, using equation D.2 and assuming $D_p^2 \neq 1$, all possible $\mathbf{M}_{SP}$ can be obtained by left multiplying $\mathbf{M}_p$ by a non-depolarizing MM that cancels out in double pass:

$$\mathbf{M}_{SP} = \mathbf{M}_A \, \mathbf{M}_p. \tag{D.3}$$

Next, it is necessary to find every $\mathbf{M}_A$ that obeys equation D.1. Because it is non-depolarizing, $\mathbf{M}_A = c_A \, \mathbf{M}_{R_A} \, \mathbf{M}_{D_A}$ using the Lu-Chipman decomposition. Define $\mathbf{m}_{q_A} \equiv \mathbf{m}_{R_A}^T \, \mathbf{q} \, \mathbf{m}_{R_A}$ and $\hat{\mathbf{v}}_A \equiv \mathbf{m}_{R_A}^T \, [0, \, 0, \, 1]^T$ where $\mathbf{m}_{R_A}$ is the lower right 3×3 submatrix of $\mathbf{M}_{R_A}$. Any 3D vector $\mathbf{D}_A$ can be written as the sum of components parallel and perpendicular to $\hat{\mathbf{v}}_A$: $\mathbf{D}_A = \mathbf{D}_\parallel + \mathbf{D}_\perp$. This implies that $\mathbf{m}_{q_A} \mathbf{D}_\parallel = -\mathbf{D}_\parallel$, $\mathbf{m}_{q_A} \mathbf{D}_\perp = \mathbf{D}_\perp$, and $\mathbf{D}_\parallel^T \mathbf{D}_\perp = 0$.

Writing for convenience $\mathbf{F} \equiv \mathbf{Q}\,\mathbf{M}_A^T\,\mathbf{Q}\,\mathbf{M}_A$, equation 5.14 becomes

$$F(1,1) = \frac{c_A^2}{(1+\sqrt{D_\perp^2 + D_\parallel^2})^2}(1 + D_\perp^2 - D_\parallel^2) \tag{D.4}$$

$$F(1,2:4) = \frac{c_A^2}{(1+\sqrt{D_\perp^2 + D_\parallel^2})^2}(\mathbf{D}_\perp^T + \mathbf{D}_\parallel^T + (\mathbf{D}_\perp^T - \mathbf{D}_\parallel^T)\mathbf{m}_{D_A}) \tag{D.5}$$

$$F(2:4,1) = \mathbf{q}F(1,2:4)^T$$

$$F(2:4,2:4) = \frac{c_A^2}{(1+\sqrt{D_\perp^2 + D_\parallel^2})^2}(\mathbf{q}\,(\mathbf{D}_\perp + \mathbf{D}_\parallel)(\mathbf{D}_\perp^T + \mathbf{D}_\parallel^T) + \mathbf{q}\,\mathbf{m}_{D_A}\,\mathbf{m}_{q_A}\,\mathbf{m}_{D_A}). \tag{D.6}$$

Using the definition of a diattenuator matrix (equation 2.29), $\mathbf{m}_{D_A}$ is given by

$$\mathbf{m}_{D_A} = \sqrt{1 - D_A^2}\mathbb{I} + a_A \mathbf{D}_A\,\mathbf{D}_A^T$$
$$a_A \equiv \frac{1 - \sqrt{1 - D_A^2}}{D_A^2}.$$

Equation D.1 requires that $\mathbf{F} = \mathbb{I}$. Starting with equation D.5, this implies that

$$\begin{aligned}
\mathbf{0} &= \mathbf{D}_\perp^T + \mathbf{D}_\parallel^T + (\mathbf{D}_\perp^T - \mathbf{D}_\parallel^T)\mathbf{m}_{D_A} \\
&= \mathbf{D}_\perp^T + \mathbf{D}_\parallel^T + (\mathbf{D}_\perp^T - \mathbf{D}_\parallel^T)\sqrt{1 - D_A^2} + a_A\,(D_\perp^2 - D_\parallel^2)\,(\mathbf{D}_\perp^T + \mathbf{D}_\parallel^T) \\
&= b_\perp \mathbf{D}_\perp^T + b_\parallel \mathbf{D}_\parallel^T \qquad (D.7) \\
b_\perp &\equiv (1 + \sqrt{1 - D_A^2} + a_A\,(D_\perp^2 - D_\parallel^2)) \\
b_\parallel &\equiv (1 - \sqrt{1 - D_A^2} + a_A\,(D_\perp^2 - D_\parallel^2)).
\end{aligned}$$

$\mathbf{D}_\perp$ and $\mathbf{D}_\parallel$ are by definition perpendicular, so equation D.7 implies both $b_\perp \mathbf{D}_\perp^T = \mathbf{0}$

and $b_\parallel \mathbf{D}_\parallel^T = \mathbf{0}$. Assume $\mathbf{D}_\parallel \neq \mathbf{0}$. Then

$$\begin{aligned}
\mathbf{0} &= b_\parallel \mathbf{D}_\parallel^T \quad \Longrightarrow \\
0 &= b_\parallel \\
&= 1 - \sqrt{1 - D_A^2} + \frac{1 - \sqrt{1 - D_A^2}}{D_\perp^2 + D_\parallel^2} (D_\perp^2 - D_\parallel^2) \\
&= \frac{2D_\perp^2 (1 - \sqrt{1 - D_A^2})}{D_A^2} \quad \Longrightarrow \\
0 &= D_\perp^2
\end{aligned}$$

because $\mathbf{D}_\parallel \neq \mathbf{0} \implies D_A^2 \neq 0 \implies (1 - \sqrt{1 - D_A^2}) \neq 0$. If on the other hand $\mathbf{D}_\parallel = \mathbf{0}$,

$$\begin{aligned}
b_\perp &= 1 + \sqrt{1 - D_\perp^2} + \frac{1 - \sqrt{1 - D_\perp^2}}{D_\perp^2} (D_\perp^2) \\
&= 2 \neq 0 \quad \therefore \\
b_\perp \mathbf{D}_\perp^T &= \mathbf{0} \quad \Longrightarrow \\
\mathbf{D}_\perp &= \mathbf{0}.
\end{aligned}$$

Therefore, in all cases $\mathbf{D}_\perp = \mathbf{0}$. Next, using equation D.4

$$\begin{aligned}
1 &= \frac{c_A^2}{(1 + |D_\parallel|)^2} (1 - D_\parallel^2) \quad \Longrightarrow \\
c_A &= \frac{1 + |D_\parallel|}{1 - |D_\parallel|}.
\end{aligned}$$

Lastly, with some algebra equation D.6 reduces to

$$\begin{aligned}
\mathbb{I} &= \frac{c_A^2}{(1 + |D_\parallel|)^2} ((1 - D_\parallel^2) \mathbf{q}\,\mathbf{m}_{q_A} + \left(1 - 2a_A \sqrt{1 - D_\parallel^2} - a_A^2 D_\parallel^2\right) \mathbf{D}_\parallel\, \mathbf{D}_\parallel^T) \\
&= \mathbf{q}\,\mathbf{m}_{q_A} \\
&= \mathbf{q}\,\mathbf{m}_{R_A}^T\, \mathbf{q}\,\mathbf{m}_{R_A}. \qquad \text{(D.8)}
\end{aligned}$$

The expression in large brackets vanishes, so the result is independent of $\mathbf{D}_A$. Subsection 5.2.1 shows that equation D.8 can only be satisfied if $\mathbf{m}_{R_A}$ is a circular retarder or half wave linear retarder. For all such matrices,

$$\begin{aligned}
\hat{\mathbf{v}}_A &= \mathbf{m}_{R_A}^T\, [0,\, 0,\, 1]^T \\
&= \mathbf{m}_{CR/HLR}^T\, [0,\, 0,\, 1]^T \\
&= [0,\, 0,\, \pm 1]^T.
\end{aligned}$$

$\mathbf{D}_A = \mathbf{D}_\parallel$ must be parallel or antiparallel to $\hat{\mathbf{v}}_A$, so in all cases $\mathbf{D}_A = [0,\, 0,\, D'_C]^T$ for $-1 < D'_C < 1$. Collecting these results, it follows that

$$\mathbf{M}_A = \frac{1 + |D'_C|}{1 - |D'_C|}\, \mathbf{M}_{CR/HLR}\, \mathbf{M}_{CD}(D'_C)$$

and finally

$$\mathbf{M}_{SP} = \frac{1 + |D'_C|}{1 - |D'_C|}\, \mathbf{M}_{CR/HLR}\, \mathbf{M}_{CD}(D'_C)\, \mathbf{M}_p \tag{D.9}$$

for all possible single pass MMs $\mathbf{M}_{SP}$.

It was assumed above that $D_p^2 \neq 1$. If $D_p = 1$, then it follows from equation 5.20 that

$$D_{DP} = \frac{2}{1 + D_p^2}\mathbf{D}_p = \mathbf{D}_p.$$

Then using equations 5.13 and 5.14 while writing $\mathbf{D} = \mathbf{D}_\parallel + \mathbf{D}_\perp$ as the sum of components parallel and perpendicular to $\hat{\mathbf{v}}$, it can be shown that $\mathbf{D} = \mathbf{D}_{DP} = \mathbf{D}_p$. Therefore, the principal diattenuation vector $\mathbf{D}_p$ is the only possible diattenuation vector.

Appendix E

Symmetric Decomposition of Reciprocal Invariant MMs

As discussed in 2.3.2, the decomposition of a MM into additive or multiplicative factors is a tool designed to aid in the physical interpretation of that MM. One multiplicative decomposition other than that due to Lu and Chipman [83] is known as the symmetric decomposition, and expresses a given MM in the form

$$\mathbf{M} = \mathbf{M}_{D2}\,\mathbf{M}_{R2}\,\mathbf{M}_{\Delta I/II}\,\mathbf{M}_{R1}\,\mathbf{M}_{D1}$$

where $\mathbf{M}_{Di}$ for $i = 1, 2$ represent diattenuator matrices, $\mathbf{M}_{Ri}$ represent retarder matrices, and $\mathbf{M}_{\Delta}$ represents a depolarizer matrix that may have one of two different forms [53, 95]. It was attempted to use the symmetric decomposition as a starting point to obtain a "double pass decomposition" of the form

$$\begin{aligned} \mathbf{M} &= (\mathbf{X}\,\mathbf{M}_{SP}^{T}\,\mathbf{X})\,\mathbf{Y}\,\mathbf{M}_{SP} \\ \mathbf{M}_{SP} &= \mathbf{M}_{\Delta}\,\mathbf{M}_{R}\,\mathbf{M}_{D}, \end{aligned} \tag{E.1}$$

which interprets $\mathbf{M}$ in view of the double pass model described in section 3.3.

Take $\mathbf{M}$ to be a RI MM satisfying $\mathbf{M} = \mathbf{X}\,\mathbf{M}^{T}\,\mathbf{X}$ (it may also obey the trace condition 3.14, but this is not necessary for any of the following results). The first step of the regular symmetric decomposition algorithm is to find the two diattenuation vectors belonging to $\mathbf{M}_{D1}$ and $\mathbf{M}_{D2}$ by solving

$$\begin{aligned} (\mathbf{M}^{T}\,\mathbf{G}\,\mathbf{M}\,\mathbf{G})\mathbf{s}_{D1} &= a^{2}\mathbf{s}_{D1} \\ (\mathbf{M}\,\mathbf{G}\,\mathbf{M}^{T}\,\mathbf{G})\mathbf{s}_{D2} &= a^{2}\mathbf{s}_{D2} \end{aligned} \tag{E.2}$$

where $G = \mathrm{diag}(1, -1, -1, -1)$, $\mathbf{s}_{Di} = (1, \mathbf{Di})^T$, $\mathbf{Di}$ are the two diattenuation vectors, and a^2 is the largest shared eigenvalue between $\mathbf{M}^T\,\mathbf{G}\,\mathbf{M}\,\mathbf{G}$ and $\mathbf{M}\,\mathbf{G}\,\mathbf{M}^T\,\mathbf{G}$ [53]. Using the double pass restriction, it follows that

$$\begin{aligned}
(\mathbf{M}^T\,\mathbf{G}\,\mathbf{M}\,\mathbf{G})\mathbf{s}_{D1} = a^2\mathbf{s}_{D1} \quad &\Longrightarrow \\
(\mathbf{X}\,\mathbf{M}\,\mathbf{X}\,\mathbf{G}\,\mathbf{M}\,\mathbf{X}^2\,\mathbf{G})\mathbf{s}_{D1} = a^2\mathbf{s}_{D1} \quad &\Longrightarrow \\
(\mathbf{X}\,\mathbf{M}\,\mathbf{G}\,\mathbf{X}\,\mathbf{M}\,\mathbf{X}\,\mathbf{G}\,\mathbf{X})\mathbf{s}_{D1} = a^2\mathbf{s}_{D1} \quad &\Longrightarrow \\
(\mathbf{M}\,\mathbf{G}\,\mathbf{M}^T\,\mathbf{G})(\mathbf{X}\,\mathbf{s}_{D1}) = a^2(\mathbf{X}\,\mathbf{s}_{D1})&
\end{aligned}$$

and so $\mathbf{s}_{D2} = \mathbf{X}\,\mathbf{s}_{D1}$. Using the expressions 2.29 to construct $\mathbf{M}_{Di}$ from the diattenuation vectors $\mathbf{Di}$, it can be shown that they must obey $\mathbf{M}_{D2} = \mathbf{X}\,\mathbf{M}_{D1}^T\mathbf{X}$. That is, $\mathbf{M}_{D2}$ is nothing other than the direction reversed version of $\mathbf{M}_{D1}$. If $\mathbf{M}^T\,\mathbf{G}\,\mathbf{M}\,\mathbf{G} = \mathbf{I}$, then the MM is nondepolarizing [53] and $\mathbf{Di}$ are not uniquely defined. In this instance, every single pass MM can be calculated as described in section 5.2.2 must be used instead. For the moment, it will also be assumed that $\mathbf{M}^T\,\mathbf{G}\,\mathbf{M}\,\mathbf{G} \neq 0$ and $|\mathbf{D1}| \neq 1$. Note that $|\mathbf{D1}| \neq 1$ implies that $|\mathbf{D2}| = |\mathbf{x}\,\mathbf{D1}| \neq 1$, and also that $\mathbf{M}_{D2}$ and $\mathbf{M}_{D1}$ are both invertible.

Once the two diattenuator matrices are known, one can compute $\mathbf{M}' = \mathbf{M}_{D2}^{-1}\,\mathbf{M}\,\mathbf{M}_{D1}^{-1} = \mathbf{M}_{R2}\,\mathbf{M}_{\Delta}\,\mathbf{M}_{R1}$. $\mathbf{M}'$ will always have the form

$$\begin{aligned}
\mathbf{M}' &= M'_{11}\begin{bmatrix} 1 & \mathbf{0}^T \\ \mathbf{0} & \mathbf{m}' \end{bmatrix} \\
&= M'_{11}\begin{bmatrix} 1 & \mathbf{0}^T \\ \mathbf{0} & \mathbf{m}_{R2}\,\mathbf{m}_{\Delta}\,\mathbf{m}_{R1} \end{bmatrix} \quad [53]
\end{aligned} \tag{E.3}$$

where $\mathbf{m}'$, $\mathbf{m}_{Ri}$, and $\mathbf{m}_{\Delta}$ are each the 3×3 submatrices of the corresponding full matrices $\mathbf{M}'$, $\mathbf{M}_{Ri}$, and $\mathbf{M}_{\Delta}$. In the original symmetric decomposition, the singular value decomposition of $\mathbf{M}'$ is used in order to determine $\mathbf{M}_{R1}$ and $\mathbf{M}_{\Delta}$ [53]. However, in order to obtain the desired form E.1, a modification is necessary. First, using the reciprocal invariance restriction 3.13,

$$
\begin{aligned}
\mathbf{M} = \mathbf{X}\,\mathbf{M}^T\,\mathbf{X} \quad &\Longrightarrow \\
\mathbf{M}_{D2}\,\mathbf{M}'\,\mathbf{M}_{D1} = \mathbf{X}\,\mathbf{M}_{D1}^T\,\mathbf{M}'^T\,\mathbf{M}_{D2}^T\,\mathbf{X} \quad &\Longrightarrow \\
\mathbf{M}_{D2}\,\mathbf{M}'\,\mathbf{M}_{D1} = \mathbf{X}\,\mathbf{M}_{D1}^T\,\mathbf{X}^2\,\mathbf{M}'^T\,\mathbf{X}^2\,\mathbf{M}_{D2}^T\,\mathbf{X} \quad &\Longrightarrow \\
\mathbf{M}_{D2}\,\mathbf{M}'\,\mathbf{M}_{D1} = \mathbf{M}_{D2}\,\mathbf{X}\,\mathbf{M}'^T\,\mathbf{X}\,\mathbf{M}_{D1} \quad &\Longrightarrow \\
\mathbf{M}' = \mathbf{X}\,\mathbf{M}'^T\,\mathbf{X} \quad &\Longrightarrow \\
(\mathbf{X}\,\mathbf{M}') = (\mathbf{X}\,\mathbf{M}')^T \quad &\Longrightarrow \\
(\mathbf{x}\,\mathbf{m}') = (\mathbf{x}\,\mathbf{m}')^T.
\end{aligned}
$$

Because $\mathbf{x}\,\mathbf{m}'$ is a real symmetric matrix, it must have an eigen decomposition of the form $\mathbf{x}\,\mathbf{m}' = \mathbf{U}^T\,\mathbf{A}\,\mathbf{U}$ where $\mathbf{U}$ is a real orthogonal matrix and $\mathbf{A}$ is a real diagonal matrix [60]. Manipulating this expression by using the fact that $\mathbf{x}^2 = \mathbf{I}$,

$$
\begin{aligned}
\mathbf{x}\,\mathbf{m}' = \mathbf{U}^T\,\mathbf{x}^2\,\mathbf{A}\,\mathbf{U} \quad &\Longrightarrow \\
\mathbf{m}' = (\mathbf{x}\,\mathbf{U}^T\,\mathbf{x})\,(\mathbf{x}\,\mathbf{A})\,\mathbf{U}. \qquad &\text{(E.4)}
\end{aligned}
$$

The eigen decomposition of a matrix is not fully unique however. Assuming there are three unique, nonzero eigenvalues, then one can obtain a new decomposition by either: multiplying any of the rows of $\mathbf{U}$ by -1, or by permuting the rows of $\mathbf{U}$ while at the same time permuting the diagonal entries of $\mathbf{A}$ in the same way. This is the same ambiguity that exists in the original symmetric decomposition [53]. There are $2^3 = 8$ possible sign combinations and six possible permutations, resulting in forty-eight different $(\mathbf{U}, \mathbf{A})$ pairs. Comparing equations E.3 and E.4, it would be favorable to take $\mathbf{m}_{R1} = \mathbf{U}$ and $\mathbf{m}_{R2} = \mathbf{x}\,\mathbf{U}^T\,\mathbf{x}$. Recall that a retarder $\mathbf{m}_R$ must be a proper rotation matrix, that is, it must have $\mathbf{m}_R\,\mathbf{m}_R^T = \mathbf{I}$ and $\det(\mathbf{m}_R) = +1$. $\mathbf{U}$ has the first property, but can have $\det(\mathbf{U}) = \pm 1$. Each of the transformations of $\mathbf{U}$ (*i.e.* swapping two rows or inverting the sign of a row) also switches the sign of $\det(\mathbf{U})$, so it follows that twenty-four of the forty-eight possible $(\mathbf{U}, \mathbf{A})$ pairs have $\det(\mathbf{U}) = +1$.

Equation E.3 also suggests taking $\mathbf{x}\,\mathbf{A} = \mathbf{m}_\Delta$. However, to make the final decomposition correspond more closely to the double pass model E.1, take

$$
\begin{aligned}
\mathbf{x}\,\mathbf{A} &= \mathbf{x} \begin{bmatrix} a_1 & 0 & 0 \\ 0 & a_2 & 0 \\ 0 & 0 & a_3 \end{bmatrix} \\
&= \mathbf{m}_{\Delta_{SP}}\,\mathbf{x}\,\mathbf{z}\,\mathbf{m}_{\Delta_{SP}}
\end{aligned}
$$

where

$$\mathbf{m}_{\Delta_{SP}} \equiv \begin{bmatrix} \sqrt{|a_1|} & 0 & 0 \\ 0 & \sqrt{|a_2|} & 0 \\ 0 & 0 & \sqrt{|a_3|} \end{bmatrix} \tag{E.5}$$

$$\mathbf{z} \equiv \begin{bmatrix} \text{sign}(a_1) & 0 & 0 \\ 0 & \text{sign}(a_2) & 0 \\ 0 & 0 & \text{sign}(a_3) \end{bmatrix}. \tag{E.6}$$

This is not the same $\mathbf{z}$ as was introduced in chapter 4. Note that because it is diagonal,

$$\begin{aligned} \mathbf{m}_{\Delta_{SP}} &= \mathbf{m}_{\Delta_{SP}}^T \\ &= \mathbf{m}_{\Delta_{SP}}^T \mathbf{x}^2 \\ &= \mathbf{x}\, \mathbf{m}_{\Delta_{SP}}^T \mathbf{x} \end{aligned}$$

Converting back to full 4×4 Mueller matrices,

$$\begin{aligned} \mathbf{M}_{R1} &\equiv \begin{bmatrix} 1 & \mathbf{0}^T \\ \mathbf{0} & \mathbf{m}_{R1} \end{bmatrix} \\ \mathbf{M}_{\Delta_{SP}} &\equiv \begin{bmatrix} 1 & \mathbf{0}^T \\ \mathbf{0} & \mathbf{m}_{\Delta_{SP}} \end{bmatrix} \\ \mathbf{Z} &\equiv \begin{bmatrix} 1 & \mathbf{0}^T \\ \mathbf{0} & \mathbf{z} \end{bmatrix}. \end{aligned}$$

Putting all of this together,

$$\begin{aligned} \mathbf{M} &= \mathbf{M}_{D2}\, \mathbf{M}_{R2}\, \mathbf{M}_{\Delta}\, \mathbf{M}_{R1}\, \mathbf{M}_{D1} \\ &= \mathbf{X}\, \mathbf{M}_{D1}^T\, \mathbf{X}\, \mathbf{X}\, \mathbf{M}_{R1}^T\, \mathbf{X}\, \mathbf{X}\, \mathbf{M}_{\Delta_{SP}}^T\, \mathbf{X}\, \mathbf{X}\, \mathbf{Z}\, \mathbf{M}_{\Delta_{SP}}\, \mathbf{M}_{R1}\, \mathbf{M}_{D1} \\ &= \mathbf{X}\, \mathbf{M}_{SP}^T\, \mathbf{X}\, (\mathbf{X}\, \mathbf{Z})\, \mathbf{M}_{SP} \\ \mathbf{M}_{SP} &\equiv \mathbf{M}_{\Delta_{SP}}\, \mathbf{M}_{R1}\, \mathbf{M}_{D1}. \end{aligned}$$

This expression matches the double pass model E.1 except for the replacement of $\mathbf{Y}$ with $\mathbf{X}\,\mathbf{Z}$. The implications of this replacement are considered in section 5.2.3.

The original symmetric decomposition algorithm [53], applied to a RI MM, would naturally have obtained $\mathbf{D2} = \mathbf{x}\,\mathbf{D1}$. However, prior knowledge of this identity allows one to significantly simplify the algorithm. The original would in general not have obtained retarders obeying $\mathbf{M}_{R2} = \mathbf{X}\,\mathbf{M}_{R1}^T\,\mathbf{X}$. This is due to the fact that it used the singular value

decomposition of $\mathbf{m}'$, while the new method uses the eigen decomposition of $\mathbf{x}\,\mathbf{m}'$ instead. Singular values are always positive, while eigenvalues can be negative. The sign differences between the two result in sign differences between the retarders $\mathbf{M}_{Ri}$ that are obtained by each method.

There are a few edge cases that should be considered. If $\mathbf{M}^T\,\mathbf{G}\,\mathbf{M}\,\mathbf{G} = 0$ (and $\mathbf{M} \neq 0$), it follows that $|\mathbf{D1}| = |\mathbf{D2}| = 1$ [53]. $\mathbf{M}$ must be non-depolarizing, and can be handled using the method of section 5.2.2. It is also possible that $|\mathbf{D1}| = |\mathbf{D2}| = 1$ and yet $\mathbf{M}^T\,\mathbf{G}\,\mathbf{M}\,\mathbf{G} \neq 0$. In this case, $\mathbf{M}$ is known as a "type II" MM, while MMs that do not have this property are "type I". Type II MMs can still be decomposed in the form

$$\mathbf{M} = \mathbf{M}_{D2II}\,\mathbf{M}_{R2}\,\mathbf{M}_{\Delta II}\,\mathbf{M}_{R1}\,\mathbf{M}_{D1II}$$

where the central depolarizer now has the peculiar form

$$\mathbf{M}_{\Delta II} = \begin{bmatrix} a_0 + a & -a & 0 & 0 \\ a & a_0 - a & 0 & 0 \\ 0 & 0 & a_2 & 0 \\ 0 & 0 & 0 & a_2 \end{bmatrix}$$
$$(0 \leq a_2 \leq a_0, \quad 0 < a) \quad [53].$$

The diattenuation vectors $(\mathbf{D1II}, \mathbf{D2II})$ are not equal to the vectors $(\mathbf{D1}, \mathbf{D2})$ which were obtained by solving E.2. Instead, a different, more complicated algorithm is necessary to find each diattenuation, retardance, and depolarization matrix [53]. Moreover, $\mathbf{M}_{\Delta II}$ can never be RI because of the requirement that $a > 0$. Suppose one was able to find a way of modifying this process for a RI $\mathbf{M}$ in order to obtain a decomposition with $\mathbf{M}_{D2II} = \mathbf{X}\,\mathbf{M}_{D1II}^T\,\mathbf{X}$ and $\mathbf{M}_{R2} = \mathbf{X}\,\mathbf{M}_{R1}^T\,\mathbf{X}$, as was done above for type I MMs. Then

$$\begin{aligned} \mathbf{M} &= \mathbf{X}\,\mathbf{M}_{D1II}^T\,\mathbf{M}_{R1}^T\,\mathbf{X}\,\mathbf{M}_{\Delta II}\,\mathbf{M}_{R1}\,\mathbf{M}_{D1II} \quad \Longrightarrow \\ \mathbf{M}_{\Delta II} &= \mathbf{X}\,((\mathbf{M}_{R1}\,\mathbf{M}_{D1II})^{-1})^T\,\mathbf{X}\,\mathbf{M}\,(\mathbf{M}_{R1}\,\mathbf{M}_{D1II})^{-1} \end{aligned}$$

which implies

$$\begin{aligned} \mathbf{X}\,\mathbf{M}_{\Delta II}^T\,\mathbf{X} &= \mathbf{X}\,((\mathbf{M}_{R1}\,\mathbf{M}_{D1II})^{-1})^T\,\mathbf{M}^T\,\mathbf{X}\,(\mathbf{M}_{R1}\,\mathbf{M}_{D1II})^{-1}\,\mathbf{X}\,\mathbf{X} \\ &= \mathbf{X}\,((\mathbf{M}_{R1}\,\mathbf{M}_{D1II})^{-1})^T\,\mathbf{X}\,\mathbf{M}\,\mathbf{X}\,\mathbf{X}\,(\mathbf{M}_{R1}\,\mathbf{M}_{D1II})^{-1} \\ &= \mathbf{M}_{\Delta II} \end{aligned}$$

using the fact that $\mathbf{M}^T = \mathbf{X}\,\mathbf{M}\,\mathbf{X}$ because $\mathbf{M}$ is RI. However, this implies that $\mathbf{M}_{\Delta II}$ is RI, which is impossible. Therefore, it must not be possible to decompose a type II matrix in

such a way that $\mathbf{M}_{D2II} = \mathbf{X}\,\mathbf{M}_{D1II}^T\,\mathbf{X}$ and $\mathbf{M}_{R2} = \mathbf{X}\,\mathbf{M}_{R1}^T\,\mathbf{X}$. Therefore type II RI MMs are incompatible with the double pass model.

It is possible for a RI MM to be type II; for example,

$$\begin{aligned}\mathbf{M} &= \begin{bmatrix} a_0 + a & -a & 0 & 0 \\ -a & -a_0 + a & 0 & 0 \\ 0 & 0 & -a_2 & 0 \\ 0 & 0 & 0 & a_2 \end{bmatrix} \\ &\qquad (0 \le a_2 \le a_0, \quad 0 < a) \\ &= \begin{bmatrix} 1 & 0 & 0 & 0 \\ 0 & -1 & 0 & 0 \\ 0 & 0 & -1 & 0 \\ 0 & 0 & 0 & 1 \end{bmatrix} \mathbf{M}_{\Delta II}\end{aligned}$$

which obeys 3.13 and 3.14 if $a_0 = a_2$, is physical due to being the product of physical MMs, and also is type II. However, type II MMs appear to be rare, occurring only in the happenstance that $|\mathbf{D1}|$ is exactly equal to one. Because of this, it was postulated that they are an edge case of limited practical importance. This idea was further validated by the simulations that were performed in section 5.4, in which no type II MMs were encountered.

Finally, if any of the eigenvalues of $\mathbf{x}\,\mathbf{m}'$ are equal to zero, or if any two are equal to one another, then there are many more possible $\mathbf{U}$ (and therefore many possible $\mathbf{m}_{R1}$). The twenty-four solutions that are found by the algorithm described above will still be valid.

Assume that $\mathbf{M}$ avoids all of these edge cases and also has the property that $\mathbf{Z}$ has exactly one negative element (it is believed on account of section 5.4 that this will be true for most if not all double pass MMs). Then, the double pass decomposition algorithm would proceed as follows: first, calculate the largest eigenvalue and associated eigenvector $\mathbf{s}_{D1}$ of $\mathbf{M}^T\,\mathbf{G}\,\mathbf{M}\,\mathbf{G}$. This can be done in Matlab using the `eig` function. $D1$ is equal to the last three elements of $\mathbf{s}_{D1}$. Then use equation 2.29 to calculate $\mathbf{M}_{D1}$, which can be used to calculate

$$\mathbf{M}' = \mathbf{X}\,\mathbf{M}_{D1}^{-1}\,\mathbf{X}\,\mathbf{M}\,\mathbf{M}_{D1}^{-1}.$$

The eigenvalue decomposition of $\mathbf{M}'$ (which can again be performed using `eig`) gives $\mathbf{U}$ and $\mathbf{A}$. If it is found that $\mathbf{Z}$ (and therefore $\mathbf{A}$) has one negative element, rearrange the entries of $\mathbf{A}$ such that it has the general form $\mathrm{diag}(+,+,-)$. Rearrange the rows of $\mathbf{U}$ in exactly the same way. Finally, if $\mathbf{U}$ has negative determinant, multiply any one row of $\mathbf{U}$ by minus one. The depolarization matrix $\mathbf{M}_{\Delta SP}$ can be calculated using E.5, while

the retardance matrix is determined by $\mathbf{m}_{R1} = \mathbf{U}$. The full single pass MM is given by $\mathbf{M}_{SP} = \mathbf{M}_{\Delta SP}\,\mathbf{M}_{R1}\,\mathbf{M}_{D1}$.

This gives only one out of the eight possible values of $\mathbf{M}_{SP}$. Section 5.2.3 discusses how the polarimetric properties of these eight are related.